Nano Research
2023, 16(8): 11221–11249

ISSN 1998-0124 CN 11-5974/O4
https://doi.org/10.1007/s12274-023-5873-x

Review Article

The function-oriented precursor selection for the preparation of carbon dots

Yalan Xu, Chan Wang (✉), Huan Zhuo, Dongrun Zhou, and Qijun Song (✉)

Key Laboratory of Synthetic and Biological Colloids, Ministry of Education, School of Chemical and Material Engineering, Jiangnan University, Wuxi 214122, China

Received: 14 April 2023 / **Revised:** 24 May 2023 / **Accepted:** 25 May 2023

ABSTRACT

As a new type of fluorescent nanomaterials, carbon dots (CDs) have exhibited excellent photoluminescence properties with tunable emission and high quantum yields, hence they have attracted an increasing interest in diverse research areas. The photoluminescence performance of CDs is primarily influenced by their precursors, which directly or indirectly determine the structures and specific functions of the resultant CDs. In this review, we aim to summarize the recent progress on synthesis of CDs using small aliphatic molecules, anilines, polyphenol, polycyclic aromatic hydrocarbons, organic dyes, or biomass as precursors. The associations of the physical and chemical properties of the CDs with their respective precursors are comprehensively investigated, and the potential applications and future development of CDs are discussed in detail. It is hoped that this review will open new horizons for CDs preparation by rational selection of the precursors from the vastly available carbon sources and the critical comments presented, here could inspire and guide future research in the design of multifunctional CDs.

KEYWORDS

carbon dots, precursors, photoluminescence, fluorophore, sensing, imaging

1 Introduction

Carbon dots (CDs) have emerged as a unique member of the carbon family due to their excellent photoluminescence characteristics [1], good biocompatibility, and the versatile preparation methods with wide availability of precursors [2]. The bright fluorescence from carbon nanoparticles was first observed in 2004 by Xu et al. during their preparation of single-walled carbon nanotubes by electric arc discharge [3]. After two years, Sun et al. synthesized various sized quasi-zero-dimensional (0D) carbon nanoparticles and named CDs for the first time [4]. Since then, a great deal of breakthroughs has been made both in theoretical understanding of the photoluminescence (PL) mechanism and the exploration of various applications in the fields, such as biomedicine, catalysis, optical devices, and anti-counterfeiting [5–7]. Currently, CDs can be divided at least into four categories, i.e., graphene quantum dots (GQDs), carbon quantum dots (CQDs), carbon nanodots (CNDs), and carbonized polymer dots (CPDs) [8, 9].

The so-called top-down or bottom-up methods are usually applied for the synthesis of CDs [8]. In the top-down route, CDs were successfully prepared from pyrolysis, laser ablation, electrochemical, or chemical oxidation etching of carbon rich materials, such as charcoal, carbon char, carbon black, carbon nanotubes, and graphite [10]. These synthetic routes, however, are often suffered from time-consuming, cumbersome procedures, and low yield of CDs. In contrast, the bottom-up route exhibits more advantages in the selection of precursors and carbonization methods. Widely available carbon sources, such as small aliphatic organic molecules, aromatic organic molecules, polymer, and natural biomass, have been used as precursors to prepare CDs by hydrothermal/solvothermal, microwave-assisted, and pyrolysis methods. Such synthetic methods have high degree of controllability [11]. The selection of carbon source has a great influence on the performance of the resultant CDs, as CDs with different sizes, morphologies, structures, and functional groups may be obtained from different carbon sources. It is interesting to note that the CDs prepared from small organic molecules usually have short emission wavelengths, while CDs obtained from more complexed organic compounds often have large conjugation domains and long emission wavelengths [12]. Besides, CDs prepared from carbon sources rich in amino or polyphenol structures tend to exhibit good reducibility [13]. CDs with large numbers of pyrrolic nitrogen show good oxidase activity [14], and CDs dopped with metal ions such as gold, silver, copper, and manganese also exhibit oxidase-like properties [15–17]. Thus, the properties of CDs are closely related to their precursor materials, and the selection of precursor strongly influences the performance of CDs and determines their applications.

Over the past decade, a large number of review papers have been published and different aspects of CDs, including the PL mechanisms of CDs [18–21], surface engineering [22, 23], large-scale synthesis [24], red/near-infrared (NIR) emission [25], the effects of plant systems [26], energy conversion and storage [27], antibacterial and antibiofilm mechanisms [28], environmental applications [29], biomedicine and sensing applications [30, 31],

Address correspondence to Chan Wang, wangchan@jiangnan.edu.cn; Qijun Song, qsong@jiangnan.edu.cn

have been comprehensively reviewed. In present work, we are trying to focus on the more recent advances in the precursor-oriented preparation of CDs with emphasis on our own experiences of CDs preparation based on scrutinizing selection of functional chemical reagents as the carbon sources. It is hoped that this review can supply some mechanistic perspectives on the formation of CDs, provide some practical guidance for the use of functionalized CDs, and promote more remarkable development of fluorescent CDs in diverse application fields.

2 Various precursor-derived CDs

Here, we mainly summarized CDs synthesized by using small aliphatic molecules, anilines, polyphenol, polycyclic aromatic hydrocarbons, organic dyes, and biomass as precursors (Table 1) and explored the specific functions of CDs inherited from precursors.

2.1 CDs obtained from small aliphatic molecules

Citric acid (CA) is perhaps the most frequently utilized precursor for the bottom-up synthesis of CDs. Its structure contains multiple hydroxyl and carboxyl groups, which allows the introduction of multiple functional groups on the surface of the resultant CDs. In addition, CA can form rings with other precursors or with itself, thereby increasing the effective conjugation length in the CDs, which makes it a versatile and popular choice for the preparation of CDs [32]. By combining CA with other small molecules containing nitrogen, sulfur, or phosphorus, a variety of CDs has been produced through methods such as calcination, hydrothermal treatment, microwave irradiation, and ultrasonic processing [8]. Yang et al. showed that the photoluminescence quantum yields (QY) of CDs prepared with only CA are generally less than 10%, and this figure increased to over 10% when CA was co-carbonized with ethylenediamine (EDA). After carefully optimizing the ratio of CA and ethylenediamine, blue-emissive CDs with QYs up to 80% were obtained (Fig. 1(a)) [33]. Schneider et al. successfully synthesized three different types of CDs by employing CA and different nitrogen sources, i.e., EDA, hexamethylenetetramine, and triethanolamine (Fig. 1(b)). They also observed that high nitrogen content typically correlates with high PL QYs of CDs [34]. Similarly, a nitrogen-doped CDs synthesized from CA and monoethanolamine was also reported [35]. The formation process of nitrogen-doped CDs was investigated with various characterization techniques, including transmission electron microscopy (TEM), fluorescence spectra, and thermogravimetric analysis, and the results revealed that the formation of CDs undergone continuous polymerization, aromatization, nucleation, and growth processes (Fig. 1(c)).

Apart from co-carbonization with EDA, nitrogen doping can also be achieved by using urea, which is a readily available nitrogen source for the preparation of multicolored fluorescent CDs via solvothermal method. In this regard, Miao et al. synthesized a series of multi-color emitting CDs with CA and urea as the raw materials, differently colored CDs were obtained by modifying the reaction temperature and the ratio of CA/urea in N,N-dimethylformamide (DMF) [36]. These authors proposed that the higher temperature and CA/urea ratio tended to increase the degree of graphitization and carboxyl content in the CDs, leading to the shift in emission color from blue/green to red. Qu's group also synthesized a series of blue-emissive CDs via microwave irradiation of CA and urea as the raw materials. The obtained CDs were found to have excellent photoluminescence properties [37]. Subsequently, they proposed a method to control the bandgap emission of CDs by solvothermal treatment of CA and urea in different solvents (water, glycerin, and DMF) to achieve panchromatic emission of CDs (Fig. 1(d)). They demonstrated that the degree of dehydration and carbonization of the precursors can be controlled by solvents, resulting in the formation of CDs with different sizes of sp^2 conjugate domains, which are accountable for the different emission colors ranging from blue to red [38]. In the formation of CDs, functional groups such as hydroxyl, carboxyl, or amine offer potential fusion sites during the dehydration process. For example, the classic preparation of CDs by solvothermal treatment of CA and urea undergoes the initial formation of short cylindrical structures with diameters ranging from 20 to 40 nm and axial lengths ranging from 7 to 20 nm, which were called as carbon nanorolls. Interestingly, under 655 nm laser irradiation, the curvilinear structure of the carbon nanorolls can unravel into carbon nanobelts with widths ranging from 7 to 20 nm and lengths reaching several hundred nanometers. Based on the special photothermal-induced PL changes during the transformation from carbon nanorolls to carbon nanobelts, multi-level anti-counterfeit encryption has been achieved (Fig. 1(e)) [39].

Ascorbic acid (AA), commonly referred to as vitamin C, possesses strong reducing properties and can act as an electron donor and reduce other molecules in the body. This characteristic of AA is significant for various reasons, including its ability to neutralize harmful free radicals and protect cells and tissues from oxidative damage. AA is frequently selected in the preparation of reductive CDs [40–43]. These CDs generally exhibit excellent reducibility and good stability. They can react with ClO^-, MnO_4^-, and NO_3^- ions, hence were used for dynamic detection of these reactants in real-time. The reduction of Fe^{3+} to Fe^{2+} could lead to a significant fluorescence change in the CDs, which was developed as fluorescent probe for Fe^{3+} sensing and monitoring the dynamic equilibrium between Fe^{3+} and Fe^{2+} [44–47].

Apart from AA, other reductive precursors such as glucose, fructose, and tannic acid (TA) are also utilized in the preparation of CDs [48]. Hallaj et al. demonstrated that ClO^- could induce direct oxidation of CDs derived from glucose pyrolysis, resulting in the generation of chemiluminescence emission. The observed chemiluminescence was proposed to stem from electron transfer annihilation and resonance energy transfer mechanisms [49]. In the presence of boric acid, urea, or sodium persulfate, CDs doped with boron, nitrogen, or sulfur were synthesized using glucose as the primary carbon source. The resulting CDs exhibited remarkable antioxidant properties, and the nitrogen-doped CDs displaying the highest free radical scavenging activity compared to AA, which was proved by the 2,2'-azino-bis(3-ethylbenzthiazoline-6-sulfonic acid) (ABTS) method [50]. The above results suggest that the CDs obtained from reductive aliphatic molecules can not only inherit the reducibility of the precursors but also exhibit good optical properties.

Briefly, in the synthesis process of CDs, the precursors play a crucial role, which not only affect the structure and composition of CDs, but also determine their optical properties and applications. The size, surface functional groups, and energy band structure of CDs can be adjusted by choosing different precursors.

2.2 CDs obtained from anilines and polyphenol

Aniline-like compounds have emerged as a promising class of precursors for the synthesis of CDs. They possess self-doped nitrogen elements and can be facilely oxidized and polymerized into large conjugated structures, thereby affording the CDs with diverse structures and properties [51]. Other heteroatom doping, including sulfur, phosphorus, or boron were also investigated to enhance the performances of CDs [52–54]. The highly conjugated structure of aniline derived CDs enables efficient electron transfer and exhibits remarkable electrical conductivity. Thus aniline-like compounds hold great potential for the preparation of CDs with advanced physiochemical properties.

By using o-phenylenediamine (o-PDA) as the sole carbon

Table 1 CDs obtained from different type of precursors

Category	Precursors	Methods	Emission color	Applications	References
Small aliphatic molecules	CA, EDA	Hydrothermal	Blue	Anticounterfeiting	[33]
	CA, monoethanolamine	Reflux	Blue	Cell imaging	[35]
	CA, urea	Solvothermal	Blue/green/red	LED	[36]
	CA, urea	Microwave	Green	Anticounterfeiting/imaging	[37]
	CA, urea	Solvothermal	Blue/green/yellow/orange/red	LED	[38]
	CA, urea	Solvothermal	Green/red	Encryptions	[39]
	AA, β-alanine	Microwave	Green	Cell imaging	[42]
	AA, glucose, and fructose	Hydrothermal	Blue	Drug loading	[48]
	Glucose	Pyrolysis	Blue	Detection of ClO^-	[49]
	Glucose, boric acid, urea, and sodium persulfate	Hydrothermal	Blue	Antibacterial	[50]
	o-PDA, catechol, and H_3PO_4	Hydrothermal	Red	Cell imaging	[52]
	o-PDA	Hydrothermal	Yellow	Detection of water in organic solvents	[55]
	p-PDA	Hydrothermal	Green/yellow/red	Cell imaging	[56]
	m-PDA	Solvothermal	Green	Cell imaging	[58]
	o-PDA, m-PDA, p-PDA, and dithiosalicylic acid	Solvothermal	Blue/green/red	Anticounterfeiting	[62]
Anilines and polyphenol	o-PDA, dopamine	Hydrothermal	Red	*Vivo* imaging/LED	[63]
	o-PDA, $AlCl_3{\cdot}6H_2O$	Solvent-free pyrolysis	Red/NIR	Cell imaging	[64]
	O-PDA, glacial acetic acid	Hydrothermal	Ultraviolet	LED	[65]
	1,2,4-Triaminobenzene	Calcination	Red	Cell imaging	[67]
	Resorcinol and AA	Hydrothermal	Blue	Cell imaging/antioxidant	[73]
	m-Aminophenol	Hydrothermal	Green	Cell/*vivo* imaging	[13]
	Phloroglucinol	Solvothermal	Blue/green/yellow/red	LED	[162]
	ANSA, EDA	Solvothermal	Green	Fluorescent ink	[76]
	PAN	Solvothermal	Yellow	Detection of Cr^{6+}	[78]
	1-Amino-2-naphthol hydrochloride, CA	Solvothermal	Orange	LED	[79]
	1,3-Dihydroxynaphthalene, KIO_4	Solvothermal	Red	LED	[80]
Polycyclic aromatic hydrocarbons	1,10-Phenanthroline, CA	Solvent-free pyrolysis	Blue	Detection of Fe^{2+}/Fe^{3+}	[89]
	5-Amino-1,10-phenanthroline, salicylic acid	Calcination	Orange	Detection of Cd^{2+}	[91]
	3,4,9,10-Tetranitroperylene	Solvothermal	Red	LED	[92]
	PTCAD, urea	Solvothermal	NIR	*Vivo* imaging	[93]
	TA	Microwave	Blue	Detection of picric acid	[94]
	TA	Calcination	Blue	Detection of Ni^{2+}	[97]
	TA	Hydrothermal	Blue	Detection of Cu^{2+}	[98]
	Cyanine dye	Solvothermal	NIR	PDT	[106]
	Polythiophene	Solvothermal	NIR	PDT	[107]
	Polythiophene derivate	Hydrothermal	Yellow	PDT	[108]
Organic dyes	Methylene blue	Hydrothermal	Red	PDT	[11]
	Curcumin	Solvothermal	Blue	PDT	[109]
	Riboflavin, EDA	Solvothermal	Green	PDT	[110]
	Mono-hydroxylphenyl triphenylporphyrin	Hydrothermal	Green	PDT	[111]
	Mn(II) phthalocyanine	Solvothermal	NIR	PDT	[102]
Biomass	Apple juice	Hydrothermal	Blue	Cell imaging	[114]
	Durian	Hydrothermal	Blue	Fluorescent ink	[117]
	Cucumber	Hydrothermal	Blue	Detection of Pb^{2+}	[119]
	Starch	Hydrothermal	Blue	Cell imaging	[120]
	Highland barley	Hydrothermal	Blue	Detection of Hg^{2+}	[121]
	Ginkgo leaves	Hydrothermal	Blue	Cell imaging	[124]
	Purslane leaves	Hydrothermal	Green	Detection of formaldehyde	[125]
	Scallions	Microwave	Blue	Detection of Cd^{2+}	[128]
	Spinach	Solvothermal	Blue/crimson/grayish white/red	Anticounterfeiting	[214]
	Taxus leaves	Solvothermal	Red	*Vivo* imaging	[215]
	Mulberry leaves	Hydrothermal	Blue	Detection of dopamine	[216]

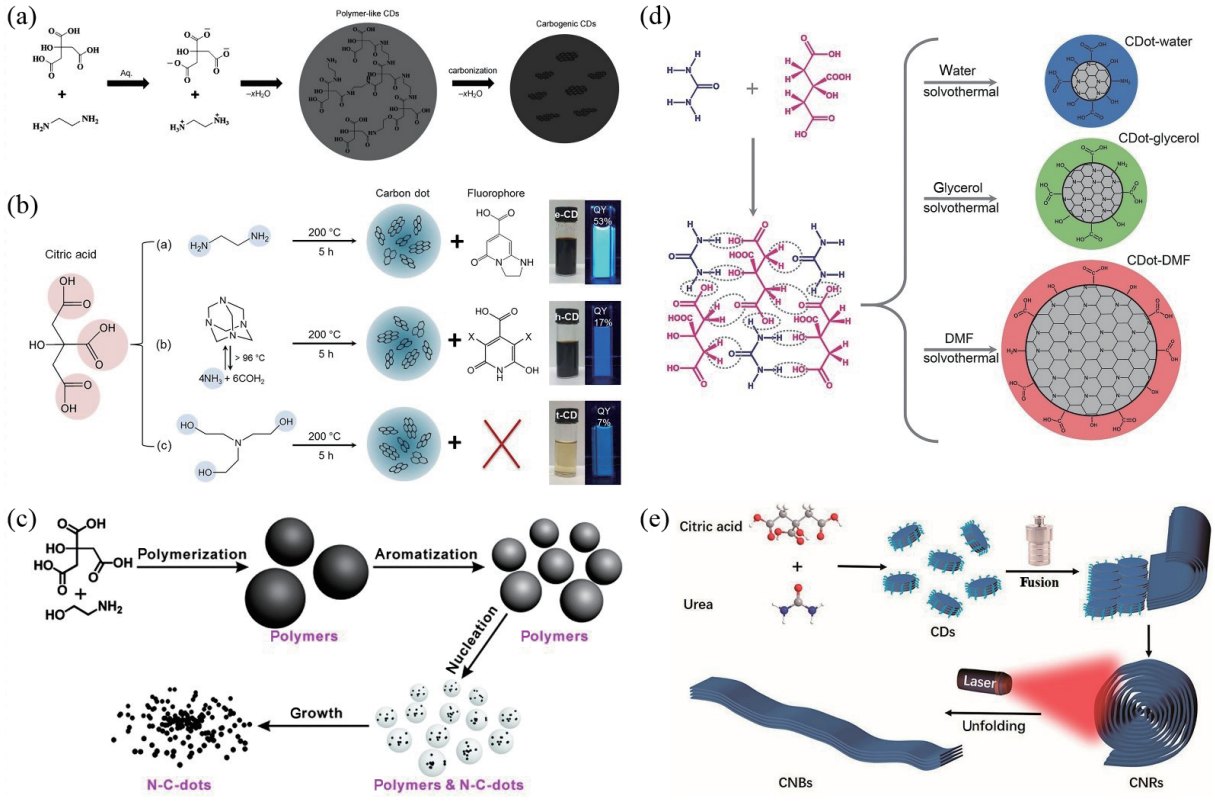

Figure 1 (a) The synthetic route of CDs using CA and EDA. Reproduced with permission from Ref. [33], © Wiley-VCH Verlag GmbH & Co. KGaA, Weinheim 2013. (b) Synthesis conditions of CA-based CDs using three different nitrogen-containing precursors. Reproduced with permission from Ref. [34], © American Chemical Society 2016. (c) The CDs prepared from CA and monoethanolamine. Reproduced with permission from Ref. [35], © The Royal Society of Chemistry 2015. (d) The growth process of CDs in different solvents. Reproduced with permission from Ref. [38], © WILEY-VCH Verlag GmbH & Co. KGaA, Weinheim 2017. (e) The structural evolution of CDs to CNRs and CNRs to CNBs via the solvothermal fusion and the photothermally induced unfolding steps, respectively. Reproduced with permission from Ref. [39], © American Chemical Society 2020.

source, Chao et al. have successfully synthesized CDs with multicolor emission in different solvents (Fig. 2(a)) [55]. Similarly, multi-color emitting CDs were obtained by hydrothermal treatment of p-phenylenediamine (p-PDA) at different pH conditions. The resultant CDs showed pH sensitive emission of red, yellow, and green color under alkaline, neutral, and acidic condition, respectively [56]. Subsequently, m-phenylenediamine (m-PDA) also was used as a precursor for the synthesis of blue, green, and red emissive CDs (Fig. 2(b)) [57–59]. However, the mechanisms behind the varied fluorescence emissions of CDs have not been fully explored. In order to gain a comprehensive understanding of the effects of different precursors on the formed CDs, researchers have conducted a systematic investigation using all three precursor materials (o-PDA, m-PDA, and p-PDA). Jiang et al. synthesized multicolored fluorescent CDs via solvothermal treatment of the three isomers, i.e., o-PDA, m-PDA, p-PDA, and the obtained CDs emitted bright blue, green, and red light, respectively (Fig. 2(c)) [60]. When the precursor is p-PDA, the resultant CDs demonstrated significantly red-shifted fluorescence and higher quantum yield compared to those obtained from the other two isomers, despite the three CDs have identical elemental compositions. A method for producing color-adjustable CDs has been proposed by hydrothermal treatment of p-aminobenzenesulfonic acid with o-, m-, or p-PDA and the resulting CDs also emit blue, green, and orange fluorescence, respectively. The different emission colors of the CDs can be attributed to differences in the particle size, degree of oxidation, and the N-related states on CDs surfaces [61]. These results indicate the optical properties of CDs were heavily dependent on the precursor selection, which gives an important guide for the design and preparation of required CDs. Solvothermal treatment of o-PDA, m-PDA, and p-PDA, along with dithiosalicylic acid in acetic acid solvent resulted in red (620 nm), green (520 nm), and blue (478 nm) emissive CDs, respectively [62]. X-ray photoelectron spectroscopy (XPS) spectra and transmission electron microscopy (TEM) images revealed that the red-shift in luminescence was accompanied by a gradual increase in particle size and C=O content of the CDs. These findings provide valuable insights into the correlation between the optical properties and structural characteristics of CDs and suggest a promising strategy for the tunable synthesis of CDs with desirable optical properties.

In the past few years, the preparation of CDs with simple organic molecules and PDA as the representative precursor have been extensively investigated. For example, the influence of hydrothermal temperature on CDs formation was systematically investigated by Yang et al. using o-PDA and dopamine as precursors (Fig. 2(d)) [63]. It was found that the dehydration reaction of the two precursors at relatively low temperatures resulted in intertwined polymer chains with benzene rings and heterocycles in the backbone. In contrast, large molecules or crosslinked polymer chains were the dominant structures in the CDs synthesized at 150 °C. When the temperature was increased to 200 °C, a carbogenic core with a large sp^2 domain was formed, with many polymer chains still linked to the carbon cores. And nearly all of the molecules and polymer chains were carbonized at 250 °C, with freshly formed C=C bonds ordered and assisting in the growth of CDs. The carbogenic cores were the dominant structure in CDs synthesized at 250 °C, hence the blue emission mostly or exclusively arose from the carbogenic cores [63]. In the following year, Yang et al. reported a nitrogen-doped CDs by using o-PDA as a carbon source with the assistance of HNO_3 [54]. It was observed that the conjugated aromatic system and

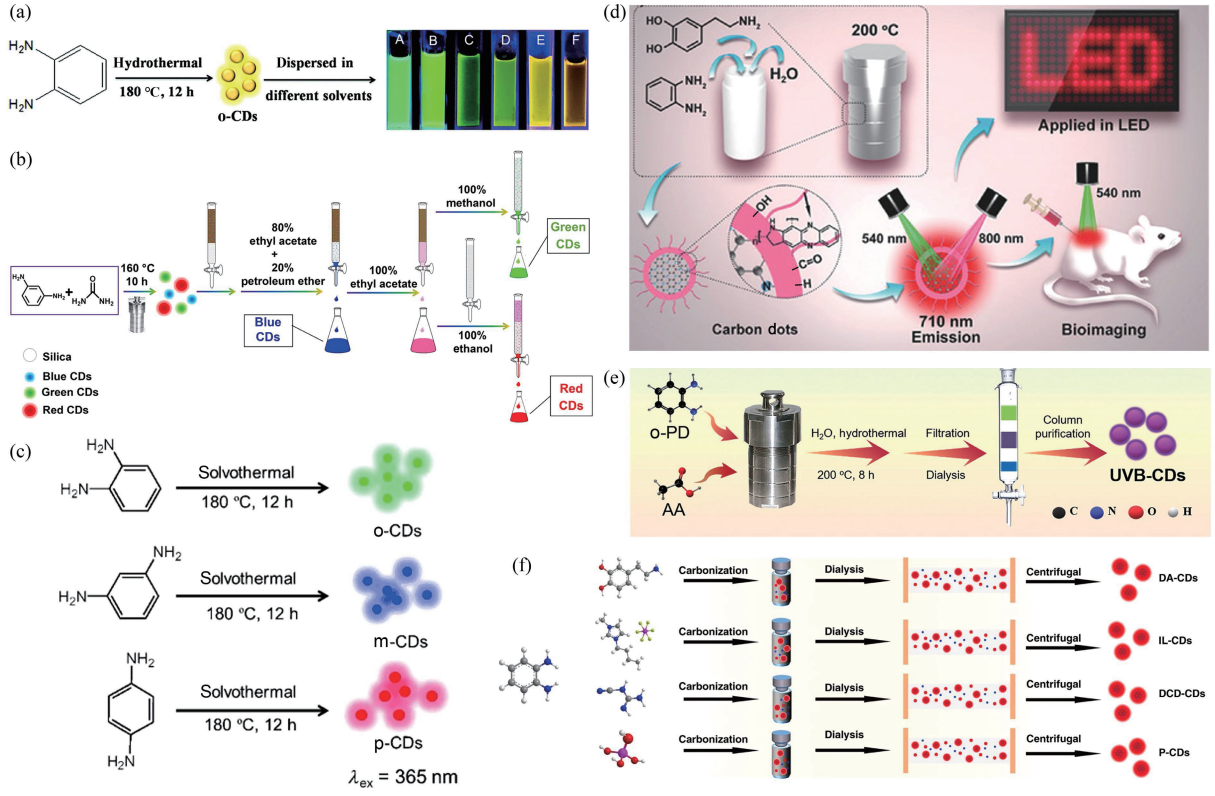

Figure 2 (a) The CDs obtained from o-PDA. Reproduced with permission from Ref. [55], © The Royal Society of Chemistry 2018. (b) Blue CDs, green CDs, and red CDs prepared from m-PDA and urea. Reproduced with permission from Ref. [57], © American Chemical Society 2021. (c) Three kinds of CDs obtained from solvothermal treatment o-PDA, m-PDA, and p-PDA, respectively. Reproduced with permission from Ref. [60], © Wiley-VCH Verlag GmbH & Co. KGaA, Weinheim 2015. (d) The CDs prepared from o-PDA and dopamine. Reproduced with permission from Ref. [63], © WILEY-VCH Verlag GmbH & Co. KGaA, Weinheim 2017. (e) The illustration of the synthesis and purification process of the UVB-CDs. Reproduced with permission from Ref. [65], © Wiley-VCH GmbH 2022. (f) Six types of CDs prepared with different method. Reproduced with permission from Ref. [51], © Wang, B. Y. et al. 2022.

hydrogen bonding were enhanced with the increase of HNO_3 dosage, resulting in the enlargement of the CDs and the achievement of red emission. Interestingly, Liu et al. reported a new red/near-infrared emissive CDs, which was formed in the presence of $AlCl_3{\cdot}6H_2O$ [64]. Their study also suggests that the formation of the sp^2-conjugated aromatic systems is a favorable pathway for achieving red/NIR emission in the CDs. On the contrary, in order to obtain fluorescence CDs with short wavelength emission, it is necessary to disrupt the conjugated structure of CDs, reducing the efficiency of the sp^2 π-system. In this respect, Xu et al. present the preparation of CDs that emit in the ultraviolet (UV) range, where o-PDA was utilized as the precursor, and acetic acid was employed as a promoter to induce sp^3 bonding in the CDs (Fig. 2(e)) [65]. This approach effectively reduced the size of sp^2 conjugated domains within the CDs, leading to a blue-shifted photoluminescence emission in the UV B (UVB) region, with a maximum emission wavelength of 308 nm. However, how to regulate the structure of CDs between sp^2 and sp^3 bonding is still challenging. It is also not clear if the fluorescence emission of CDs depends solely on the size of the sp^2/sp^3 hybridized domains. To address this challenge, Wang and colleagues have tried to validate the hypothesis by preparing CDs with CA (sp^3 hybridized structures) and o-PDA (sp^2 hybridized structures) as the precursors [66]. Multicolor CDs were obtained by manipulating the reaction conditions to alter the ratio of hybridized domains and meticulous tuning the temperature and pH during the hydrothermal reaction. Seven unique colors of fluorescent CDs were successfully synthesized, and their maximum emission wavelengths are located at 413, 445, 472, 505, 567, 592, and 635 nm, which span the entire visible spectrum. Theoretical and experimental investigations revealed that the blue emission increases with the increase of the sp^3 hybridization in CDs, whereas a decrease in the proportion of sp^3 hybridization leads to a prevalence of sp^2 hybridization, resulting in a gradual red shift in the fluorescence emission peak of CDs. Therefore, it is possible to design CDs that emit multiple colors by modifying the proportion of sp^2 and sp^3 hybridized domains. Recently, Lu et al. found that most red fluorescent CDs prepared from o-PDA as precursor exhibit similar optical characteristics [51]. As shown in Fig. 2(f), six kinds of fluorescent CDs were prepared by reacting o-PDA with dopamine, ionic liquid (1-butyl-3-methylimidazolium hexafluorophosphate), dicyandiamide, phosphoric acid, sulfuric acid, or nitric acid, respectively [51]. These CDs exhibit the same PL emission and absorbance spectra, furthermore, the sizes and X-ray diffraction peaks of these six CDs obtained are identical, but the number and orientation of lattice fringes vary. They believe that different preparation methods had almost no effect on the carbon nuclei structure of the CDs, only affect the degree of carbon core stacking and different surface polymers. Thus, they have concluded that the carbon core regulates the emission center of CDs, while the polymer shell regulates the intensity of PL emission.

In addition to utilizing the sp^2 conjugation properties of simple organic molecules, the protonation, deprotonation, and reducibility of aromatic molecules containing specific functional groups could also be inherited in the resultant CDs. For example, we have prepared a kind of pH-sensitive fluorescent CDs through direct calcination of 1,2,4-triaminobenzene, which is known as a pH sensitive precursor [67]. Upon increasing the pH from 4.0 to 8.0, the fluorescence emission of the CDs is shifted from 650 to 585 nm. The pH dependence of CDs is ascribed to the reversible transformation between azo and quinone structures, which is induced by protonation and deprotonation (Figs. 3(a) and 3(b)). Zhang et al. used p-PDA as the carbon source and successfully synthesized red-fluorescent CDs via a hydrothermal method with

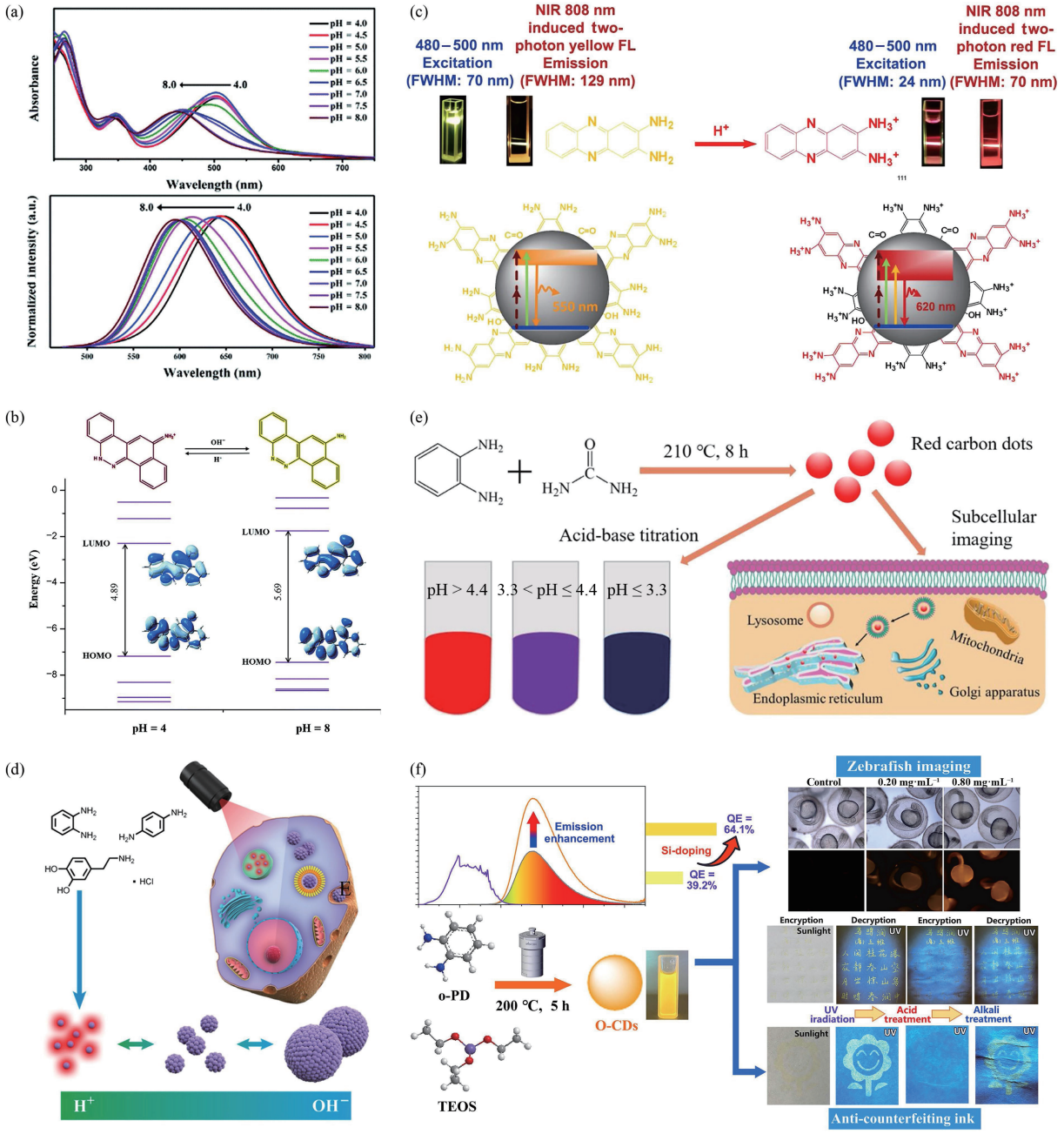

Figure 3 (a) Ultraviolet–visible (UV–vis) absorption spectra and fluorescent spectra of a series of CDs at different pH values with an excitation of 444 nm. (b) The structures of CDs at different pH values by DFT calculations. Reproduced with permission from Ref. [67], © The Royal Society of Chemistry 2020. (c) Protonation of surface 2,3-diaminophenazine fluorophore strongly affects the molecular state of CDs. Reproduced with permission from Ref. [68], © Zhang, Q. et al. 2021. (d) The pH-responsive CDs obtained from o-PDA, p-PDA, and dopamine. Reproduced with permission from Ref. [69], © WILEY-VCH Verlag GmbH & Co. KGaA, Weinheim 2019. (e) and (f) The CDs based o-PDA. Reproduced with permission from Ref. [70], © Elsevier Ltd. 2021. Reproduced with permission from Ref. [71], © American Chemical Society 2021.

the assistance of sodium sulfate, which is also pH-sensitive (Fig. 3(c)) [68]. Systematic analysis revealed that the molecular state of CDs is affected by the protonation and deprotonation of 2,3-diaminophenazine, which is an oxidation product of the reactant o-PDA. The protonation and deprotonation occur, respectively, in acidic and alkaline environments, leading to changes in the photon transition band gap and triggering red fluorescence emission with a significantly altered emissive peak width. Coincidentally, o-PDA, p-PDA, and dopamine were used to fabricate red emissive two-photon fluorescent CDs via a hydrothermal method (Fig. 3(d)). The resultant CDs exhibit a pH-dependent response in the pH range of 1.0 to 9.0, and a linear response was observed within the pH range of 3.5 to 6.5. These properties are particularly useful for monitoring the changes of intracellular pH [69]. Under strongly acidic conditions, the $-NH_2$ groups of the CDs undergo protonation, which helps to prevent aggregation by creating electrostatic repulsion. On the other hand, the CDs exhibit partial deprotonation in alkaline conditions, leading to a near-complete quenching of fluorescence. The CDs derived from aniline-like compounds have demonstrated a great potential for pH sensing applications due to the protonation and deprotonation induced transformation. Based on such mechanism, pH-responsive orange and red emissive CDs obtained from o-PDA were also used for anti-counterfeiting and endoplasmic reticulum (ER) imaging, respectively (Figs. 3(e) and 3(f)) [70, 71]. Hence with simple precursors and synthetic methods, the obtained CDs can retain the unique optical properties, making them an attractive candidate for pH sensing applications.

The precursors containing aromatic amino or phenolic

hydroxyl groups are easily oxidizable, thus they have used for preparation of CDs with redox applications. The CDs rich in –OH usually exhibit free radical scavenging activity, which highlights their potential in biomedical applications. Lu et al. have developed a one-step hydrothermal method for the synthesis of biocompatible CDs with rich hydroxyl groups by using phloroglucinol and phenol as precursors [72]. The prepared CDs have demonstrated excellent antioxidant property, thus have been used for scavenging free radicals and protecting cells from harmful effects. Using catechol and AA as precursors, Wang et al. reported a blue fluorescent CDs that can efficiently eliminate reactive oxygen species (ROS) (Fig. 4(a)) [73]. The excellent antioxidant properties of CDs can be attributed to their polyphenol-like structures with inherent antioxidant capabilities. The addition of AA not only enhances the fluorescent efficiency of CDs, making them suitable for various sensing applications, but also prevents the oxidation of resorcinol during the polymerization and carbonization process. It has been demonstrated that the phenolic H-atoms in the CDs can effectively scavenge free radicals and form intermediate phenoxyl radicals, which further undergo p-π orbital overlap to achieve resonance stabilization (Fig. 4(b)) [74, 75]. Therefore, the CDs with phenol-like groups can act as efficient H-atom donors to capture ROS and mitigate chronic inflammation. It is worth noting that aromatic molecules with both phenolic hydroxyl and amino groups, i.e., m-aminophenol have been employed as carbon sources to prepare CDs for dynamics monitoring oxidative stress *in vivo* [13]. Comprehensive characterizations and theoretical calculations revealed that the luminescent centers of CDs consist of a six-membered aromatic ring with abundant phenolic hydroxyl and amino groups, which act as active sites for the removal of ROS, accompanying with the fluorescence changing from yellow-green to blue (Fig. 4(c)). However, above mentioned CDs usually lack selectivity, as they can react non-specifically with various ROS. To address this issue, our group proposed a new strategy by using phosphate to partially protect the active sites, intending to differentiate between different ROS (Fig. 4(d)) [52]. To achieve this purpose, we initially synthesized a yellow fluorescent CDs by using o-PDA and catechol as the precursors. The resultant CDs show the similar characteristics to above mentioned CDs, i.e., they have sensitive fluorescence response to ROS but lack of selectivity. After further treatment of the yellow emissive CDs with phosphoric acid, it is interesting to note that a kind of narrow bandwidth red fluorescent CDs was obtained, which displayed sensitive colorimetric and fluorescent responses to hydroxyl radicals (·OH), superoxide anion radicals ($\cdot O_2^-$), and singlet oxygen ($^1O_2$), but have no response to H_2O_2 (Fig. 4(e)). We think this is a significant finding, because H_2O_2 is ubiquitously existing in various biological samples, hence could be a primary interference for ROS detection. The structures of the CDs were comprehensively investigated experimentally and theoretically and the results revealed that the as-prepared CDs consist of two five-membered aromatic rings joined together by pyrophosphate groups. The phosphate group protects the amino terminals of the aromatic ring, which is the underlying reason for the inactivity of the CDs to H_2O_2 [52]. All these results tend to conclude that the CDs obtained from polyphenol and aniline-like precursors as the carbon source can perfectly inherit their unique antioxidant properties. Although the

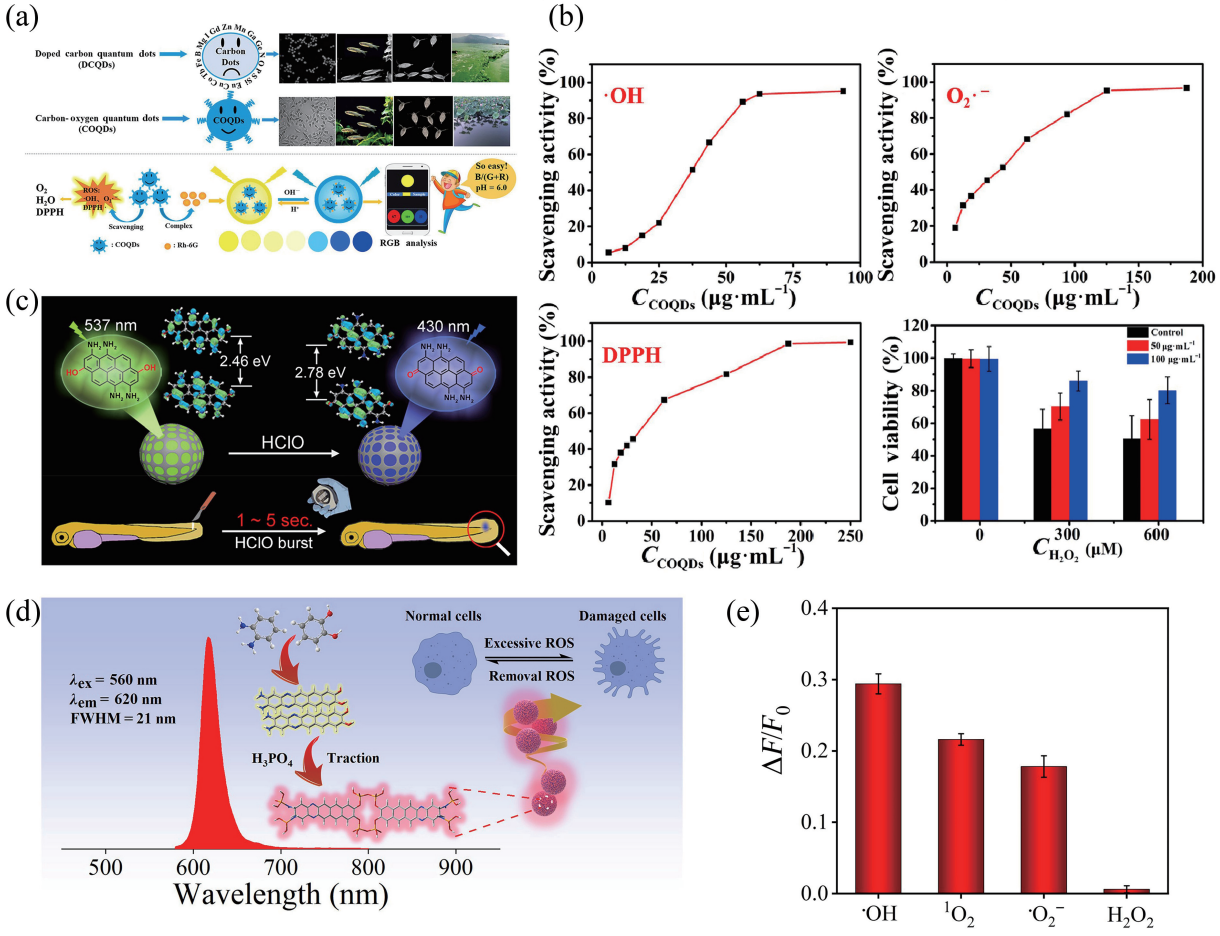

Figure 4 (a) and (b) The free radical scavenging activity of CDs. Reproduced with permission from Ref. [73], © Elsevier Ltd. 2022. (c) Mechanism diagram for the alteration of CDs emission performances caused by oxidation. Reproduced with permission from Ref. [13], © American Chemical Society 2020. (d) The CDs obtained from o-PDA, catechol, and H_3PO_4. (e) Fluorescence responses of the CDs for different ROS. Reproduced with permission from Ref. [52], © The Royal Society of Chemistry 2023.

CDs synthesized so far are still not able to distinguish all kinds of ROS, the novel strategy introduced in this work should have a great potential in the designing species selective CDs sensors.

In conclusion, the CDs obtained from anilines and polyphenol precursors can inherit and retain the following properties: (1) the conjugated structures of precursors, which facilitate long-wavelength emission of CDs; (2) the abundant amino functional groups, making the resulting CDs highly sensitive to pH based on protonation and deprotonation mechanisms; and (3) the reducibility of the precursors, as CDs inherit a large number of easily oxidizable aromatic phenolic hydroxyl and amino groups, which can be used to remove ROS.

2.3 CDs obtained from polycyclic aromatic compounds

In many applications, it is often desirable for CDs to have a long-wavelength emission. In this regard, the polycyclic aromatic hydrocarbons (PAHs) have emerged as a promising class of precursors for the synthesis of CDs. PAHs possess large conjugated structures, facilitating the formation of long-wavelength CDs with the large sp^2 domain. Accordingly, they have garnered significant attention as a platform for the development of novel CDs with tunable optical properties.

Naphthalene and its derivatives belong to PAHs with two benzene rings, whose conjugated bonds can be formed between the sp^2 hybridized carbon atoms on the naphthalene ring, resulting in a larger conjugated structure. Green-emitting CDs (G-CDs) were successfully synthesized with microwave-assisted solvothermal method by using 1-amino-2-naphthol-4-sulfonic acid (ANSA) and EDA as precursors, and ethanol as the solvent (Fig. 5(a)) [76]. The carbon core of as-prepared G-CDs is surrounded by functional groups such as hydroxyl, sulfonyl, and amino groups. At high temperatures and pressure, ANSA and EDA undergo dehydration and deamination reactions, producing molecular copolymers. These copolymers further polymerize, resulting in the formation of large conjugated structures. As single emission behavior was observed, Long et al. speculate the G-CDs might have a unique PL center, which is independent of the size. The surface defects of G-CDs, primarily caused by the edge S–O and $–NH_2$ groups, were considered to be closely related to the PL center of the G-CDs. Another naphthalene derivatives, 1-(2-pyridylazo)-2-naphthol (PAN) was also employed by Feng et al. for CDs preparation. As a chelating agent, PAN is able to trap Mn^{2+} in solution. With the proceeding of the carbonization process, Mn^{2+} cations can act as connectors between the chelating agents, forming the metal-coordinated functional groups in the carbon framework, which ultimately promote the formation of yellow CDs [77]. Following their previous work, Feng and colleagues utilized PNA as a precursor and coordinated it with transition metal Co^{2+} to synthesize yellow fluorescent CDs (Y-CDs) via a solvent-thermal reaction. The resulting CDs show high sensitivity in detecting Cr^{6+} ions (Fig. 5(b)) [78]. Although the naphthalene-based carbon sources form a conjugated structure during the preparation of CDs, their long side chains and excessive functional groups limit the further expansion of the conjugated domain of the CDs. Therefore, some researchers attempted to use simple naphthalene-based precursors as carbon sources, which make it easier to synthesize CDs with larger conjugated systems. For example, 1-amino-2-naphthol hydrochloride and CA were used as raw materials to prepare orange emissive CDs (Fig. 5(c)) [79]. Yang et al. have successfully fabricated red emissive CDs with an emission center at 628 nm, and they concluded that the precursor of 1,3-dihydroxynaphthalene is crucial in determining the distinctive structure of red emissive CDs (Fig. 5(d)) [80]. 1,3-dihydroxynaphthalene can be considered as the smallest sp^2 domain containing –OH groups. Under strong oxidation conditions using KIO_4, 1,3-dihydroxynaphthalene acts as a building block to form large conjugated sp^2 clusters with –OH groups at the edge sites, via a series of dehydrative condensation and dehydrogenative planarization processes. Meanwhile, a polarity-sensitive red emissive CDs (emission center at 640 nm) were synthesized from 2,7-dihydroxynaphthalene, CA, and L-methionine, using solvothermal method. The red emission of the CDs is mainly due to the inheritance of the conjugated structure of 2,7-dihydroxynaphthalene, while the nitrogen and sulfur doping is resulted from L-methionine. Thus, the retention of amino, hydroxyl, carboxyl, and methylthio groups on the surface of CDs was achieved to enhance the fluorescence stability, emission wavelength, and quantum yield [81]. It was found that the electron cloud density of sp^2 hybridization in the carbon cores increases with the increase of solvent polarity, which reduces the energy gap between highest occupied molecular orbital (HOMO) and d lowest unoccupied molecular orbital (LUMO) orbitals. As a result, the transition of π–π^* electrons from the first excited S_1 state to the ground S_0 state is promoted, resulting in a red shift of the emission wavelength of CDs.

Quinoline, also called as nitrogen-containing naphthalene, is a heterocyclic aromatic organic compound composed of a benzene ring fused to a pyridine ring. To construct nucleic acid-targeting CDs, quinoline derivatives were selected as the ideal structure-inherent carbon sources. This is because quinoline moieties are present in most nucleic acid probes, and are highly effective at binding to the grooves of nucleic acids through electrostatic and π–π interactions [82–84]. Using quinoline derivatives, 4-methylquinoline as carbon source, Peng et al. prepared RNA-targeting red-emitting CDs by solvothermal method [85]. After dehydration and carbonization process, quinoline molecules construct stable conjugated carbon cores of CDs, which inherit the groove structure of quinoline. The combination of the single-stranded nucleic acids RNA with the grooves of CDs induces the aggregation of CDs, leading to the fluorescence quenching of CDs (Fig. 5(e)). Lu et al. prepared a new type of CDs by using 4,7-dibromo-2,1,3-benzothiadiazole, and 2-aminoquinoline as the precursors, and the obtained CDs have been proved to have a flexible molecule (N4, N7-di(quinolin-2-yl) benzo[c] [1,2,5] thiadiazole-4,7-diamine), consisting of a planar conjugated benzothiadiazole (BTD) unit as the chromophore and two aminoquinoline (4AQ) terminal units [86]. At thermodynamic equilibrium, the large quinoline groups force the entire molecule into a planar conformation. Conversely, the molecule can maintain a non-coplanar conformation, with an increased dihedral angle between the terminal quinolines and the BTD core (Fig. 5(f)). They inferred that the non-coplanar conformation and associated spatial constraints trigger dynamic self-assembly. During the preparation of CDs, functional groups or carbon skeletons of the precursor molecules may be retained on the surface or within the interior of the CDs. Additionally, carbon bonds typically form five- or six-membered aromatic rings that extend into the sp^2 carbon network of the CDs. As a result, non-covalent π–π interactions can exist between individual layers, which are the primary driving force behind molecular self-assembly [86].

Phenanthrene is another frequently utilized PAHs that consists of three fused benzene rings. Similarly, phenanthroline and its derivatives are simple PAHs formed by the fusion of one benzene ring and two pyridinium heterocyclic rings, which not only have large conjugated structures, but also have good coordination ability with metal ions. Among them, 1,10-phenanthroline is the classic analytical reagent for colorimetric determination of Fe^{2+}. Thus 1,10-phenanthroline has been frequently employed as the

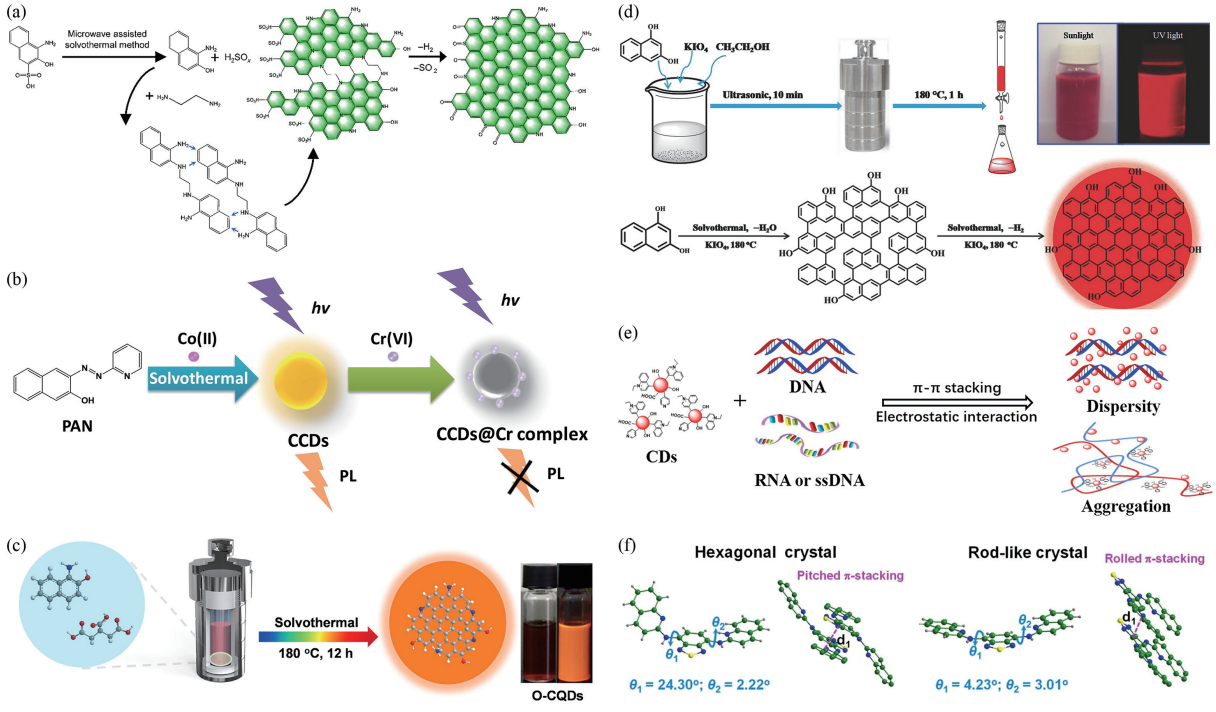

Figure 5 (a) The possible autocatalytic reaction mechanism of CDs based ASNA. Reproduced with permission from Ref. [76], © Elsevier B.V. 2022. (b) The CDs obtained from PAN. Reproduced with permission from Ref. [78], © Elsevier B.V. 2016. (c) The orange emissive CDs prepared from 1-amino-2-naphthol hydrochloride and CA. Reproduced with permission from Ref. [79], © American Chemical Society 2022. (d) The preparation and growth mechanism of red emissive CDs. Reproduced with permission from Ref. [80], © WILEY-VCH Verlag GmbH & Co. KGaA, Weinheim 2017. (e) The binding mechanism of CDs with nucleic acids. Reproduced with permission from Ref. [85], © Elsevier B.V. 2021. (f) Molecular structure, torsion angles, and intermolecular stacking of hexagonal crystal and rod-like crystal. Reproduced with permission from Ref. [86], © Wiley-VCH GmbH 2022.

carbon source to synthesize CDs that have fluorescence response to iron ions [87, 88]. For example, through a one-step solid-state synthesis method, Iqbal et al. prepared blue-emitting CDs (B-CDs) by using CA and 1,10-phenanthroline as the precursors (Fig. 6(a)) [89]. The B-CDs inherited the strong metal chelation ability of 1,10-phenanthroline, which can form non-fluorescent products with Fe^{3+} and Fe^{2+}, quenches the fluorescence of B-CDs. These quenching-type CDs respond to both Fe^{2+} and Fe^{3+}, however, they cannot distinguish between Fe^{3+} and Fe^{2+}. Recently, our group prepared a new type of CDs with hydrothermal treatment of 5-amino-1,10-phenanthroline and salicylic acid, the resultant blue colored CDs exhibit colorimetric and fluorometric dual-mode responses to Fe^{2+} and Fe^{3+} (Fig. 6(b)) [90]. Through the optimization of parameters such as reaction time, temperature, and precursor ratio, the obtained CDs effectively retain the structure of phenanthroline moieties. It was found that Fe^{2+} can specifically bind to the pyridinic N on the surface of the CDs, which induced the aggregation of CDs and form a large conjugated configuration with substantially enhanced fluorescence. Meanwhile, Fe^{3+} can oxidize the CDs, leading to the decrease of fluorescence intensity (Fig. 6(c)). Interestingly, when this solution was allowed to stand for ca. 20 min, the fluorescence could be recovered due to the increased formation of Fe^{2+}. When the same precursors 5-amino-1,10-phenanthroline and salicylic acid with slightly different ratio were subjected to direct calcination, an orange-red fluorescent CDs (OR-CDs) were obtained [91]. The as-prepared OR-CDs not only retained the chelating functional groups, but also have specific-sized cavity that is capable of selectively embedding Cd^{2+}. Our experimental characterizations and density functional theory (DFT) calculations revealed that the OR-CDs are composed of nine aromatic ring basic units with their spacing perfectly match the radius of Cd^{2+}. Thus, the OR-CDs exhibited aggregation-induced emission enhancement (AIEE) in the presence of Cd^{2+} (Fig. 6(d)).

Perylene is another commonly encountered PAHs that has a large conjugated structure. When perylene and HNO_3 were refluxed together, 3,4,9,10-tetranitroperylene was obtained, where $-NO_2$ group underwent nucleophilic substitution and more C=O functional groups were generated under the solvothermal conditions [92]. Consequently, red emissive CDs with an emission center at 610 nm are obtained through a sequence of dehydration, carbonization, and polymerization reactions (Fig. 6(e)). Recently, Qu et al. also reported a new type of CDs by solvothermal treatment of perylene tetracarboxylic dianhydride (PTCDA) and urea (Fig. 6(f)) [93]. Under DMF solvothermal conditions, PTCAD and urea undergo fusion to form large π-conjugated structure, and as-prepared CDs solution exhibit unprecedented near-infrared absorption band at 720 nm and emission band at 745 nm [93]. DFT study revealed that the trimeric product of PTCDA and urea is the luminescent unit of the CDs. Therefore, the fusion of large conjugated benzenoid derivatives has enabled the expansion of conjugation and achieved narrow bandgap near-infrared emission of CDs. The surface of CDs could be further modified with polyethyleneimine (PEI) after solvothermal treatment, which prevents the interaction of water molecules with their conjugated carbon cores, leading to enhanced near-infrared emission in aqueous solution.

It is worth noting that not all organic compounds containing multiple benzene rings can be used to produce CDs with long-wavelength emission. TA is a polyphenolic compound composed of ten pyrogallol (1,2,3-trihydroxybenzene) units and one glucose molecule. After microwave assisted hydrolyzing TA in ammonia solution, Anappara et al. obtained a kind of UV-emitting CDs. They suggested that TA is a complex ester of pyrogallol and glucose, which undergoes hydrolysis to yield glucose and gallic acid derivatives in alkaline condition. When the hydrolysis products were subjected to microwave-assisted treatment, the clusters of sp^2-bonded graphite were formed [94]. By using TA as the sole carbon source, Huang et al. produced a kind of blue emissive CDs via a hydrothermal method. The CDs exhibit a

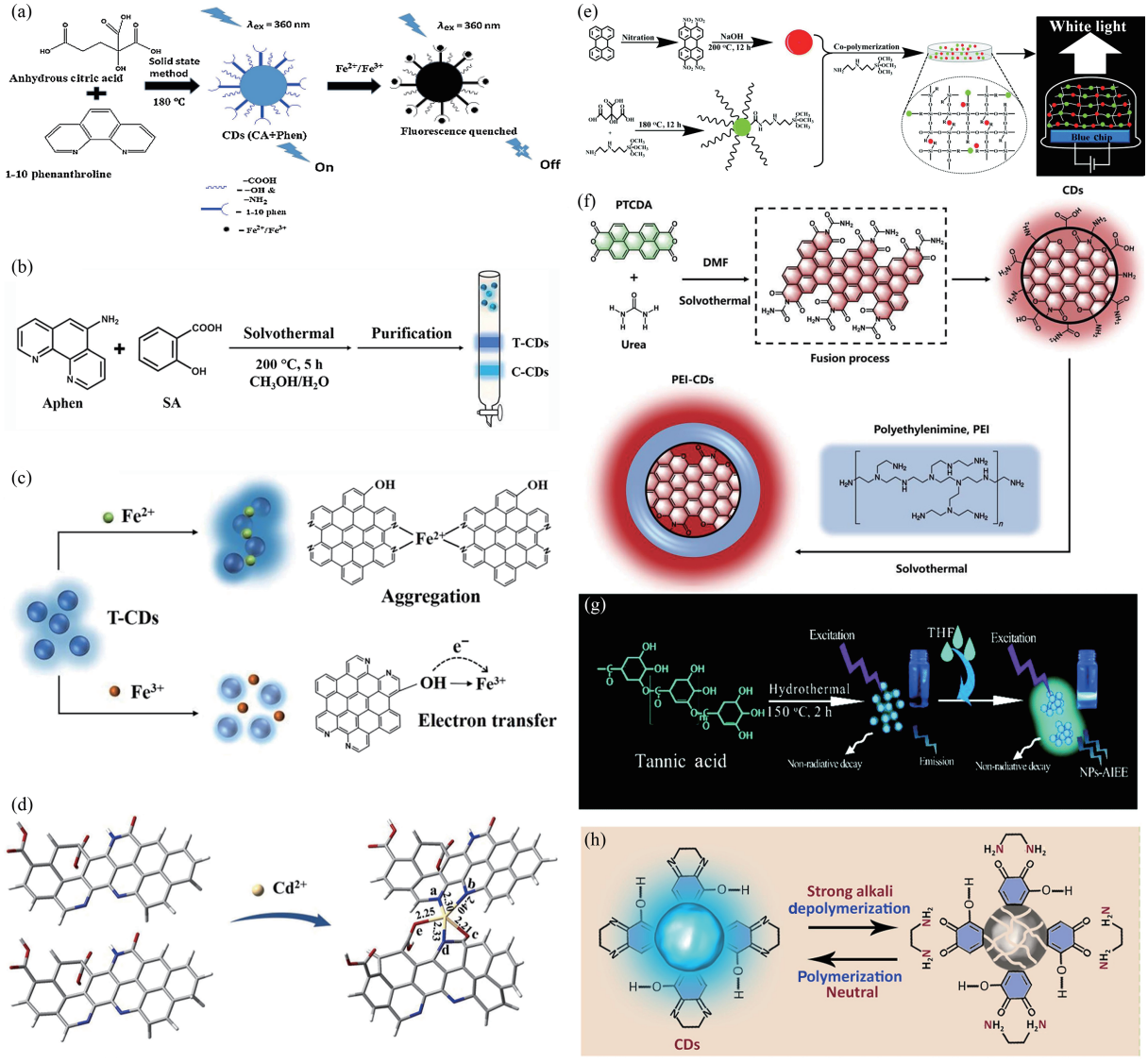

Figure 6 (a) The formation of CDs, and the quenching off CDs by Fe^{2+} and Fe^{3+}. Reproduced with permission from Ref. [89], © Elsevier B.V. 2016. (b) The CDs obtained from 5-amino-1,10-phenanthroline and salicylic acid. (c) The recognition mechanism of CDs for Fe^{2+} and Fe^{3+}. Reproduced with permission from Ref. [90], © Jiang, T. et al., under exclusive licence to The Japan Society for Analytical Chemistry 2022. (d) The formation of the Cd-OR-CDs aggregate. Reproduced with permission from Ref. [91], © Elsevier B.V. 2021. (e) and (f) The formation of CDs based perylene. Reproduced with permission from Ref. [92], © The Royal Society of Chemistry 2018. Reproduced with permission from Ref. [93], © Liu, Y. P. et al., Advanced Science published by Wiley-VCH GmbH 2022. (g) and (h) The CDs obtained from TA. Reproduced with permission from Ref. [95], © The Royal Society of Chemistry 2016. Reproduced with permission from Ref. [96], © Elsevier Inc. 2022.

maximum PL emission center at 455 nm when excited by 350 nm incident light (Fig. 6(g)) [95]. Similarly, Elsayed Hafez et al. also synthesized a blue-emitting CDs by one-pot Schiff base reaction using TA and EDA precursors (Fig. 6(h)) [96]. They believe that the precursor molecules are cross-linked via imine bonds to form the CDs. By controlling the pH of the solution, the imine bonds could be further manipulated to break or re-bond, achieving photo-switchable cycling based on the reversible aggregation reaction. Liu et al. reported a kind of stable blue fluorescent CDs via solvent-free calcination method using the TA as the precursor [97]. They found that the synthesis temperature had a significant impact on the QY and surface properties of the CDs. At a reaction temperature of 300 °C, the CDs underwent a high degree of graphitization, resulting in a high C=C/C–C ratio and the highest QY of 35.4% in comparison with the CDs obtained from other temperatures. The surface of the CDs was rich in oxygen-containing functional groups, which facilitated selective coordination with Ni^{2+}. Therefore, CDs synthesized at this temperature were found to be suitable for use as a fluorescent Ni^{2+} sensor [97]. Although different synthesis methods were used, the resulting CDs could only exhibit short-wavelength light emission, which suggests that CDs prepared from TA have a relatively small conjugated structure [98]. This could be due to the fact that TA itself has a small conjugated configuration, and during the formation of CDs, the TA structure with glucose as the central unit is disrupted, rather than being polymerized to form a larger conjugated structure. Since TA has the polyphenolic structure, the CDs prepared from it still inherit good reducibility. Kawasaki et al. obtained a type of blue emitting nitrogen doped CDs (N-CDs) by using TA and polyethyleneimine. It was found that the N-CDs have unique ability to directly reduce chloroauric acid and form gold nanoparticles without requiring any additional reducing agents or stabilizers [99]. The retention of abundant phenolic hydroxyl groups in CDs is believed to be responsible for their reducibility.

Although PAHs precursors contain large numbers of aromatic rings, not all of them are suitable for the synthesis of CDs with long-wavelength emission. Precursors with multiple aromatic rings that are not in the same plane tend to form CDs that emit blue or green light. When PAHs with larger conjugated systems

are used as the carbon sources, the resultant CDs usually exhibit higher stability and red or near-infrared emission.

2.4 CDs obtained from organic dyes

Photodynamic therapy (PDT) has emerged as a highly selective and non-invasive cancer treatment, offering several advantages over traditional therapies [100]. PDT relies on the use of photosensitizers, which generate singlet oxygen ($^1O_2$) or other ROS upon light irradiation at the tumor site. These ROS selectively destroy cancer cells by disrupting biomolecules. One of the major benefits of PDT is its minimal invasiveness and low drug toxicity, which make it a highly attractive option for treating various types of cancers. Additionally, PDT offers high selectivity, broad application range, and minimal side effects [101, 102]. It is widely acknowledged that the success of PDT largely depends on the choice of photosensitizer [103]. In this regard, a variety of organic dyes as photosensitizers have been investigated and developed for PDT applications. Among them, phthalocyanine compounds, porphyrin compounds, phenothiazine compounds, chlorin e6, and methylene blue are commonly used and have shown promising results in preclinical and clinical studies. The inherent characteristics of CDs make them suitable candidate for PDT, which have garnered significant interest in cancer therapy and other biomedical applications. The versatile physicochemical properties of CDs, including their size, shape, surface chemistry, and fluorescence, can be modulated to optimize their photodynamic efficacy and selectivity.

In 2012, Huang et al. first demonstrated the photodynamic cytotoxicity of CDs as a PDT agent against cancer cells [104]. However, their strategy involved the modification of the photosensitizer chlorin e6 on the surface of CDs, whereby the therapeutic effect is predominantly attributed to the chlorin e6 molecule, and the CDs only serve as a delivery vehicle. Although this approach has been demonstrated to improve the efficacy of PDT, it still fails to address the inherent issue of photo-bleaching [105]. Further research is needed to overcome this challenge, to fully harness the potential of CDs as an effective platform for photodynamic therapy. Thus, the preparation of CDs directly from organic dyes was investigated, aiming to produce CDs that possess favorable optical properties, biocompatibility, resistance to photobleaching, and high yield of singlet oxygen. A hydrophobic cyanine dye was used as photosensitive molecules to make PDT active CDs (Fig. 7(a)) [106]. After modification with poly (ethylene glycol) (PEG 800), a hydration layer was formed on the surface of CDs. Thus, the water solubility of CDs was increased, making them more readily available in aqueous systems. The

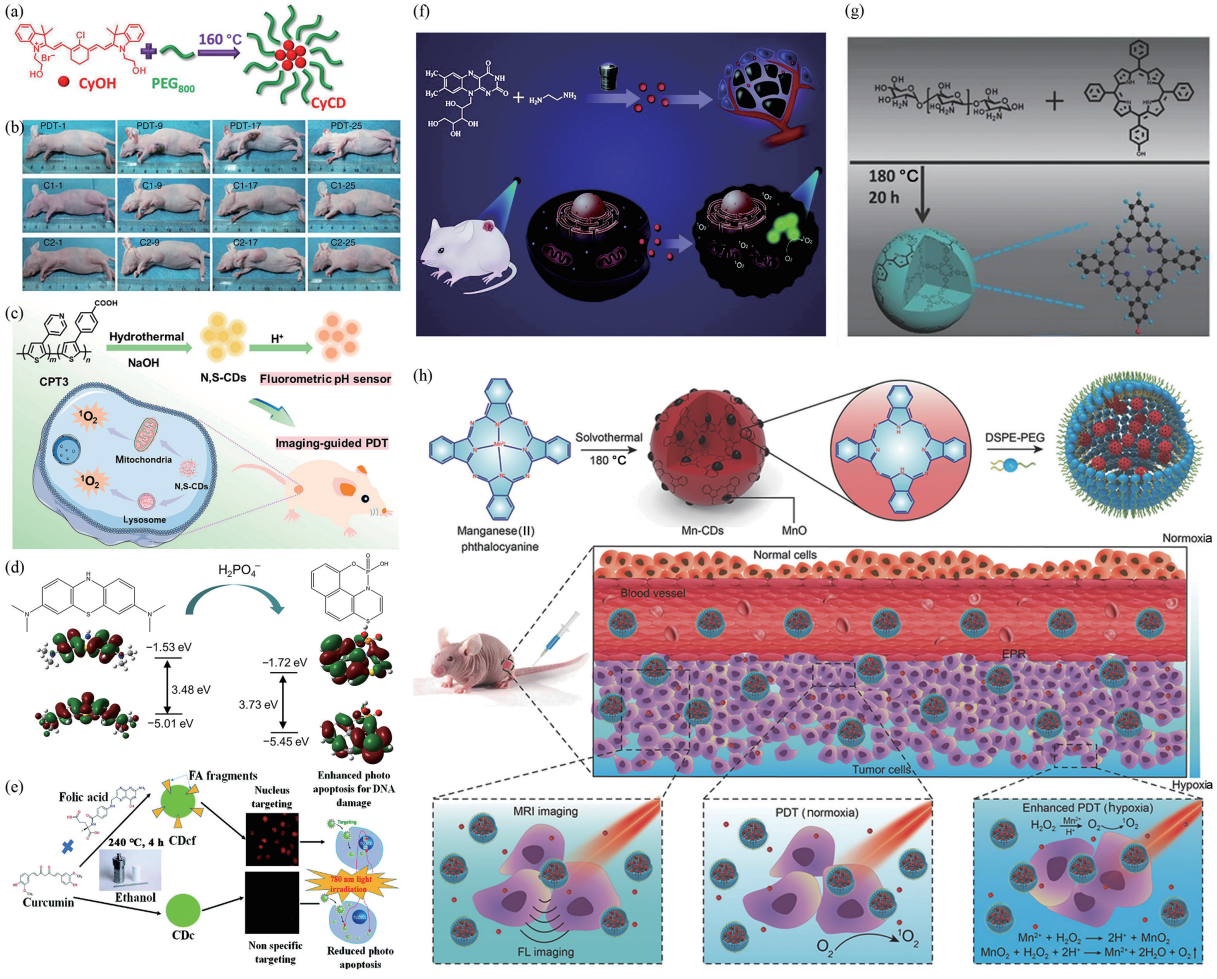

Figure 7 (a) The CDs prepared with cyanine dye. Reproduced with permission from Ref. [106], © American Chemical Society 2016. (b) Photographs of mice after various treatments on the 1st, 9th, 17th, and 25th day. (PDT: CDs light irradiation; C1: GQDs only; and C2: light irradiation only). Reproduced with permission from Ref. [107], © Macmillan Publishers Limited 2014. (c) Preparing N,S-CDs, and its application in imaging-guided PDT. Reproduced with permission from Ref. [108], © American Chemical Society 2021. (d) The CDs obtained from methylene blue. Reproduced with permission from Ref. [11], © American Chemical Society 2021. (e) The formation of CDs based on photosensitizer riboflavin. Reproduced with permission from Ref. [109], © The Royal Society of Chemistry 2020. (f) The riboflavin-based CDs with high singlet oxygen generation for photodynamic therapy. Reproduced with permission from Ref. [110], © The Royal Society of Chemistry 2021. (g) Synthetic route of TPP CDs. Reproduced with permission from Ref. [111], © WILEY-VCH Verlag GmbH & Co. KGaA, Weinheim 2016. (h) The Mn-CDs assembly as an acidic H_2O_2-driven oxygenerator to enhance the anticancer efficiency of PDT in a solid tumor. Reproduced with permission from Ref. [102], © WILEY-VCH Verlag GmbH & Co. KGaA, Weinheim 2018.

obtained CDs show a strong absorption and NIR emission within the range from 600 to 900 nm. Under light irradiation with an 808 nm NIR laser at a power of 2.0 W/cm^2, the CDs can effectively inhibit tumor growth [106]. In 2014, Ge et al. have successfully synthesized red emissive CDs via hydrothermal method, using polythiophene as the precursor [107]. It is noteworthy that the $^1O_2$ generation capability of the prepared CDs surpasses that of other PDT reagents by up to 1.3 times. Owing to their outstanding $^1O_2$ generation properties, this kind of CDs have demonstrated promising efficacy for PDT *in vitro* and *in vivo*. Under irradiation with white light (400–800 nm, 80 mW·cm^{-2}), the dimension of mice tumor in CDs treatment group exhibited a remarkable decrease (Fig. 7(b)). Lan and colleagues have developed a facile hydrothermal method for preparing N,S-doped CDs (N,S-CDs) derived from polythiophene derivate (Fig. 7(c)) [108]. The resultant N,S-CDs exhibit pH-sensitive fluorescence characteristics, enabling them to distinguish between tumor cells and normal cells. Upon exposure to light, the N,S-CDs generate $^1O_2$ to induce cell death to cancer cells. Moreover, the N,S-CDs can accumulate in lysosomes and mitochondria, generating intracellular $^1O_2$. These subcellular-targeted CDs can effectively enhance the efficacy of PDT. Our group also developed red fluorescent CDs with PDT activity by using methylene blue as the sole carbon source and phosphate as an assisting agent (Fig. 7(d)) [11]. The active therapeutic molecule methylene blue can be integrated into the sp^2 carbon framework of the red fluorescent CDs while maintaining high $^1O_2$ yield of the precursor molecule. Furthermore, the incorporation of phosphate groups into the CDs prevents them from binding to DNA phosphate groups and thereby overcomes the issue of methylene blue mediated DNA damage. These features enable the obtained CDs to function as an effective agent for PDT without causing harmful side effects. Gomes et al. have developed cancer cell-targeting CDs using curcumin and folic acid as precursors (Fig. 7(e)) [109]. The CDs were found to interact with cancer cells through folate receptor-mediated pathways, and demonstrated clear nuclear localization. The generation of intracellular $^1O_2$ was enhanced with the increase of irradiation time, ultimately improved the PDT efficacy. Similarly, green-emitting CDs were synthesized using organic dyes riboflavin, a naturally occurring vitamin, and the CDs also exhibited a higher capacity to produce $^1O_2$ than riboflavin itself (Fig. 7(f)) [110]. CDs based on porphyrin were synthesized using mono-hydroxylphenyl triphenylporphyrin (TPP) and chitosan (Fig. 7(g)). These TPP CDs possess the unique ability to generate cytotoxic $^1O_2$ and exhibit good water solubility [111]. In the study, mice with tumors were exposed to 625 nm spotlight at a power intensity of 60 mW·cm^2 for 1 h. After 13 days, it was observed that the TPP CDs treatment group exhibited smaller tumor volumes compared to the control group. These findings validate the therapeutic efficacy of TPP CDs *in vivo*, demonstrating their ability to efficiently suppress the growth of solid tumors. Although PDT using CDs has shown promise as a potential treatment for cancer, the hypoxic conditions within tumor microenvironments and rapid oxygen consumption during PDT can significantly hinder the effectiveness of this approach, which relies on the presence of oxygen. Addressing these challenges is crucial for improving the therapeutic potential of CDs in PDT for cancer treatment. Using Mn(II) phthalocyanine as the carbon source, Jia et al. have developed a novel Mn doped CDs (Mn-CDs), which enables the generation O_2 *in situ* for PDT (Fig. 7(h)) [102]. The Mn(II) in Mn-CDs can catalyze the production of O_2 from H_2O_2 in cancer cells, allowing Mn-CDs to generate O_2 even in low-oxygen environments. When exposed to light, Mn-CDs continuously react with self-supplied O_2 to generate $^1O_2$, thereby enhancing the effectiveness of PDT. As a result, photosensitive molecules can be used directly as carbon sources and fused into the sp^2 framework of CDs during the process of dehydration carbonization, forming CDs with photosensitive activity. This approach can not only preserve the ability of photosensitive molecules to produce $^1O_2$, but also improve their photostability.

Therefore, it is reasonable to select photosensitizers as precursors for the preparation of photoactive CDs. Embedding the active unit of the photosensitizer into the conjugated structure of CDs can not only improve the photostability and biocompatibility of the photosensitizer but also enhances the effectiveness of PDT.

2.5 CDs obtained from biomass

Compared to other precursors, biomass carbon sources are an environmentally friendly natural product, which has the advantages of low cost, easily accessible, green, nontoxic, and renewable in the preparation of CDs [112]. In addition, biomass contains rich heteroatoms of nitrogen, oxygen, phosphorus, or sulfur owing to the existence of carbohydrate, protein, lipid, and glutathione. Converting biomass into value-added CDs can not only achieves the rational waste usage, but also conforms to the sustainable development strategy of green energy [113]. In the recent years, a wide range of biomass materials have been employed as carbon sources for the synthesis of CDs. The biomass used includes apple [114], banana [115], durian [116, 117], rice husk [118], cucumber [119], starch [120], highland barley [121], egg [122], ginkgo leaves [123, 124], purslane leaves [125], lichi leaves [126], rose [127], scallions [128], fish scales [129], honey [130], and milk [131]. The CDs derived from biomass have found various applications such as biological imaging, drug delivery, sensors, and catalysis [132, 133].

Sachdev et al. prepared CDs with uniform sizes by hydrothermal treatment of coriander leaves as carbon source at 240 °C for 4 h (Fig. 8(a)) [134]. The resulting CDs show a maximum emission wavelength at 400 nm with a quantum yield of 6.48% when the excitation wavelength was 350 nm. With the increase of excitation wavelength, there was an observable red shift in the emission wavelength of CDs, and the emission intensity gradually decreased. The fluorescence of the CDs can be effectively quenched by Fe^{3+}, due to the exceptional coordination between Fe^{3+} and hydroxyl groups on the surface of the CDs [134]. Eggshells, egg whites, and egg yolks have been used as carbon sources to synthesize CDs [135–137]. Wu et al. successfully obtained nitrogen-doped CDs with an average size of 2.1 nm by hydrothermal treatment of egg white at 220 °C for 48 h (Fig. 8(b)) [138]. They found that egg white is hydrolyzed into small molecular weight peptides and amino acids in the initial stage of the hydrothermal treatment. Subsequently, the amino acids partially polymerize and carbonize into a carbon core, which could be enveloped by large numbers of oligomers. When the carbon core surrounded by oligomers grows larger, the outer layer of oligomers decreases or disappears. Finally, nitrogen-doped CDs with abundant hydroxyl and carboxyl groups are obtained [138]. By varying the excitation wavelength in the range of 290 to 450 nm, there is also a noticeable red shift in the emission peak from 415 to 540 nm, accompanied by a rapid decrease in intensity. When magnolia flower was hydrothermally treated at 200 °C for 8 h, blue emissive CDs were produced (Fig. 8(c)), and their fluorescence can be quenched by Fe^{3+} [139]. Further study revealed that the strong interaction between Fe^{3+} and the –OH, –NH_2, and –COOH on the CDs surface induced the aggregation of CDs. Shuang et al. fabricated a bright blue fluorescent N-CDs using astragalus as precursor (Fig. 8(d)) [140]. The fluorescence of N-CDs also can be quenched by Fe^{3+}. As the average lifetime of N-CDs is the same as that of N-CDs-Fe^{3+}, they attributed the selective response to the static quenching, resulting from the formation of a

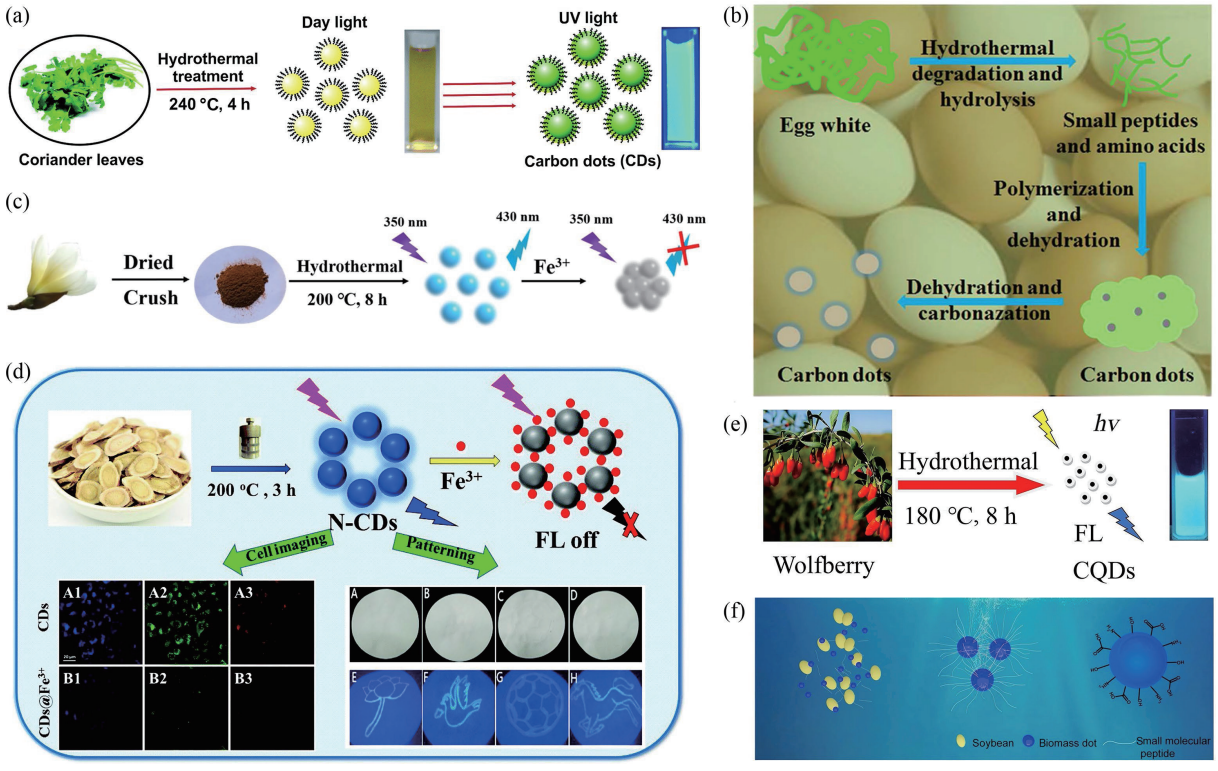

Figure 8 (a) One-step synthesis of CDs from coriander leaves. Reproduced with permission from Ref. [134], © The Royal Society of Chemistry 2015. (b) The formation process of the CDs based on egg white. Reproduced with permission from Ref. [138], © American Chemical Society 2015. (c) The synthesis of biomass CDs from magnolia flower by hydrothermal treatment and the mechanism of Fe^{3+} detection. Reproduced with permission from Ref. [139], © Elsevier Ltd. 2019. (d) The CDs obtained from astragalus. Reproduced with permission from Ref. [140], © The Royal Society of Chemistry 2020. (e) The hydrothermal synthesis of N-CDs from wolfberry. Reproduced with permission from Ref. [141], © Elsevier Ltd. 2021. (f) The preparation process of the CDs from soybeans by ultrasonic method. Reproduced with permission from Ref. [142], © Zhao, W. B. et al. 2019.

non-fluorescent complex between N-CDs and Fe^{3+}. Wolfberry contains polysaccharides, sugars, betaine, various amino acids, and carotenoids, thus N-CDs was also obtained from hydrothermal treatment of wolfberry (Fig. 8(e)) [141]. Gu et al. found that this N-CDs can reduce Fe^{3+} to Fe^{2+}, as evidenced by the appearance of red color in the presence of o-phenanthroline. The surface defects on N-CDs were formed during the reduction of Fe^{3+}, which causes the failure of the electron transition from the excited state to the ground state, thus the fluorescence quenching occurs for the N-CDs. Zhao et al. reported a kind of blue fluorescent CDs, which was prepared from soybeans using ultrasonic method (Fig. 8(f)) [142]. The resultant CDs also show sensitive fluorescence response to Fe^{3+} in a quenching mode. They reasoned that the redox potential of Fe^{3+}/Fe^{2+} couple ($E°$ = 0.77) is located between the LUMO and HOMO energy levels of the CDs, which induces photo-induced electron transfer from the LUMO energy level to the complex states of Fe^{3+}. Table 2 summarizes the CDs produced from various biomasses that exhibit the capability for Fe^{3+} detection. It is worth noting that these CDs mainly show blue fluorescence and have an excitation-dependent behavior. The excitation-dependent emissions of CDs are commonly attributed to the inhomogeneity of CDs, including in size distributions and the surface states. Natural biomasses usually consist of many carbohydrate and amino acid moieties, hence the synthesized CDs could have different functional groups on their surface, such as –OH, $–NH_2$, and –COOH groups. The fluorescence responses of the CDs to Fe^{3+} can be primarily classified into two mechanisms: static quenching and electron transfer [10]. Static quenching mechanism refers the formation of non-fluorescent complex between CDs and Fe^{3+}, resulting in a decrease in the fluorescence intensity of CDs. Meanwhile, the outer electron structure of Fe^{3+} has a half-filled $3d^5$ orbitals, which are prone to be filled by the excited state electrons from the CDs via the coordination interaction, resulting in nonradiative electron/hole recombination. Above mentioned studies have thoroughly revealed the responsive mechanisms of biomass CDs to Fe^{3+}, however, it is still not clear why these CDs exhibit special selectivity for Fe^{3+}, which obviously deserves further investigations in the future.

The preservation of some distinct functionalities from biomasses precursors have also extended to the synthesis of CDs with antimicrobial and antioxidant properties. The CDs synthesized from natural antimicrobial plants may have excellent biocompatibility while retaining the antimicrobial ability of the parent plants. For example, Sun et al. used natural antibacterial plant garlic as raw materials and synthesized nitrogen-sulfur co-doped antibacterial CDs using a simple one-step hydrothermal method (Fig. 9(a)) [143]. The obtained CDs possess a graphite lattice structure with positive charge, hence these CDs are capable of adsorbing onto the surface of negatively charged bacteria. This electrostatic interaction can disturb the normal function of the bacterial cell membrane, resulting in membrane damage and the excessive accumulation of ROS. Furthermore, once the small-sized CDs particles enter the bacterial cell, they suppress the activity of bacterial antioxidant enzymes, exacerbating oxidative stress and ultimately leading to bacterial death. Tea polyphenols are the most significant components of tea, which include catechins, epicatechins, flavonoids, and theaflavins. Several types of polyphenols such as anthocyanins, resveratrol, and flavonoids are the effective components found in grapes that possess strong antioxidant properties. Similarly, flavonoids and organic acids in date and clementine peel exhibit potent antioxidant and anti-inflammatory activities. In this regard, the effective components of these four plants have antioxidant properties and can scavenge free radicals and protect cells from oxidative damage. It is interesting to note that the CDs derived from these biomasses inherit the antioxidant property [144]. Murru et al. and Šafranko

Table 2 CDs prepared from different biomass carbon sources and their application in Fe^{3+} detection

Carbon source	Method	Range	LOD	Mechanism	References
Coriander leaves	Hydrothermal	0–6 μM	0.4 μM	Static quenching	[134]
Egg white	Hydrothermal	50–250 μM	—	—	[138]
Magnolia flower	Hydrothermal	0.2–1 μM	0.088 μM	Static quenching	[139]
Astragalus	Hydrothermal	50–250 μM	42 nM	Static quenching	[140]
Wolfberry	Hydrothermal	0–100 μM	3.0 μM	Electron transfer	[141]
Soybean	Ultrasonic	0–30 μM	2.9 μM	Electron transfer	[142]
Citrus clementina	Hydrothermal	7–50 μM	4.57 μM	—	[146]
Cherry blossom	Hydrothermal	0–0.6 mM	—	Static quenching	[217]
Hemps	Hydrothermal	0–60 μM	0.47 μM	Static quenching	[218]
Chicken cartilage	Hydrothermal	2–500 μM	0.47 μM	Static quenching	[219]
Chrysanthemum	Hydrothermal	0–100 μM	5.4 μM	Static quenching	[220]
Honey	Hydrothermal	0.005–100 μM	1.7 nM	Static quenching	[221]
Momordica charantia	Hydrothermal	0–150 μM	0.175 μM	Static quenching	[222]
Lychee	Hydrothermal	0–22 μM	23.6 nM	Static quenching	[223]
Spirulina algae	Hydrothermal	0.05–1 μM	14.8 nM	Static quenching	[224]
Green bean	Hydrothermal	10–70 μM	3.6 nM	Static quenching	[225]
Cranberry beans	Hydrothermal	30–600 μM	9.55 μM	Static quenching	[226]
Miscanthus	Hydrothermal	0.02–2000 μM	20 nM	Static quenching	[227]
Green pepper	Hydrothermal	1–500 μM	0.1 μM	Static quenching	[228]
Mopan persimmons	Hydrothermal	0–100 μM	0.324 μM	Static quenching	[229]
Water hyacinth	Hydrothermal	0–330 μM	0.77 μM	Static quenching	[230]
Pine needles	Hydrothermal	0.1–540 μM	0.02 μM	Static quenching	[231]
Banana peel	Hydrothermal	5–25 μM	0.66 μM	Static quenching	[232]
Pomelo peel	Hydrothermal	0.1–160 μM	0.086 μM	Static quenching	[233]
Pork rib bones	Hydrothermal	0.15–5 μM	0.064 μM	Static quenching	[234]
Tar	Hydrothermal	0.06–1400 μM	60 nM	Static quenching	[235]
Tar	Calcination	0–100 μM	0.22 μM	Static quenching	[236]
Cellulose and lignin	Pyrolysis	0–400 μM	19.1 nM	Static quenching	[237]
Poa pratensis	Hydrothermal	5.0–25 μM	1.4 μM	Electron transfer	[238]
Red pitaya	Hydrothermal	2–40 nM	1.2 nM	Electron transfer	[239]
Coffee beans	Hydrothermal	0–0.10 mM	15.4 nM	Electron transfer	[240]
Coffee grounds	Hydrothermal	0–50 μM	9 nM	Electron transfer	[241]
Prunus leaves	Hydrothermal	0–250 μM	1.60 μM	Electron transfer	[242]
Cassava stem	Hydrothermal	15.6–62.5 μM	0.91 μM	Electron transfer	[243]
Corn cob	Hydrothermal	0.78–3.9 μM	0.8550 μM	Electron transfer	[244]
Lignin	Hydrothermal	0–300 μM	0.77 μM	Electron transfer	[245]
Milk	Hydrothermal	0.1–20 μM	0.6 μM	Electron transfer	[246]
Crop	Hydrothermal	0–500 μM	5.23 μM	Electron transfer	[247]
Wintersweet flowers	Hydrothermal	0.05–100 μM	0.15 μM	Electron transfer	[248]
Siberian elm seeds	Hydrothermal	0–500 μM	3.18 μM	Electron transfer	[249]
Borassus flabellifer	Calcination	0–30 nM	10 nM	Electron transfer	[250]

et al. fabricated CDs from tea, grapes, and clementine peel with a hydrothermal method [145, 146]. Using date as carbon source, Dhara et al. prepared CDs by microwave irradiation method [147]. The antioxidant activities of CDs have been explored by 2,2-diphenyl-1-picrylhydrazyl (DPPH) and Folin-Ciocelteau assays in aqueous media. Compared with standard antioxidant compounds such as AA and vitamin E, the CDs obtained from tea, grapes, clementine peel, or date showed substantially improved antioxidant properties [145, 147]. *Artemisia argyi* is herbaceous perennial plant commonly found in China, which has been traditionally used as a herb-medicine to prevent conditions such as plague, inflammatory diseases, and cancer. The active ingredients of *A. argyi* leaves are mainly volatile oil and bitter glycosides. The volatile oil contains a variety of compounds such as citronellol, camphor, and pinene, which have strong antimicrobial, insecticidal, analgesic, and anti-inflammatory

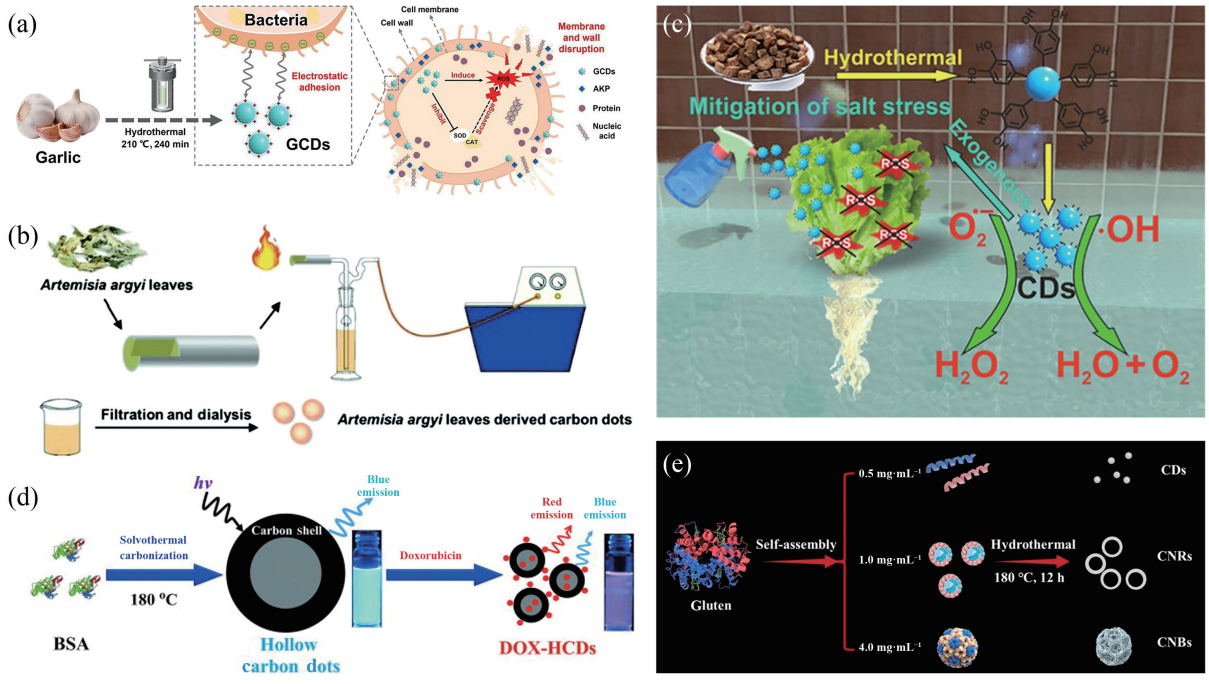

Figure 9 (a) The CDs prepared from natural antibacterial plant garlic. Reproduced with permission from Ref. [143], © Elsevier B.V. 2023. (b) Synthesis process diagram of CDs with *A. argyi* leaves. Reproduced with permission from Ref. [148], © The Royal Society of Chemistry 2020. (c) The mechanism of CDs alleviating the oxidative damage of Italian lettuce under salt stress. Reproduced with permission from Ref. [152], © American Chemical Society 2020. (d) The synthesis of luminescent HCDs. Reproduced with permission from Ref. [213], © Elsevier Ltd. 2013. (e) Formation of CDs, CNRs, and CNBs. Reproduced with permission from Ref. [158], © American Chemical Society 2022.

effects. The bitter glycosides are the main source of bitterness in *A. argyi* leaves and have various physiological effects, such as anti-inflammatory, antibacterial, analgesic, hypotensive, and immune regulatory activities. Kang et al. synthesized CDs with *A. argyi* leaves through a smoking simulation method (Fig. 9(b)) [148]. The resultant CDs have demonstrated superior antibacterial activity on the Gram-negative bacteria. They concluded that the CDs inhibit approximately 50% of the enzyme activity that is related to bacterial wall synthesis, resulting in bacterial death. *Salvia miltiorrhiza* is a plant of the *Salvia genus*. It is commonly used in traditional Chinese medicine [149]. Many studies have shown that salvianic acid and its analogues are the main active ingredients of *S. miltiorrhiza*, which have strong antioxidant properties [149–151]. Lei et al. synthesized blue emissive CDs by using *S. miltiorrhiza* as the precursor (Fig. 9(c)). After hydrothermal treatment of *S. miltiorrhiza*, many miltiorrhiza-like polymers are formed on the surface of CDs, endowing the CDs with high antioxidant capacity. Analysis revealed that these CDs possessed multiple enzyme activities, which can effectively scavenge DPPH·, $\cdot O_2^-$, and ·OH, exhibiting stronger antioxidant activity than that of the pure *S. miltiorrhiza* extract [152]. Moreover, spraying CDs on the leaves of Italian lettuce seedlings can effectively alleviate oxidative damage caused by salt stress.

In general, small molecule carbon sources can be readily carbonized into zero-dimensional CDs, but it is difficult to prepare morphology-controllable carbon nanomaterials using these carbon sources [153]. In contrast, natural protein molecules, possess inherent biocompatibility and can self-assemble into unique structures via hydrogen bonding, electrostatic interactions, or hydrophobic interactions. Despite this potential, the studies by utilizing proteins as the precursors and employing peptide assembly to direct nanoparticle synthesis are still relatively rare [154]. Bovine serum albumin (BSA) is a single-chain globular protein widely present in bovine serum, consisting of 583 amino acid residues with a molecular weight of approximately 66.5 kDa. BSA has high solubility and stability, and is extensively used in biological and biochemical research. BSA has a structure composed of α-helices and random coil structures, which play important roles in the function of proteins [155–157]. By utilizing the self-assembly characteristics of BSA, hollow luminescent CDs (HCDs) were prepared by Wang et al. using a simple solvothermal method (Fig. 9(d)) [213]. The as-prepared HCDs possess a diameter of approximately 6.8 nm with a pore size of ca. 2 nm. They inferred that BSA monomers tended to form uniform aggregates with a size of approximately 453 nm when initially dispersed in ethanol. After solvothermal treatment for 4 h, BSA was denatured and formed non-uniform aggregates with sizes ranging from approximately 10 to 80 nm. The size of the aggregates gradually decreased with the increase of reaction time, and these aggregates separated into carbon nanoparticles under extreme solvothermal conditions. At this time, carbonization was found only on the surface of small aggregates, and was not yet complete, potentially preventing the shell from sinking or breaking. After incubation for 12 h, the incompletely carbonized interior was carbonized, and the HCDs were produced. More recently, we used gluten from wheat as a carbon source to prepare three different types of carbon nanomaterials by using a template-free method (Fig. 9(e)) [158]. Specifically, we found that concentration-dependent self-assembly of gluten played an important role in the formation of carbon nanostructures. Three unique shaped carbon nanomaterials, namely, CDs, carbon nanorings (CNRs), and porous carbon nanospheres (CNBs) were obtained with this self-assembly approach. These three types of carbon nanomaterials were successfully used for cell imaging. In addition, due to the large surface area and low toxicity, CNRs can serve as an excellent drug carrier for chemotherapy. The formation of polymorphic carbon nanoparticles is mainly attributed to the unique structure of gluten, which can be divided into three parts, namely N-terminus, C-terminus, and a hydrophobic region in the middle. The N-terminus and C-terminus are composed of 81–104 and 42 amino acids, respectively, exhibiting strong hydrophilicity, while the central hydrophobic region of gliadin is composed of 440–680 hydrophobic amino acids. Therefore, gluten can self-assemble into

micelles in aqueous solution, with the hydrophobic segments forming the core and the hydrophilic parts forming the expanded corona.

Most biomass-derived CDs have the characteristic of emitting short-wavelength light with low QY. In recent years, researchers have made continuous efforts to regulate the emission wavelength of biomass-derived CDs and tried to improve corresponding QYs. Using spinach as the raw material, Wang et al. prepared four kinds of CDs in different solvents (water, ethanol, acetone or the mixture of ethanol, and acetone). The resultant CDs have blue, dark, gray-white, and red emission with QYs of 8.9%, 12.3%, 10.8%, and 14.4%, respectively [120]. It was found that the multicolor luminescence is mainly attributed to the changes in boiling point and polarity of the solvents, which alter the carbonization process of polysaccharides and chlorophyll in spinach, thereby modifying the particle size, surface functional groups, and luminescent properties of the spinach-derived CDs. Yang et al. prepared a type of deep red emissive CDs from taxus leaves by solvothermal method [121]. After column chromatographic purification, the CDs with a narrow full width at half maximum (FWHM) of 20 nm and a high QY of 59% were obtained (Fig. 10(a)). By using mulberry leaves as the precursor and solvothermal method, Xiong et al. fabricated CDs with strong near-infrared fluorescence, the absolute QY of the CDs reached up to 73%, and the maximum FWHM was 20 nm (Fig. 10(b)) [122]. Interestingly, when feeding silkworms with these CDs, the silkworms with bright red fluorescence still grew healthily, and spun cocoons normally. Qin et al. prepared CDs by ethanol-thermal treatment of camphor leaves, hellebore leaves, oleander leaves, clover leaves, and bamboo leaves, respectively (Fig. 10(c)) [197]. The obtained CDs showed identical red fluorescence emission, which is ascribed to the same fluorophore of chlorophyll.

3 Luminescence mechanism

Many different mechanisms have been proposed to elucidate the luminescence of CDs, such as quantum confinement effect, surface state, molecule state, conjugation effect, AIEE, and cross-linked enhanced emission (CEE) effect, etc. [8, 20, 159]. Up to now, the quantum confinement effect, surface state, and molecule state are widely accepted mechanisms. Herein, we primarily summarize the recent advances in these three mechanisms for the luminescence of CDs.

3.1 Quantum confinement effect

The quantum confinement effect (size effect) refers to the phenomenon observed in nanoscale materials, where the behavior

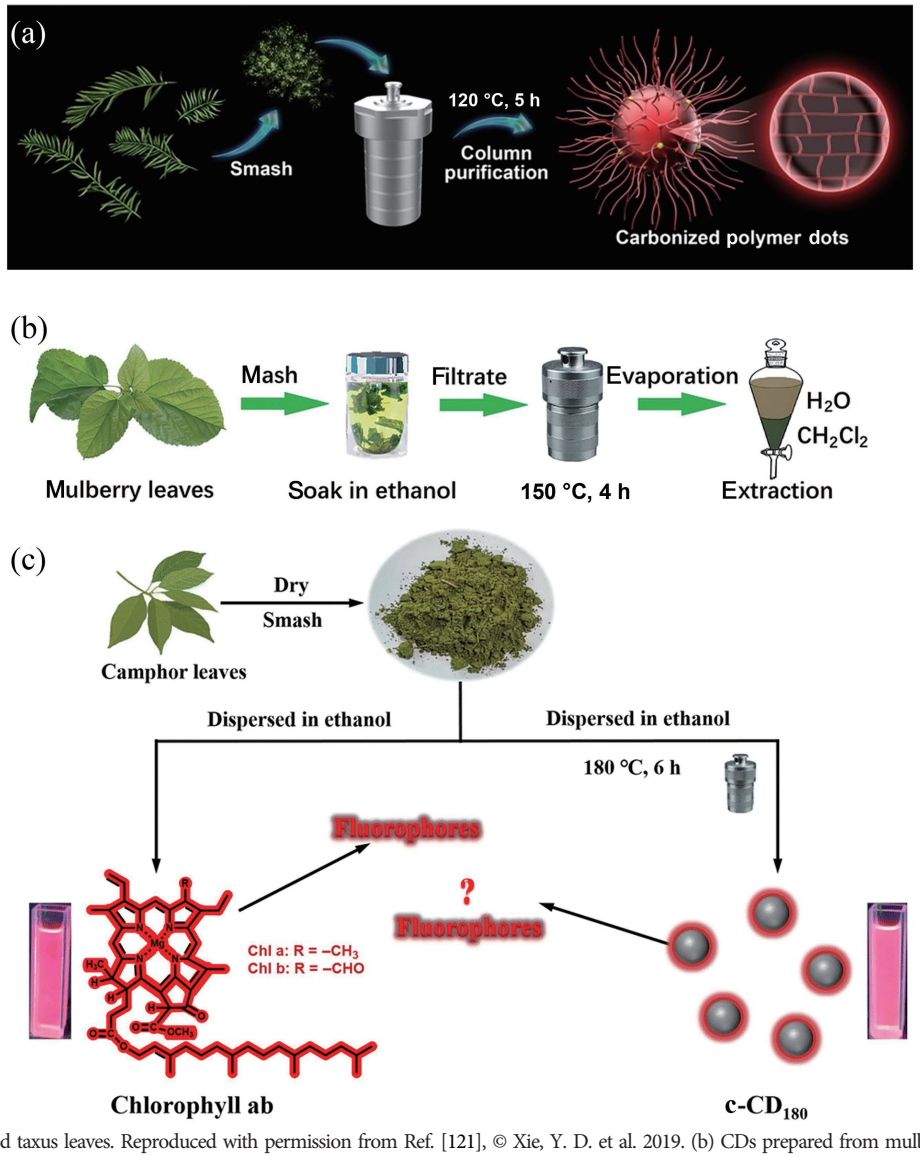

Figure 10 (a) CDs based taxus leaves. Reproduced with permission from Ref. [121], © Xie, Y. D. et al. 2019. (b) CDs prepared from mulberry leaves. Reproduced with permission from Ref. [122], © Wiley-VCH Verlag GmbH & Co. KGaA, Weinheim 2012. (c) CDs obtained from camphor, hellebore, oleander, clover, and bamboo leaves. Reproduced with permission from Ref. [197], © The Royal Society of Chemistry 2019.

of electrons and other charge carriers is influenced by their spatial confinement within a small volume [160]. The quantum confinement effect in CDs leads to changes in the band structure and energy levels. As the size of CDs decreases, their bandgap increases, resulting in a shift towards higher energy wavelengths in the emission spectra [18]. In 2014, Alam Sk et al. utilized theoretical calculation to simulate the influence of CDs sizes on the emission wavelength [161]. The results showed that as the sizes of CDs increased from 0.46 to 2.31 nm, the corresponding emission wavelength shifted from the blue region to the near-infrared region, which is attributed to the increased degree of π electron delocalization with size enlargement (Fig. 11(a)). Using CA and urea as precursors, three types of CDs with average diameters of 1.7, 2.8, and 4.5 nm were prepared by altering the reaction solvent during the preparation process [38]. It was observed that with the increase of the CDs sizes, the fluorescence shifted from blue to red color. In 2018, Fan et al. synthesized triangular CDs (T-CDs) by refluxing phloroglucinol in ethanol or sulfuric acid, the obtained CDs have nearly defect-free graphene crystal structure with uniform size distribution, high color purity, and narrow FWHM of only 29–30 nm [162]. They observed that as the size increased from 1.9 to 2.4, 3.0, and 3.9 nm, the emission peak of T-CDs gradually shifted from the blue emissive region to the green, yellow, and red emissive regions (Fig. 11(b)). Recently, Wang et al. also observed that CDs measuring approximately 1.2 nm emit UV light at around 350 nm, and the CDs ranging from 1.5 to 3 nm emit visible light within the range of 400 to 700 nm [163]. The bandgap energies of CDs gradually decrease from 2.76 to 1.88 eV with the increase of the sizes, which further confirms the relationship between quantum confinement effect and the fluorescence emission wavelength.

3.2 Surface state

The surface states, including the functional groups, defects, and traps on the surface of CDs, have a great influence on the optical properties of CDs [164]. These surface states usually could lead to increased non-radiative recombination, resulting in a decrease in the photoluminescence intensity. Also, the changes in surface states could alter the energy levels or the band structure of CDs, leading to shifts in the emission wavelength. Therefore, photoluminescence property of CDs can often be tuned by controlling and modifying the surface states of CDs. A comprehensive quantum chemical DFT study conducted by Kundelev et al. revealed that amino groups on the surface of CDs

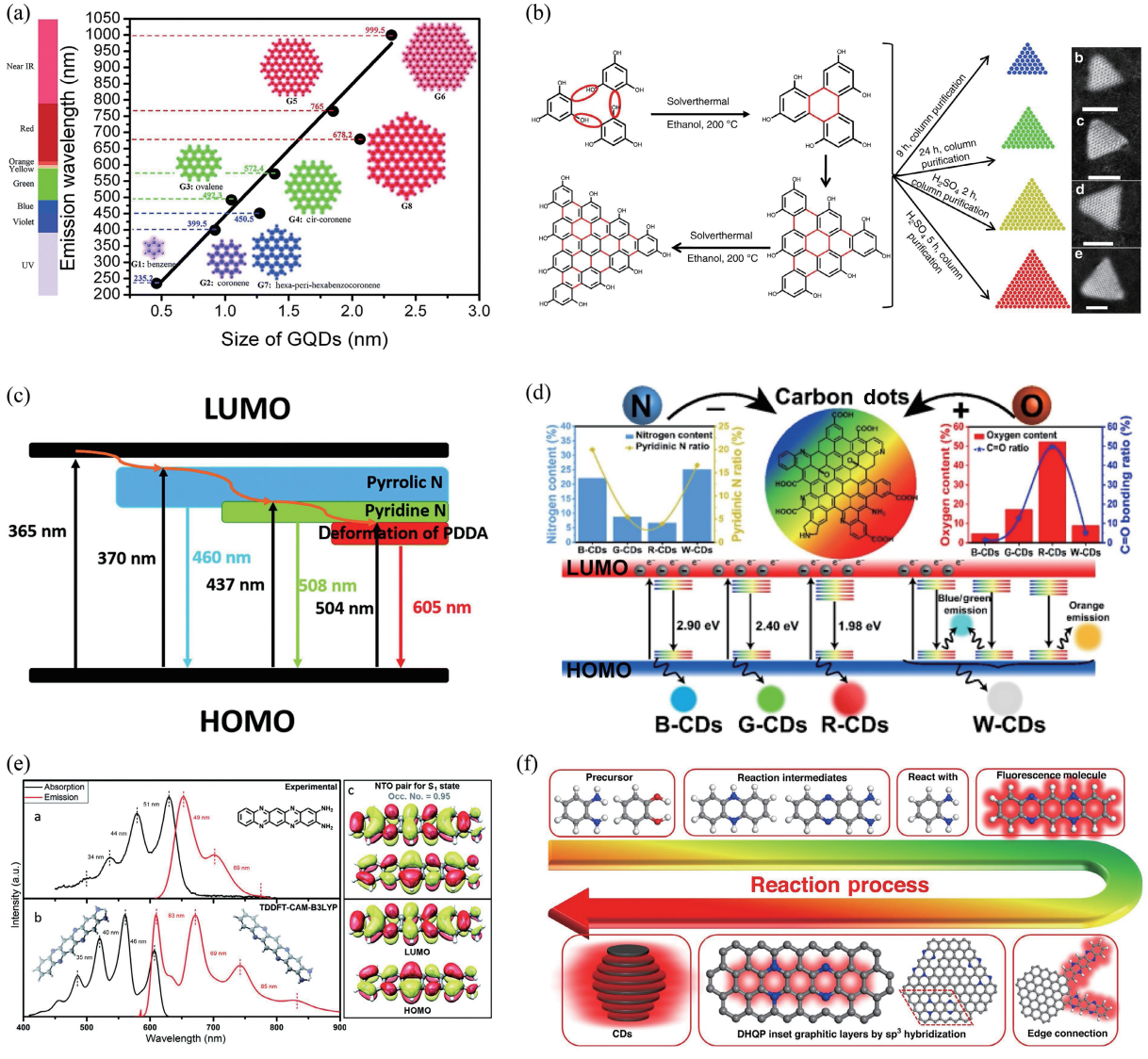

Figure 11 Luminescence origin of CDs ((a) and (b)) size effect. Reproduced with permission from Ref. [161], © The Royal Society of Chemistry 2014. Reproduced with permission from Ref. [162], © Yuan, F. L. et al. 2018. (c) and (d) Surface state. Reproduced with permission from Ref. [164], © Chinese Chemical Society and Institute of Materia Medica, Chinese Academy of Medical Sciences. Published by Elsevier B.V. 2021. Reproduced with permission from Ref. [165], © The Royal Society of Chemistry 2018. (e) and (f) Molecule state. Reproduced with permission from Ref. [5], © Li, P. F. et al. 2022. Reproduced with permission from Ref. [170], © Soni, N. et al. 2021.

can not only cause the redshift of emission wavelength, but also enhance the inherent high fluorescence intensity of CDs [32]. Using p-PDA and EDTA, polyethyleneimine or L-proline as raw materials, controllable emission of CDs was achieved with varied N-doping [165]. The TEM images show that these CDs are well-dispersed and possess similar nanoscale particle sizes. The presence of multiple emission states in CDs is associated with the nitrogen speciation on their surface, including pyridinic N, pyrrolic N, graphitic N, and amino N. The red emission is attributed to the formation of fluorophore resulting from the deformation of p-phenylenediamine, while the green emission state is governed by pyridinic N, and the blue emission is enhanced by pyrrolic N (Fig. 11(c)). Qu et al. found that the S=O/C=O groups present in dimethyl sulfoxide (DMSO)/DMF interact with the CDs, resulting in increased surface oxidation potential of the CDs, contributing to the enhancement of near-infrared absorption band and near-infrared fluorescence. Li et al. also demonstrated that the luminescence wavelength of the CDs redshifted as the ratio of oxygen- and nitrogen-related components increased [164]. These results tend to suggest that nitrogen substitution (pyridinic nitrogen/pyrrolic nitrogen) dominates the blue emission, while the introduction of oxygen functional groups lowers the LUMO energy level, resulting in the redshift of emission wavelength (Fig. 11(d)). In conclusion, the surface condition of CDs is not dictated by individual side chains or functional groups alone, instead, it is also influenced by the hybridization of the carbon skeleton with interconnected chemical groups. More complete carbonization could reduce the surface functional groups and side chains, thus the fluorescence emission becomes primarily governed by the size effect. Hence, the fluorescence of CDs can be finely tuned by manipulating both the inner core and surface functional groups.

3.3 Molecule state

In recent years, researchers discovered the presence of organic fluorescent chromophores in CDs, which dominate their fluorescence emission. Yang et al. synthesized blue-emitting CDs through a hydrothermal method using CA and EDA as precursors [166]. The presence of 5-oxo-1,2,3,5-tetrahydroimidazo[1,2-a] pyridine-7-carboxylic acid (IPCA) structure was identified in the mass spectrum. The optimal conformation was determined through Gauss simulation and the HOMO and LUMO energy levels were calculated to be 1.494 and 5.350 eV, respectively. The predicted absorbance and PL spectra closely match the experimental measurements, indicating that molecular fluorophore IPCA is the origin of the fluorescence emission in CDs. Subsequently, Chen et al. prepared a kind of N, S co-doped CDs using CA and cysteine as raw materials, and two organic fluorophores, i.e., 5-oxo-3,5-dihydro-2H-thiazolo [3,2-a] pyridine-3,7-dicarboxylic acid (TPDCA) and 5-oxo-3,5-dihydro-2H-thiazolo [3,2-a] pyridine-7-carboxylic acid (TPCA), were identified as the main fluorescence origins of the CDs [167]. Similarly, a kind of green emissive CDs was prepared by Kasprzyk et al. by microwave treatment of CA and urea, where it was found that the green emission of the CDs is derived from the molecular fluorophore 4-hydroxy-1H-pyrrolo[3,4-c] pyridine-1,3,6(2H,5H)-trione (HPPT) [168]. 2,3-Diaminophenazine (DAP) and 2-Amino-3-hydroxyphenazine (AHP) were found to be the dominant species in the yellow emissive CDs that were obtained from o-PDA precursor [169]. Through systematic purification and characterization, Soni et al. found that the red emissive CDs obtained from o-PDA contain the molecular structured quinoline [2,3-b] phenazine-2, 3-diamine (QXPDA), which was confirmed by nuclear magnetic resonance (NMR) and MS [170]. The fluorophore was further verified by the fact that QXPDA has the identical emission characteristics with that of CDs. Also, the excitation-independent behavior of QXPDA is very similar to that of the red emissive CDs (Fig. 11(e)). More recently, Sun et al. fabricated another kind of red emissive CDs from o-PDA and catechol [5]. The luminescence was attributed to the presence of molecular state fluorophores, i.e., 5,14-dihydroquinoxalino[2,3-b] phenazine (DHQP), which is either incorporated into graphene or connected with graphene edge by sp^3 hybridization (Fig. 11(f)). In conclusion, molecular fluorophores are generally formed through the dehydration and condensation reactions among small molecules in the polymerization process. As a result, CDs with molecule-state fluorescence often exhibit a polymer-like structure or a weakly crystallized structure. In comparison to the emission originating from the surface state or the size effect, the fluorescence governed by the molecule state is highly sensitive to the surrounding environment [21].

4 Applications

CDs inheriting the characteristics of their precursors have shown excellent optical performance and versatile surface functionalities, which endows the resultant CDs with wide applicability in diverse areas [171, 172]. In this section, we briefly summarize the applications of CDs derived from different precursors in the fields of sensing, bioimaging, light emitting devices (LED), and anti-counterfeiting.

4.1 Sensing

Compared to the small molecular fluorescent probes, CDs usually exhibit improved photostability and their fluorescence can be more sensitive to the surrounding environment due to the presence of abundant functional groups on the surface of CDs. Thus, CDs obtained from various precursors have been exploited for fluorescence sensing applications, including cationic ion detections (Ca^{2+}, Fe^{2+}, Fe^{3+}, Cu^{2+}, Ag^{+}, Pb^{2+}, Hg^{2+}, Cd^{2+} etc.) [91, 173–178], anion detections (F^{-}, ClO^{-}, NO_2^{-}, HPO_4^{2-}, MnO_4^{-}, I^{-} etc.) [174, 179–181] and biological molecules analysis (ascorbic acid, glutathione, cysteine, uric acid, glucose etc.) [47, 182–185]. Furthermore, there has been a growing development of CDs that are specifically designed for temperature sensing. In this respect, the CDs with "turn off" fluorescence responses have been initially reported as an effective temperature sensor (Fig. 12(a)) [186, 187]. The increase in thermal energy can lead to increased nonradiative decay, i.e., the energy absorbed by the CDs is dissipated as heat rather than light emission. Consequently, the fluorescence intensity decreases with the increase of temperature [188]. However, the heating-induced fluorescence "turn off" of CDs is susceptible to environmental interferences, which could lead to false temperature signals. Also, the decrease in fluorescence tends to have poor resolution in temperature sensing and imaging. To address these issues, our group has developed a series of "turn on" type temperature-sensitive CDs. Using CA and urea as precursors, a kind of Y-CDs was successfully prepared with a facile solvothermal method (Fig. 12(b)) [189]. It was found that the obtained Y-CDs exhibit a significant fluorescence enhancement with the increase of temperature, and show a good linearity in the range of 15–85 °C with a thermal sensitivity of 5.3%/°C and temperature resolution of 0.09 °C. Comprehensive characterizations revealed that the fluorescence intensity is reliant on intramolecular hydrogen bonds in the Y-CDs. Theoretical simulations also confirm that the partially breaking of the hydrogen bonds amplifies the electron cloud density within the conjugated system and stabilizes the coplanar arrangement of molecular chromophores in the Y-CDs (Fig. 12(c)) [189]. As a result, a distinct "turn-on" fluorescent response is observed in

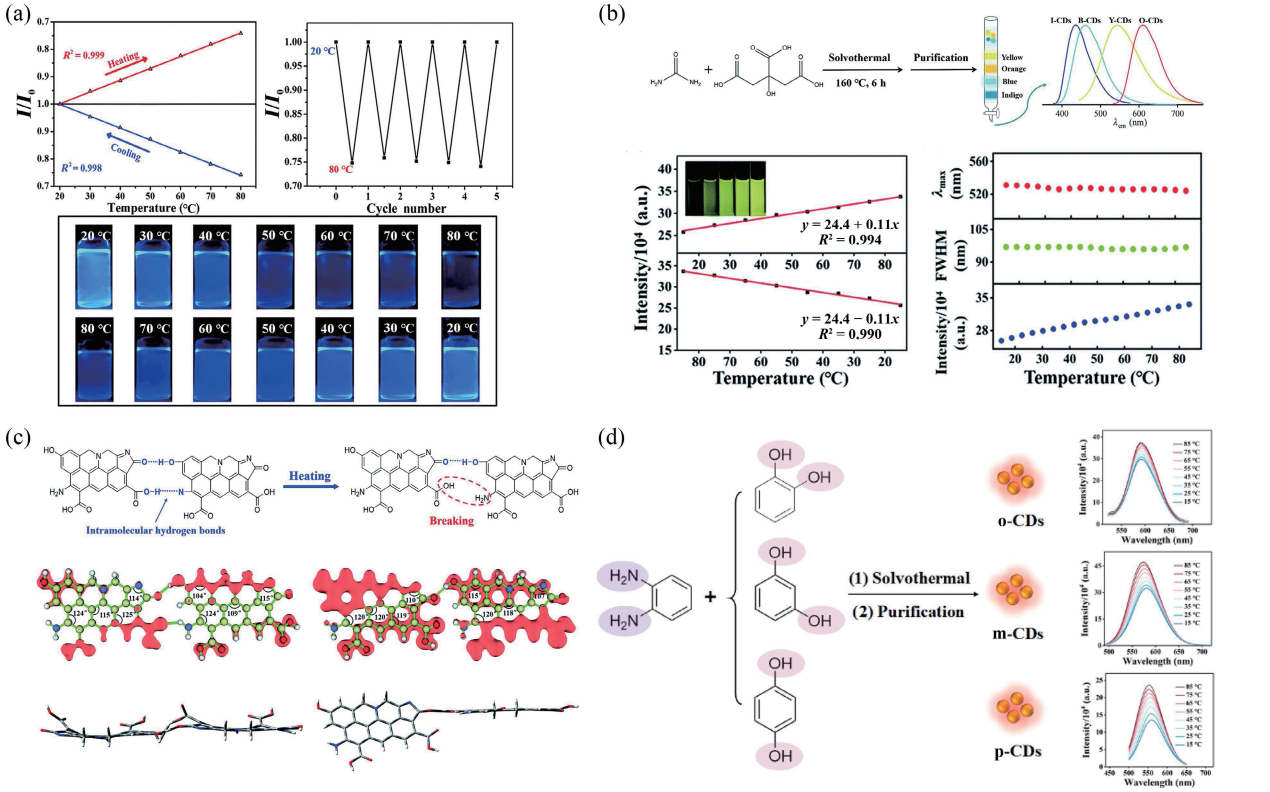

Figure 12 (a) "Turn off" type temperature-sensitive CDs. Reproduced with permission from Ref. [187], © The Royal Society of Chemistry 2017. (b) "Turn on" type temperature-sensitive Y-CDs, and (c) The effects of intermolecular hydrogen bond on the structure of Y-CDs. Reproduced with permission from Ref. [189], © The Royal Society of Chemistry 2022. (d) The CDs obtained from o-PDA and three isomers of dihydroxybenzene. Reproduced with permission from Ref. [190], © Elsevier Inc. 2022.

response to temperature increment. Based on the influence of intramolecular hydrogen bonding on the thermosensitivity of CDs, we subsequently prepared more "turn-on" type CDs with varied thermosensitivities by utilizing o-PDA and three isomers of dihydroxybenzene as carbon sources (Fig. 12(d)) [190]. Through comprehensive experimental characterizations and theoretical calculations, it was revealed that even slight variations in the positions of substituents on the phenyl ring of the precursors can have a significant impact on the formation of intramolecular hydrogen bonds. In general, the CDs with strong intramolecular hydrogen bonds tended to have low thermosensitivities.

4.2 Imaging

With the rapid development of synthetic methods and precursor selections, many CDs with outstanding photoluminescence property have been prepared, and they also exhibit other unique advantages, including adjustable emission wavelength, controllable sizes, low cytotoxicity, and good photostability, which make them an ideal candidate for fluorescence imaging applications. For example, a kind of photoluminescent CDs with a quantum yield of 30.2% was obtained by microwave-assisted pyrolysis of CA [191]. These CDs exhibit an excitation-dependent characteristics. When they were incubated with the L929 cells, blue, green, and red fluorescence were observed, respectively, under the excitation at wavelengths of 405, 488, and 543 nm (Fig. 13(a)). However, the CDs are evenly distributed throughout the cell, which limited their ability to distinguish the different organelles. Recently, researchers have designed the CDs that can target specific organelles. For example, lipophilic cationic probes can be employed for targeting mitochondria within living cells, because mitochondria usually possess high negative transmembrane potential (up to 180–200 mV) [192]. As a naturally occurring lipophilic cationic dye, rhodamine exhibits a strong attraction towards mitochondria. Inspired by this, Wang et al. utilized a reverse design strategy, synthesized a mitochondria-targeting CDs that have rhodamine fluorescent center by microwave-assisted treatment of CA and m-aminophenol (Fig. 13(b)) [193]. Wei and colleagues prepared a kind of orange emissive CDs (O-CDs) using L-cysteine and neutral red as precursors, which can target the Golgi apparatus (Fig. 13(c)) [194]. Golgi apparatus contains L-cysteine receptors, which could form disulfide bonds with the L-cysteine residues on the O-CDs. Furthermore, a kind of dual-emissive CDs was synthesized by Chen et al. using hydrophobic lysine and electrophilic o-PDA. Lysine, as the hydrophobic component, contributed to the hydrophobicity of the CDs, while o-PDA imparts electrophilicity to the CDs. This design enabled the CDs responsive to changes in the polarity of the ER (Fig. 13(d)) [195]. Leblanc et al. fabricated a kind of cationic CDs using 1,2,4,5-benzenetetramine as raw material, which can interact electrostatically with negatively charged DNA within cell nucleus, achieving targeted imaging of the cell nucleus (Fig. 13(e)) [196]. Using CA and N,N-dimethylaniline as the precursors, the CDs targeting to intracellular lysosomes have also been reported [197]. Compared to the commercial lysosomal probe (LysoTracker Deep Red), the resulting CDs have stronger photobleaching resistance and can stably label HeLa cells for more than 48 h (Fig. 13(f)). All these results have demonstrated that the CDs with specific functions could be facilely prepared by selecting the appropriate precursors, achieving imaging of targeted organelles for cellular labeling.

4.3 LEDs

As a new type of photoluminescene materials, solid-state luminescent CDs can be used as phosphor layer in optoelectronic devices. By coating CDs on LED chips with different emission wavelengths, colorful LED devices could be fabricated. To avoid the aggregation-induced emission quenching of CDs, Qu et al. immobilized the CDs in a silicon dioxide network, which can

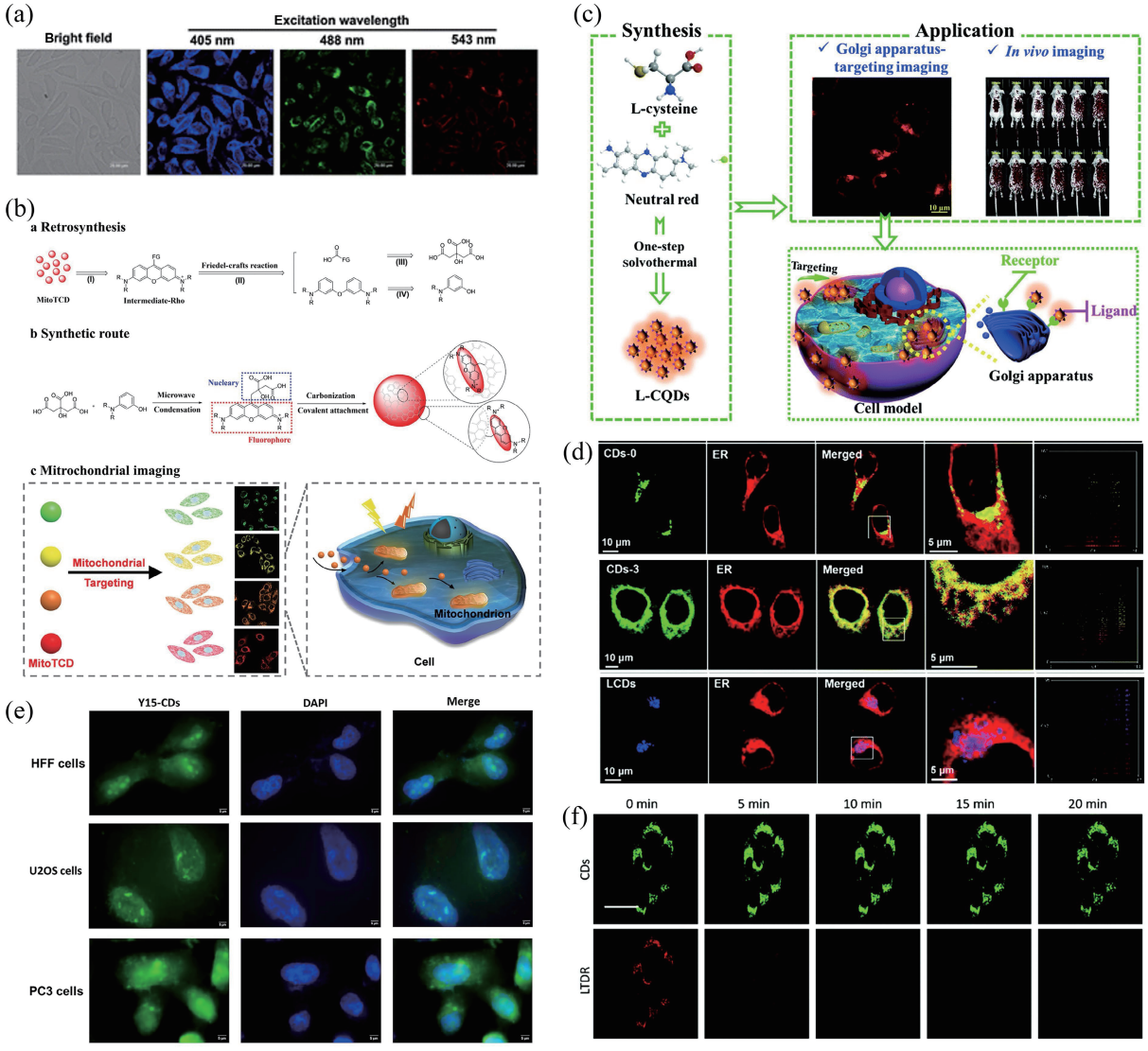

Figure 13 (a) Images of CDs labeled L929 cells with different excitation wavelength. Reproduced with permission from Ref. [191], © The Royal Society of Chemistry 2012. (b) Mitochondrial targeted CDs. Reproduced with permission from Ref. [193], © WILEY-VCH Verlag GmbH & Co. KGaA, Weinheim 2019. (c) Golgi targeting CDs. Reproduced with permission from Ref. [194], © The Royal Society of Chemistry 2022. (d) EA targeting CDs. Reproduced with permission from Ref. [195], © The Royal Society of Chemistry 2020. (e) Nuclear targeted CDs. Reproduced with permission from Ref. [196], © Elsevier Inc. 2023. (f) Lysosome targeting CDs. Reproduced with permission from Ref. [197], © The Royal Society of Chemistry 2019.

effectively prevent the aggregation of CDs. The resulting CDs composite exhibited a high fluorescence quantum yield of 30%–40%. By appropriately mixing red, green, and blue emissive CDs powder, white luminescent phosphors with Commission Internationale de L'Eclairage (CIE) coordinates of (0.34, 0.31) were obtained, which is very close to the CIE coordinates (0.33, 0.33) of natural white light standards (Fig. 14(a)) [38]. The fluorescence quenching of CDs could also be prevented by mixing CDs with starch. Hu et al. reported that LED obtained from orange emissive CDs/starch has promising warm white light characteristics, including a CIE of (0.41, 0.37) (Fig. 14(b)), a low correlated color temperature (CCT) of 3265 K, and an improved color rendering index (CRI) of 90. These values satisfy the standard requirements for indoor illumination, where a CCT below 4000 K and a CRI greater than 80 are desired [198]. Similarly, Shen et al. fabricated green, yellow, and orange LEDs by incorporating CDs into a polyethylene pyrrolidone (PVP) matrix (Fig. 14(c)) [199]. Three types of matrices, namely polymethyl methacrylate (PMMA), melamine-formaldehyde resin (MF), and epoxy resin A and B (ERG), are also used as solid dispersants for fabricating LED. Peng et al. constructed three warm white light WLED systems with high color rendering index by dispersing yellow, green, and red light-emitting CDs in these three matrices (Fig. 14(d)) [200]. To avoid the π–π stacking induced quenching to the powder emission, Wang et al. introduced organic semiconductors, polymer semiconductors PVK, and poly(9,9-dioctylfluorene-co-N-(4-(3-methylpropyl)) diphenylamine) (TFB), as host materials to prevent direct contact among the CDs (Fig. 14(e)) [201]. These CDs-LEDs exhibited excellent performance, with maximum luminance reaching 1414–4917 cd·m^{-2} and external quantum efficiencies ranging from 0.08% to 0.87%.

4.4 Anti-counterfeiting

In the so-called information age, information forgery and product counterfeiting become a great concern in product manufactory and public safety. Therefore, it is urgently needed to develop effective coding strategies and anti-counterfeiting technologies to make genuine items difficult to replicate and replace. Owing to the versatile optical property, low cost, and low toxicity, CDs have become increasingly popular as materials for a new generation of secure anti-counterfeiting inks [202]. The fluorescent or phosphorescent properties exhibited by CDs are unique and difficult to replicate, hence labelling products with CDs could provide a reliable means for the verification of product

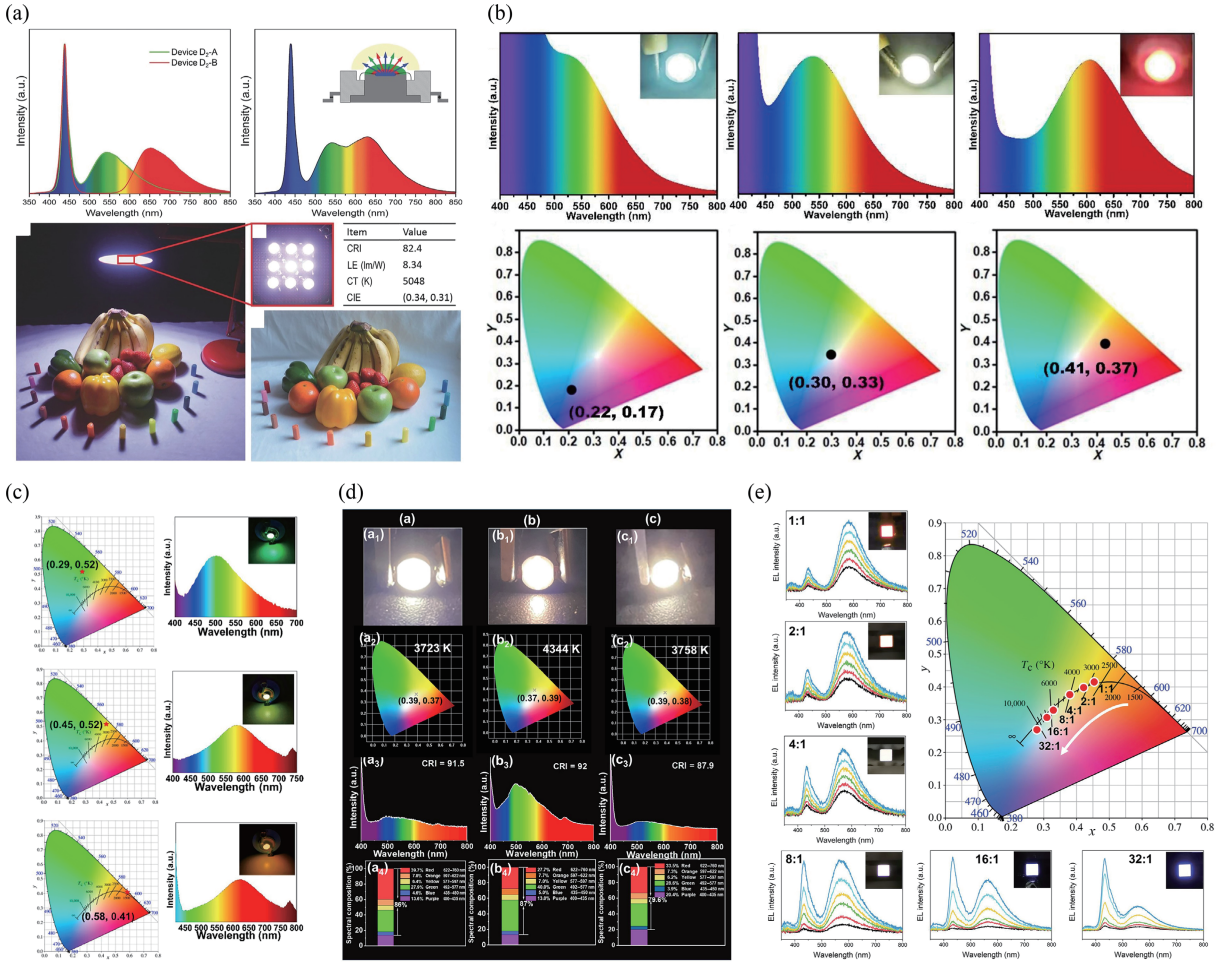

Figure 14 (a) The CDs dispersed in silicon dioxide for LEDs. Reproduced with permission from Ref. [38], © WILEY-VCH Verlag GmbH & Co. KGaA, Weinheim 2017. (b) CDs mixed in starch for LEDs. Reproduced with permission from Ref. [198], © Elsevier B.V. 2021. (c) CDs@PVP for LEDs. Reproduced with permission from Ref. [199], © American Chemical Society 2023. (d) CDs@PMMA, CDs@MF, and CDs@ERG for LEDs. Reproduced with permission from Ref. [200], © American Chemical Society 2022. (e) CDs dispersed in TFB for LED. Reproduced with permission from Ref. [201], © Wiley-VCH GmbH 2021.

authenticity. For example, Shen et al. reported such a label with CDs ink printed patterns, which can achieve information encryption under sunlight and information decryption under ultraviolet light [203]. As shown in Fig. 15(a), the printed patterns exhibit bright yellow-green fluorescence under ultraviolet light and completely disappear once the excitation is turned off. Our group has also developed a thermalsensitive label by mixing temperature-sensitive CDs with rhodamine B (RhB) to form a cartridge ink. Under UV light, the printed patterns exhibited significantly different fluorescence at different temperatures (Fig. 15(b)) [204]. Meanwhile, multiple information encryption can be achieved by using CDs with phosphorescent properties. Yang et al. prepared the CDs with blue and green phosphorescence, with which colorful patterns were observable under 365 nm UV irradiation (Fig. 15(c)) [205]. Once the excitation is turned off, only the encrypted patterns with CDs can be seen, and the afterglow can last for several seconds. In this aspect, we have prepared a kind of CDs with long phosphorescent lifetime and excitation-dependent phosphorescence using the molten salt method [206]. The CDs, C_3N_4, or their mixture were used for the preparation of the ink. Under 365 nm excitation, the emblem pattern, and letters "A, B, C, and D" can be seen, exhibiting different fluorescence colors. Once the light was turned off, the emblem circular pattern encoded with C_3N_4 powder and letters "A" and "C" became invisible, while the encoded emblem pattern with CDs and C_3N_4 mixture displayed a green color, along with letters "B" and "D". After removing the 395 nm excitation light source, the color of the emblem pattern and letters "B" and "D" turned yellow (Fig. 15(d)). All these results demonstrated that the unusual color changes generated by the excitation dependent phosphorescence can provide multiple security for anti-counterfeiting and information protection systems.

4.5 Other fields

In addition to above applications, multifunctional CDs have also been applied in other relevant fields. For example, CDs have been integrated into energy storage devices like supercapacitors and batteries to enhance the charge storage capacity, cycling stability, and rate capability of these devices [9]. Some CDs exhibit high catalytic efficiency, hence they were used as catalysts in many redox reactions and photocatalysis [207]. The CDs with large surface area and hierarchical structures have been explored as carriers for drug delivery systems [208]. Their small size, biocompatibility, and ability to penetrate cellular membranes make them suitable for targeted drug delivery and controlled release. Some CDs can remove contaminants like heavy metals and organic pollutants from water sources, hence they were successfully applied in water purification and environmental remediation processes [209]. By incorporation of CDs into polymers, textiles, and coatings, they can act as flame retardant additives by releasing non-flammable gases upon exposure to heat or flame [210]. Furthermore, CDs can be applied as foliar sprays or incorporated into the soil to improve nutrient uptake, photosynthesis, and overall plant growth [211]. CDs are also utilized for crop protection against pests and diseases [212]. They can be formulated into nanopesticides or used as part of

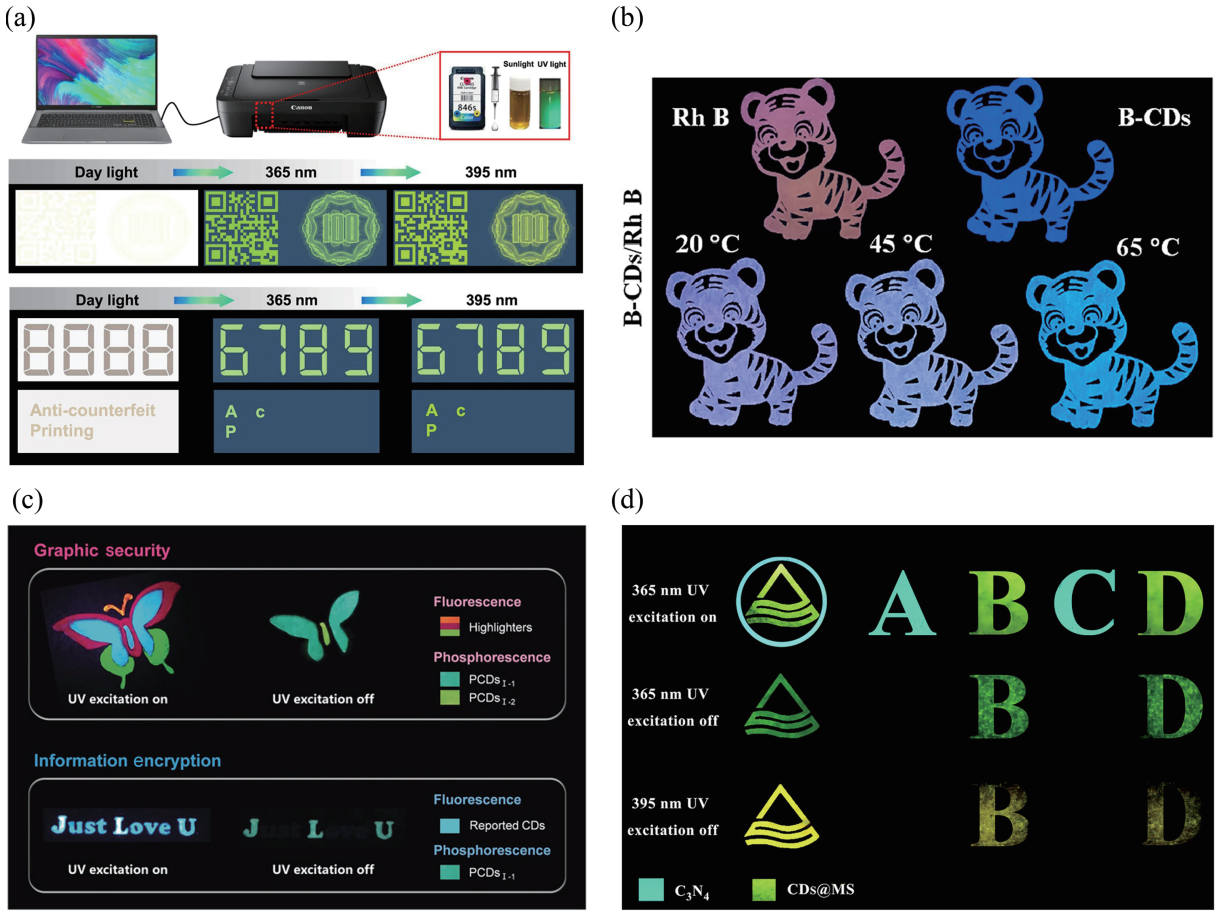

Figure 15 (a) Application of fluorescent CDs in information encryption. Reproduced with permission from Ref. [203], © American Chemical Society 2021. (b) Temperature-sensitive CDs are used for anti-counterfeiting. Reproduced with permission from Ref. [204], © Elsevier B.V. on behalf of Chinese Chemical Society and Institute of Materia Medica, Chinese Academy of Medical Sciences 2023. (c) and (d) Multiple anti-counterfeiting of phosphorescent CDs. Reproduced with permission from Ref. [205], © Wiley-VCH Verlag GmbH & Co. KGaA, Weinheim 2018. Reproduced with permission from Ref. [206], © The Royal Society of Chemistry 2019.

biocontrol strategies to inhibit the growth of pathogens and pests, reducing the need for traditional chemical pesticides. In brief, the application fields of CDs have expanded rapidly in the last few years. It is foreseeable that with the fast development of high-quality CDs, such an expansion will be continued in the future.

5 Summary and challenge

In summary, this paper reviews the recent advances in preparing fluorescent CDs using different types of precursors, focusing on the formation process and applications.

The properties exhibited by multifunctional CDs are not arbitrary, their optical characteristics are intimately related to the precursor molecules. The small molecule precursors undergo dehydration and condensation to form the emissive center of fluorescent CDs, while aromatic precursors are more likely to form large conjugated structures during carbonization, resulting in CDs with long emission wavelengths. The CDs obtained from precursors such as aniline or phenol exhibit excellent antioxidant properties due to the good reducibility of these carbon source, and can be used for scavenging ROS. CDs with pH-sensitive response are derived from the inheritance of amino or carboxyl groups of their precursors. This inheritance leads to changes in the fluorescence wavelength and intensity of CDs during the protonation or deprotonation processes. The CDs prepared by PAHs not only has good optical properties, but also inherits the metal chelating ability of their precursor, realizing the specific detection of metal ions. The CDs prepared by using organic dyes as carbon sources not only retain their photosensitizing properties but also improve their optical stability, enhancing the effectiveness of PDT. The CDs obtained from natural biomass as a carbon source have been successfully used for the detection of Fe^{3+}. Additionally, CDs obtained from biomass with pharmacological properties can retain their drug activity and exhibited a great potential in anti-inflammatory and antibacterial applications. By using the biomass with self-assembly capabilities as a carbon source, the morphologies of the resultant carbon nanomaterials can be controlled with a great certainty.

The influence of precursors on the properties and functions of CDs are thoroughly discussed in this paper, which intend to provide some useful guidance for the synthesis of CDs with specific functionalities. The study of CDs is still an area of rapid development. Despite the huge advances have been made in the last decade, we are soberly aware of the enormous challenges in the field of CDs, which have limited the wide applications of CDs in many practical scenarios. These limitations may include but not restricted to following issues:

(1) Purification of CDs: The commonly used purification methods are dialysis, centrifugation, and column chromatography separation. These approaches are time consuming and ineffective in obtaining pure products, therefore, more effective, and clean purification method are urgently needed.

(2) The yield of CDs: Currently the yield and purity of CDs are still relatively low, and large-scale production of CDs is difficult in many circumstances, thus restricted many researches and practical applications.

(3) The luminescent origin of CDs: There are many attributions to the origin of the luminescence of CDs, and there is still controversy and no unified conclusion at present, which requires further investigation.

Acknowledgements

This work was supported by the National Natural Science Foundation of China (No. 51973083) and Fundamental Research Funds for the Central Universities (No. JUSRP22027). We would like to acknowledge the work of Central Laboratory, School of Chemical and Material Engineering, Jiangnan University. We also would like to acknowledge the support of China Scholarship Council.

References

[1] Yang, X.; Li, X.; Wang, B. Y.; Ai, L.; Li, G. P.; Yang, B.; Lu, S. Y. Advances, opportunities, and challenge for full-color emissive carbon dots. *Chin. Chem. Lett.* **2022**, *33*, 613–625.

[2] Ai, L.; Song, Z. Q.; Nie, M. J.; Yu, J. K.; Liu, F. K.; Song, H. Q.; Zhang, B.; Waterhouse, G. I. N.; Lu, S. Y. Solid-state fluorescence from carbon dots widely tunable from blue to deep red through surface ligand modulation. *Angew. Chem., Int. Ed.* **2023**, *62*, e202217822.

[3] Xu, X. Y.; Ray, R.; Gu, Y. L.; Ploehn, H. J.; Gearheart, L.; Raker, K.; Scrivens, W. A. Electrophoretic analysis and purification of fluorescent single-walled carbon nanotube fragments. *J. Am. Chem. Soc.* **2004**, *126*, 12736–12737.

[4] Sun, Y. P.; Zhou, B.; Lin, Y.; Wang, W.; Fernando, K. A. S.; Pathak, P.; Meziani, M. J.; Harruff, B. A.; Wang, X.; Wang, H. F. et al. Quantum-sized carbon dots for bright and colorful photoluminescence. *J. Am. Chem. Soc.* **2006**, *128*, 7756–7757.

[5] Li, P. F.; Xue, S. S.; Sun, L.; Zong, X. P.; An, L.; Qu, D.; Wang, X. Y.; Sun, Z. C. Formation and fluorescent mechanism of red emissive carbon dots from o-phenylenediamine and catechol system. *Light Sci. Appl.* **2022**, *11*, 298.

[6] Tao, S. Y.; Feng, T. L.; Zheng, C. Y.; Zhu, S. J.; Yang, B. Carbonized polymer dots: A brand new perspective to recognize luminescent carbon-based nanomaterials. *J. Phys. Chem. Lett.* **2019**, *10*, 5182–5188.

[7] Zhu, S. J.; Song, Y. B.; Zhao, X. H.; Shao, J. R.; Zhang, J. H.; Yang, B. The photoluminescence mechanism in carbon dots (graphene quantum dots, carbon nanodots, and polymer dots): Current state and future perspective. *Nano Res.* **2015**, *8*, 355–381.

[8] Li, J. R.; Gong, X. The emerging development of multicolor carbon dots. *Small* **2022**, *18*, 2205099.

[9] Liu, J. J.; Li, R.; Yang, B. Carbon dots: A new type of carbon-based nanomaterial with wide applications. *ACS Cent. Sci.* **2020**, *6*, 2179–2195.

[10] Liang, L. L.; Veksha, A.; Amrad, M. Z. B. M.; Snyder, S. A.; Lisak, G. Upcycling of exhausted reverse osmosis membranes into value-added pyrolysis products and carbon dots. *J. Hazard. Mater.* **2021**, *419*, 126472.

[11] Xu, Y. L.; Wang, C.; Ran, G. X.; Chen, D.; Pang, Q. F.; Song, Q. J. Phosphate-assisted transformation of methylene blue to red-emissive carbon dots with enhanced singlet oxygen generation for photodynamic therapy. *ACS Appl. Nano Mater.* **2021**, *4*, 4820–4828.

[12] Wei, Z. T.; Lu, W. Y.; Wang, X. M.; Ni, J. P.; Prova, U. H.; Wang, C. X.; Huang, G. Y. Harnessing versatile dynamic carbon precursors for multi-color emissive carbon dots. *J. Mater. Chem. C* **2022**, *10*, 1932–1967.

[13] Wang, Y.; Guo, G.; Gao, J. L.; Li, Z. B.; Yin, X. E.; Zhu, C. Q.; Xia, Y. S. Multicenter-emitting carbon dots: Color tunable fluorescence and dynamics monitoring oxidative stress *in vivo*. *Chem. Mater.* **2020**, *32*, 8146–8157.

[14] Wang, H. B.; Zhang, M. L.; Wei, K. Q.; Zhao, Y. J.; Nie, H. D.; Ma, Y. R.; Zhou, Y. J.; Huang, H.; Liu, Y.; Shao, M. W. et al. Pyrrolic nitrogen dominated the carbon dot mimic oxidase activity. *Carbon* **2021**, *179*, 692–700.

[15] Zhao, J.; Wang, H. H.; Geng, H. Q.; Yang, Q.; Tong, Y. P.; He, W. W. Au/N-doped carbon dot nanozymes as light-controlled anti- and pro-oxidants. *ACS Appl. Nano Mater.* **2021**, *4*, 7253–7263.

[16] Zhao, N.; Song, J. Q.; Zhao, L. S. Metallic deep eutectic solvents-assisted synthesis of Cu, Cl-doped carbon dots as oxidase-like and peroxidase-like nanozyme for colorimetric assay of hydroquinone and H_2O_2. *Colloids Surf. A* **2022**, *648*, 129390.

[17] Zhuo, S. J.; Fang, J.; Li, M.; Wang, J.; Zhu, C. Q.; Du, J. Y. Manganese(II)-doped carbon dots as effective oxidase mimics for sensitive colorimetric determination of ascorbic acid. *Microchim. Acta* **2019**, *186*, 745.

[18] Xue, S. S.; Li, P. F.; Sun, L.; An, L.; Qu, D.; Wang, X. Y.; Sun, Z. C. The formation process and mechanism of carbon dots prepared from aromatic compounds as precursors: A review. *Small*, in press, https://doi.org/10.1002/smll.202206180.

[19] Zhi, B.; Yao, X. X.; Cui, Y.; Orr, G.; Haynes, C. L. Synthesis, applications and potential photoluminescence mechanism of spectrally tunable carbon dots. *Nanoscale* **2019**, *11*, 20411–20428.

[20] Ai, L.; Yang, Y. S.; Wang, B. Y.; Chang, J. B.; Tang, Z. Y.; Yang, B.; Lu, S. Y. Insights into photoluminescence mechanisms of carbon dots: Advances and perspectives. *Sci. Bull.* **2021**, *66*, 839–856.

[21] He, C.; Xu, P.; Zhang, X. H.; Long, W. J. The synthetic strategies, photoluminescence mechanisms and promising applications of carbon dots: Current state and future perspective. *Carbon* **2022**, *186*, 91–127.

[22] Liu, W. J.; Li, C.; Ren, Y. J.; Sun, X. B.; Pan, W.; Li, Y. H.; Wang, J. P.; Wang, W. J. Carbon dots: Surface engineering and applications. *J. Mater. Chem. B* **2016**, *4*, 5772–5788.

[23] Xu, X. K.; Li, Y. D.; Hu, G. Q.; Mo, L. Q.; Zheng, M. T.; Lei, B. F.; Zhang, X. J.; Hu, C. F.; Zhuang, J. L.; Liu, Y. L. Surface functional carbon dots: Chemical engineering applications beyond optical properties. *J. Mater. Chem. C* **2020**, *8*, 16282–16294.

[24] Zhang, J.; Yu, S. H. Carbon dots: Large-scale synthesis, sensing and bioimaging. *Mater. Today* **2016**, *19*, 382–393.

[25] Han, Y.; Liccardo, L.; Moretti, E.; Zhao, H. G.; Vomiero, A. Synthesis, optical properties and applications of red/near-infrared carbon dots. *J. Mater. Chem. C* **2022**, *10*, 11827–11847.

[26] Li, Y. D.; Xu, X. K.; Wu, Y.; Zhuang, J. L.; Zhang, X. J.; Zhang, H. R.; Lei, B. F.; Hu, C. F.; Liu, Y. L. A review on the effects of carbon dots in plant systems. *Mater. Chem. Front.* **2020**, *4*, 437–448.

[27] Hu, C.; Li, M. Y.; Qiu, J. S.; Sun, Y. P. Design and fabrication of carbon dots for energy conversion and storage. *Chem. Soc. Rev.* **2019**, *48*, 2315–2337.

[28] Yu, M. Z.; Li, P. L.; Huang, R. B.; Xu, C. N.; Zhang, S. Y.; Wang, Y. L.; Gong, X. D.; Xing, X. D. Antibacterial and antibiofilm mechanisms of carbon dots: A review. *J. Mater. Chem. B* **2023**, *11*, 734–754.

[29] Hebbar, A.; Selvaraj, R.; Vinayagam, R.; Varadavenkatesan, T.; Kumar, P. S.; Duc, P. A.; Rangasamy, G. A critical review on the environmental applications of carbon dots. *Chemosphere* **2023**, *313*, 137308.

[30] Jaleel, J. A.; Pramod, K. Artful and multifaceted applications of carbon dot in biomedicine. *J. Control. Release* **2018**, *269*, 302–321.

[31] Xu, D.; Lin, Q. L.; Chang, H. T. Recent advances and sensing applications of carbon dots. *Small Methods* **2020**, *4*, 1900387.

[32] Kundelev, E. V.; Tepliakov, N. V.; Leonov, M. Y.; Maslov, V. G.; Baranov, A. V.; Fedorov, A. V.; Rukhlenko, I. D.; Rogach, A. L. Amino functionalization of carbon dots leads to red emission enhancement. *J. Phys. Chem. Lett.* **2019**, *10*, 5111–5116.

[33] Zhu, S. J.; Meng, Q. N.; Wang, L.; Zhang, J. H.; Song, Y. B.; Jin, H.; Zhang, K.; Sun, H. C.; Wang, H. Y.; Yang, B. Highly photoluminescent carbon dots for multicolor patterning, sensors, and bioimaging. *Angew. Chem., Int. Ed.* **2013**, *52*, 3953–3957.

[34] Schneider, J.; Reckmeier, C. J.; Xiong, Y.; Von Seckendorff, M.; Susha, A. S.; Kasák, P.; Rogach, A. L. Molecular fluorescence in citric acid-based carbon dots. *J. Phys. Chem. C* **2017**, *121*, 2014–2022.

[35] Hu, Y. P.; Yang, J.; Tian, J. W.; Yu, J. S. How do nitrogen-doped carbon dots generate from molecular precursors? An investigation of the formation mechanism and a solution-based large-scale synthesis.. *J. Mater. Chem. B* **2015**, *3*, 5608–5614.

[36] Miao, X.; Qu, D.; Yang, D.; Nie, B.; Zhao, Y. K.; Fan, H. Y.; Sun,

Z. C. Synthesis of carbon dots with multiple color emission by controlled graphitization and surface functionalization. *Adv. Mater.* **2018**, *30*, 1704740.

[37] Qu, S. N.; Wang, X. Y.; Lu, Q. P.; Liu, X. Y.; Wang, L. J. A biocompatible fluorescent ink based on water-soluble luminescent carbon nanodots. *Angew. Chem., Int. Ed.* **2012**, *51*, 12215–12218.

[38] Tian, Z.; Zhang, X. T.; Li, D.; Zhou, D.; Jing, P. T.; Shen, D. Z.; Qu, S. N.; Zboril, R.; Rogach, A. L. Full-color inorganic carbon dot phosphors for white-light-emitting diodes. *Adv. Opt. Mater.* **2017**, *5*, 1700416.

[39] Liang, T.; Liu, E. S.; Li, M. H.; Ushakova, E. V.; Kershaw, S. V.; Rogach, A. L.; Tang, Z. K.; Qu, S. N. Morphology control of luminescent carbon nanomaterials: From dots to rolls and belts. *ACS Nano* **2021**, *15*, 1579–1586.

[40] Wang, L.; Choi, W. M.; Chung, J. S.; Hur, S. H. Multicolor emitting N-doped carbon dots derived from ascorbic acid and phenylenediamine precursors. *Nanoscale Res. Lett.* **2020**, *15*, 222.

[41] Xu, Y.; Fan, Y.; Zhang, L.; Wang, Q.; Fu, H. Y.; She, Y. B. A novel enhanced fluorescence method based on multifunctional carbon dots for specific detection of Hg^{2+} in complex samples. *Spectrochim. Acta Part A* **2019**, *220*, 117109.

[42] Edison, T. N. J. I.; Atchudan, R.; Sethuraman, M. G.; Shim, J. J.; Lee, Y. R. Microwave assisted green synthesis of fluorescent N-doped carbon dots: Cytotoxicity and bio-imaging applications. *J. Photochem. Photobiol. B: Biol.* **2016**, *161*, 154–161.

[43] Hao, A. J.; Guo, X. J.; Wu, Q.; Sun, Y.; Cong, C. R.; Liu, W. J. Exploring the interactions between polyethyleneimine modified fluorescent carbon dots and bovine serum albumin by spectroscopic methods. *J. Lumin.* **2016**, *170*, 90–96.

[44] Lv, P. Y.; Xu, Y. Y.; Liu, Z.; Li, G. P.; Ye, B. X. Carbon dots doped lanthanide coordination polymers as dual-function fluorescent probe for ratio sensing $Fe^{2+/3+}$ and ascorbic acid. *Microchem. J.* **2020**, *152*, 104255.

[45] Tu, J. Q.; Yang, X. Y.; Liu, H. P.; Chen, P.; Liu, K.; Gao, J. A "on-off-on" fluorescent probe for sensitive detection of Fe^{3+} and ascorbic acid by cross-linking agent protected carbon dots. *Int. J. Environ. Anal. Chem.* **2020**, *102*, 243–253.

[46] Raveendran, V.; Babu, A. R. S.; Renuka, N. K. Mint leaf derived carbon dots for dual analyte detection of Fe(III) and ascorbic acid. *RSC Adv.* **2019**, *9*, 12070–12077.

[47] Cui, J. J.; Zhu, X. X.; Liu, Y. P.; Liang, L. M.; Peng, Y. S.; Wu, S. G.; Zhao, Y. N-doped carbon dots as fluorescent "turn-off" nanosensors for ascorbic acid and Fe^{3+} detection. *ACS Appl. Nano Mater.* **2022**, *5*, 7268–7277.

[48] Cailotto, S.; Amadio, E.; Facchin, M.; Selva, M.; Pontoglio, E.; Rizzolio, F.; Riello, P.; Toffoli, G.; Benedetti, A.; Perosa, A. Carbon dots from sugars and ascorbic acid: Role of the precursors on morphology, properties, toxicity, and drug uptake. *ACS Med. Chem. Lett.* **2018**, *9*, 832–837.

[49] Hallaj, T.; Amjadi, M.; Manzoori, J. L.; Shokri, R. Chemiluminescence reaction of glucose-derived graphene quantum dots with hypochlorite, and its application to the determination of free chlorine. *Microchim. Acta* **2015**, *182*, 789–796.

[50] Ezati, P.; Rhim, J. W.; Molaei, R.; Priyadarshi, R.; Roy, S.; Min, S.; Kim, Y. H.; Lee, S. G.; Han, S. Preparation and characterization of B, S, and N-doped glucose carbon dots: Antibacterial, antifungal, and antioxidant activity. *Sustainable Mater. Technol.* **2022**, *32*, e00397.

[51] Wang, B. Y.; Wei, Z. H.; Sui, L. Z.; Yu, J. K.; Zhang, B. W.; Wang, X. Y.; Feng, S. N.; Song, H. Q.; Yong, X.; Tian, Y. X. et al. Electron-phonon coupling-assisted universal red luminescence of o-phenylenediamine-based carbon dots. *Light Sci. Appl.* **2022**, *11*, 172.

[52] Xu, Y. L.; Wang, C.; Sui, L. Z.; Ran, G. X.; Song, Q. J. Phosphoric acid densified red emissive carbon dots with a well-defined structure and narrow band fluorescence for intracellular reactive oxygen species detection and scavenging. *J. Mater. Chem. C* **2023**, *11*, 2984–2994.

[53] Gao, D.; Liu, A. M.; Zhang, Y. S.; Zhu, Y. D.; Wei, D.; Sun, J.; Luo, H. R.; Fan, H. S. Temperature triggered high-performance carbon dots with robust solvatochromic effect and self-quenching-resistant deep red solid state fluorescence for specific lipid droplet imaging. *Chem. Eng. J.* **2021**, *415*, 128984.

[54] Liu, J. J.; Li, D. W.; Zhang, K.; Yang, M. X.; Sun, H. C.; Yang, B. One-step hydrothermal synthesis of nitrogen-doped conjugated carbonized polymer dots with 31% efficient red emission for *in vivo* imaging. *Small* **2018**, *14*, 1703919.

[55] Chao, D. Y.; Lyu, W.; Liu, Y. B.; Zhou, L.; Zhang, Q. R.; Deng, R. P.; Zhang, H. J. Solvent-dependent carbon dots and their applications in the detection of water in organic solvents. *J. Mater. Chem. C* **2018**, *6*, 7527–7532.

[56] Jiao, Y.; Liu, Y.; Meng, Y. T.; Gao, Y. F.; Lu, W. J.; Liu, Y.; Gong, X. J.; Shuang, S. M.; Dong, C. Novel processing for color-tunable luminescence carbon dots and their advantages in biological systems. *ACS Sustainable Chem. Eng.* **2020**, *8*, 8585–8592.

[57] Arkin, K.; Zheng, Y. X.; Hao, J. W.; Zhang, S. Y.; Shang, Q. K. Polychromatic carbon dots prepared from m-phenylenediamine and urea as multifunctional fluorescent probes. *ACS Appl. Nano Mater.* **2021**, *4*, 8500–8510.

[58] Zhu, T. T.; Cao, L.; Zhou, Z. Q.; Guo, H. Z.; Ge, M. F.; Dong, W. F.; Li, L. Ultra-bright carbon quantum dots for rapid cell staining. *Analyst* **2022**, *147*, 2558–2566.

[59] Zhan, Y. J.; Luo, F.; Guo, L. H.; Qiu, B.; Lin, Y. H.; Li, J.; Chen, G. N.; Lin, Z. Y. Preparation of an efficient ratiometric fluorescent nanoprobe (m-CDs@$[Ru(bpy)_3]^{2+}$) for visual and specific detection of hypochlorite on site and in living cells. *ACS Sens.* **2017**, *2*, 1684–1691.

[60] Jiang, K.; Sun, S.; Zhang, L.; Lu, Y.; Wu, A. G.; Cai, C. Z.; Lin, H. W. Red, green, and blue luminescence by carbon dots: Full-color emission tuning and multicolor cellular imaging. *Angew. Chem., Int. Ed.* **2015**, *54*, 5360–5363.

[61] Jia, J.; Lu, W.; Cui, S.; Dong, C.; Shuang, S. Synthesis of multicolor luminescent adjustable carbon dots and their application in anti-counterfeiting. *Mater. Today Chem.* **2022**, *25*, 100972.

[62] Xu, X. K.; Mo, L. Q.; Li, W.; Li, Y. D.; Lei, B. F.; Zhang, X. J.; Zhuang, J. L.; Hu, C. F.; Liu, Y. L. Red, green and blue aggregation-induced emissive carbon dots. *Chin. Chem. Lett.* **2021**, *32*, 3927–3930.

[63] Lu, S. Y.; Sui, L. Z.; Liu, J. J.; Zhu, S. J.; Chen, A. M.; Jin, M. X.; Yang, B. Near-infrared photoluminescent polymer-carbon nanodots with two-photon fluorescence. *Adv. Mater.* **2017**, *29*, 1603443.

[64] Liu, K. K.; Song, S. Y.; Sui, L. Z.; Wu, S. X.; Jing, P. T.; Wang, R. Q.; Li, Q. Y.; Wu, G. R.; Zhang, Z. Z.; Yuan, K. J. et al. Efficient red/near-infrared-emissive carbon nanodots with multiphoton excited upconversion fluorescence. *Adv. Sci.* **2019**, *6*, 1900766.

[65] Xu, J. H.; Liang, Q. J.; Li, Z. J.; Osipov, V. Y.; Lin, Y. J.; Ge, B. H.; Xu, Q.; Zhu, J. F.; Bi, H. Rational synthesis of solid-state ultraviolet B emitting carbon dots via acetic acid-promoted fractions of sp^3 bonding strategy. *Adv. Mater.* **2022**, *34*, 2200011.

[66] Wang, B. Y.; Yu, J. K.; Sui, L. Z.; Zhu, S. J.; Tang, Z. Y.; Yang, B.; Lu, S. Y. Rational design of multi-color-emissive carbon dots in a single reaction system by hydrothermal. *Adv. Sci.* **2021**, *8*, 2001453.

[67] Chen, Y. Y.; Wang, C.; Xu, Y. L.; Ran, G. X.; Song, Q. J. Red emissive carbon dots obtained from direct calcination of 1,2,4-triaminobenzene for dual-mode pH sensing in living cells. *New J. Chem.* **2020**, *44*, 7210–7217.

[68] Zhang, Q.; Wang, R. Y.; Feng, B. W.; Zhong, X. X.; Ostrikov, K. Photoluminescence mechanism of carbon dots: Triggering high-color-purity red fluorescence emission through edge amino protonation. *Nat. Commun.* **2021**, *12*, 6856.

[69] Ye, X. X.; Xiang, Y. H.; Wang, Q. R.; Li, Z.; Liu, Z. H. A red emissive two-photon fluorescence probe based on carbon dots for intracellular pH detection. *Small* **2019**, *15*, 1901673.

[70] Sun, Z. S.; Zhou, W. Y.; Luo, J. B.; Fan, J. Q.; Wu, Z. C.; Zhu, H. N.; Huang, J. Q.; Zhang, X. G. High-efficient and pH-sensitive orange luminescence from silicon-doped carbon dots for information encryption and bio-imaging. *J. Colloid Interface Sci.* **2022**, *607*, 16–23.

[71] Zhu, Z.; Liu, C. L.; Song, X. M.; Mao, Q. X.; Ma, T. Y. Carbon dots as an indicator of acid-base titration and a fluorescent probe

for endoplasm reticulum imaging. *ACS Appl. Bio Mater.* **2021**, *4*, 3623–3629.

[72] Lu, F.; Yang, S. W.; Song, Y. X.; Zhai, C. M.; Wang, Q. G.; Ding, G. Q.; Kang, Z. H. Hydroxyl functionalized carbon dots with strong radical scavenging ability promote cell proliferation. *Mater. Res. Express* **2019**, *6*, 065030.

[73] Wang, X.; Zhao, L.; Hu, J. S.; Wei, H.; Liu, X. Y.; Li, E. S.; Yang, S. H. Rational design of novel carbon-oxygen quantum dots for ratiometrically mapping pH and reactive oxygen species scavenging. *Carbon* **2022**, *190*, 115–124.

[74] Liu, Y. L.; Shi, J. J. Antioxidative nanomaterials and biomedical applications. *Nano Today* **2019**, *27*, 146–177.

[75] Ingold, K. U.; Pratt, D. A. Advances in radical-trapping antioxidant chemistry in the 21st century: A kinetics and mechanisms perspective. *Chem. Rev.* **2014**, *114*, 9022–9046.

[76] Long, X.; Zhang, Y. Y.; Chen, X.; Zhong, Y. Q.; Wu, S. G.; Hao, L. Synthesis of highly efficient green emissive carbon dots towards UV encryption fluorescent ink. *Opt. Mater.* **2022**, *132*, 112829.

[77] Wang, Y.; Zhang, Y.; Jia, M. Y.; Meng, H.; Li, H.; Guan, Y. F.; Feng, L. Functionalization of carbonaceous nanodots from Mn^{II}-coordinating functional knots. *Chem.—Eur. J.* **2015**, *21*, 14843–14850.

[78] Zhang, H. Y.; Wang, Y.; Xiao, S.; Wang, H.; Wang, J. H.; Feng, L. Rapid detection of Cr(VI) ions based on cobalt(II)-doped carbon dots. *Biosens. Bioelectron.* **2017**, *87*, 46–52.

[79] Guo, H. Z.; Liu, Z. K.; Shen, X. Y.; Wang, L. One-pot synthesis of orange emissive carbon quantum dots for all-type high color rendering index white light-emitting diodes. *ACS Sustainable Chem. Eng.* **2022**, *10*, 8289–8296.

[80] Wang, Z. F.; Yuan, F. L.; Li, X. H.; Li, Y. C.; Zhong, H. Z.; Fan, L. Z.; Yang, S. H. 53% efficient red emissive carbon quantum dots for high color rendering and stable warm white-light-emitting diodes. *Adv. Mater.* **2017**, *29*, 1702910.

[81] Yang, Z.; Li, H.; Xu, T. T.; She, M. Y.; Chen, J.; Jia, X. D.; Liu, P.; Liu, X. R.; Li, J. L. Red emissive carbon dots as a fluorescent sensor for fast specific monitoring and imaging of polarity in living cells. *J. Mater. Chem. A* **2023**, *11*, 2679–2689.

[82] Li, Q.; Chang, Y. T. A protocol for preparing, characterizing and using three RNA-specific, live cell imaging probes: E36, E144 and F22. *Nat. Protoc.* **2006**, *1*, 2922–2932.

[83] Gill, M. R.; Garcia-Lara, J.; Foster, S. J.; Smythe, C.; Battaglia, G.; Thomas, J. A. A ruthenium(II) polypyridyl complex for direct imaging of DNA structure in living cells. *Nat. Chem.* **2009**, *1*, 662–667.

[84] Peng, X. J.; Wu, T.; Fan, J. L.; Wang, J. Y.; Zhang, S.; Song, F. L.; Sun, S. G. An effective minor groove binder as a red fluorescent marker for live-cell DNA imaging and quantification. *Angew. Chem., Int. Ed.* **2011**, *50*, 4180–4183.

[85] Xu, N.; Du, J. J.; Yao, Q. C.; Ge, H. Y.; Shi, C.; Xu, F.; Xian, L. M.; Fan, J. L.; Peng, X. J. Carbon dots inspired by structure-inherent targeting for nucleic acid imaging and localized photodynamic therapy. *Sens. Actuators B: Chem.* **2021**, *344*, 130322.

[86] Yang, J. Y.; Guo, L. K.; Yong, X.; Zhang, T. J.; Wang, B. Y.; Song, H. Q.; Zhao, Y. S.; Hou, H. W.; Yang, B.; Ding, J. et al. Simulating the structure of carbon dots via crystalline π-aggregated organic nanodots prepared by kinetically trapped self-assembly. *Angew. Chem., Int. Ed.* **2022**, *61*, e202207817.

[87] Xu, Y. Y.; Zhang, Z. Z.; Lv, P. Y.; Duan, Y. H.; Li, G. P.; Ye, B. X. Ratiometric fluorescence sensing of $Fe^{2+/3+}$ by carbon dots doped lanthanide coordination polymers. *J. Lumin.* **2019**, *205*, 519–524.

[88] Sun, X. B.; Zhang, J. L.; Wang, X. Y.; Zhao, J. R.; Pan, W.; Yu, G. F.; Qu, Y. J.; Wang, J. P. Colorimetric and fluorimetric dual mode detection of Fe^{2+} in aqueous solution based on a carbon dots/phenanthroline system. *Arabian J. Chem.* **2020**, *13*, 5075–5083.

[89] Iqbal, A.; Tian, Y. J.; Wang, X. D.; Gong, D. Y.; Guo, Y. L.; Iqbal, K.; Wang, Z. P.; Liu, W. S.; Qin, W. W. Carbon dots prepared by solid state method via citric acid and 1,10-phenanthroline for selective and sensing detection of Fe^{2+} and Fe^{3+}. *Sens. Actuators B: Chem.* **2016**, *237*, 408–415.

[90] Jiang, T.; Huang, J. F.; Ran, G. X.; Song, Q. J.; Wang, C. A colorimetric and fluorometric dual-mode carbon dots probe derived from phenanthroline precursor for the selective detection of Fe^{2+} and Fe^{3+}. *Anal. Sci.* **2023**, *39*, 325–333.

[91] Xu, Y. L.; Wang, C.; Jiang, T.; Ran, G. X.; Song, Q. J. Cadmium induced aggregation of orange-red emissive carbon dots with enhanced fluorescence for intracellular imaging. *J. Hazard. Mater.* **2022**, *427*, 128092.

[92] Yuan, B.; Xie, Z.; Chen, P.; Zhou, S. Y. Highly efficient carbon dots and their nanohybrids for trichromatic white LEDs. *J. Mater. Chem. C* **2018**, *6*, 5957–5963.

[93] Liu, Y. P.; Lei, J. H.; Wang, G.; Zhang, Z. M.; Wu, J.; Zhang, B. H.; Zhang, H. Q.; Liu, E. S.; Wang, L. M.; Liu, T. M. et al. Toward strong near-infrared absorption/emission from carbon dots in aqueous media through solvothermal fusion of large conjugated perylene derivatives with post-surface engineering. *Adv. Sci.* **2022**, *9*, 2202283.

[94] Joseph, J.; Anappara, A. A. Microwave-assisted hydrothermal synthesis of UV-emitting carbon dots from tannic acid. *New J. Chem.* **2016**, *40*, 8110–8117.

[95] Liu, Z. X.; Wu, Z. L.; Gao, M. X.; Liu, H.; Huang, C. Z. Carbon dots with aggregation induced emission enhancement for visual permittivity detection. *Chem. Commun.* **2016**, *52*, 2063–2066.

[96] Chen, B. B.; Chang, S.; Jiang, L.; Lv, J.; Gao, Y. T.; Wang, Y.; Qian, R. C.; Li, D. W.; Hafez, M. E. Reversible polymerization of carbon dots based on dynamic covalent imine bond. *J. Colloid Interface Sci.* **2022**, *621*, 464–469.

[97] Li, Y.; Liu, C.; Chen, M. L.; An, Y. L.; Zheng, Y. W.; Tian, H.; Shi, R.; He, X. H.; Lin, X. Solvent-free preparation of tannic acid carbon dots for selective detection of Ni^{2+} in the environment. *Int. J. Mol. Sci.* **2022**, *23*, 6681.

[98] Achadu, O. J.; Revaprasadu, N. Tannic acid-derivatized graphitic carbon nitride quantum dots as an "on-off-on" fluorescent nanoprobe for ascorbic acid via copper(II) mediation. *Microchim. Acta* **2019**, *186*, 87.

[99] Nozaki, T.; Kakuda, T.; Pottathara, Y. B.; Kawasaki, H. A nanocomposite of N-doped carbon dots with gold nanoparticles for visible light active photosensitisers. *Photochem. Photobiol. Sci.* **2019**, *18*, 1235–1241.

[100] Zhang, Q. Z.; He, J.; Yu, W. M.; Li, Y. C.; Liu, Z. H.; Zhou, B. N.; Liu, Y. M. A promising anticancer drug: A photosensitizer based on the porphyrin skeleton. *RSC Med. Chem.* **2020**, *11*, 427–437.

[101] Sun, S.; Chen, J. Q.; Jiang, K.; Tang, Z. D.; Wang, Y. H.; Li, Z. J.; Liu, C. B.; Wu, A. G.; Lin, H. W. Ce6-modified carbon dots for multimodal-imaging-guided and single-NIR-laser-triggered photothermal/photodynamic synergistic cancer therapy by reduced irradiation power. *ACS Appl. Mater. Interfaces* **2019**, *11*, 5791–5803.

[102] Jia, Q. Y.; Ge, J. C.; Liu, W. M.; Zheng, X. L.; Chen, S. Q.; Wen, Y. M.; Zhang, H. Y.; Wang, P. F. A magnetofluorescent carbon dot assembly as an acidic H_2O_2-driven oxygenerator to regulate tumor hypoxia for simultaneous bimodal imaging and enhanced photodynamic therapy. *Adv. Mater.* **2018**, *30*, 1706090.

[103] Wang, B. Y.; Song, H. Q.; Qu, X. L.; Chang, J. B.; Yang, B.; Lu, S. Y. Carbon dots as a new class of nanomedicines: Opportunities and challenges. *Coord. Chem. Rev.* **2021**, *442*, 214010.

[104] Huang, P.; Lin, J.; Wang, X. S.; Wang, Z.; Zhang, C. L.; He, M.; Wang, K.; Chen, F.; Li, Z. M.; Shen, G. X. et al. Light-triggered theranostics based on photosensitizer-conjugated carbon dots for simultaneous enhanced-fluorescence imaging and photodynamic therapy. *Adv. Mater.* **2012**, *24*, 5104–5110.

[105] Ji, D. K.; Dali, H.; Guo, S.; Malaganahally, S.; Vollaire, J.; Josserand, V.; Dumortier, H.; Ménard-Moyon, C.; Bianco, A. Multifunctional carbon nanodots: Enhanced near-infrared photosensitizing, photothermal activity, and body clearance. *Small Sci.* **2022**, *2*, 2100082.

[106] Zheng, M.; Li, Y.; Liu, S.; Wang, W. Q.; Xie, Z. G.; Jing, X. B. One-pot to synthesize multifunctional carbon dots for near infrared fluorescence imaging and photothermal cancer therapy. *ACS Appl. Mater. Interfaces* **2016**, *8*, 23533–23541.

[107] Ge, J. C.; Lan, M. H.; Zhou, B. J.; Liu, W. M.; Guo, L.; Wang, H.; Jia, Q. Y.; Niu, G. L.; Huang, X.; Zhou, H. Y. et al. A graphene quantum dot photodynamic therapy agent with high singlet oxygen generation. *Nat. Commun.* **2014**, *5*, 4596.
[108] Zhao, S. J.; Yang, K.; Jiang, L. R.; Xiao, J. F.; Wang, B. H.; Zeng, L. T.; Song, X. Z.; Lan, M. H. Polythiophene-based carbon dots for imaging-guided photodynamic therapy. *ACS Appl. Nano Mater.* **2021**, *4*, 10528–10533.
[109] Nasrin, A.; Hassan, M.; Gomes, V. G. Two-photon active nucleus-targeting carbon dots: Enhanced ROS generation and photodynamic therapy for oral cancer. *Nanoscale* **2020**, *12*, 20598–20603.
[110] Yue, J.; Li, L.; Jiang, C. Y.; Mei, Q.; Dong, W. F.; Yan, R. H. Riboflavin-based carbon dots with high singlet oxygen generation for photodynamic therapy. *J. Mater. Chem. B* **2021**, *9*, 7972–7978.
[111] Li, Y.; Zheng, X. H.; Zhang, X. Y.; Liu, S.; Pei, Q.; Zheng, M.; Xie, Z. G. Porphyrin-based carbon dots for photodynamic therapy of hepatoma. *Adv. Healthc. Mater.* **2017**, *6*, 1600924.
[112] Meng, W. X.; Bai, X.; Wang, B. Y.; Liu, Z. Y.; Lu, S. Y.; Yang, B. Biomass-derived carbon dots and their applications. *Energy Environ. Mater.* **2019**, *2*, 172–192.
[113] Zhu, L. L.; Shen, D. K.; Wu, C. F.; Gu, S. State-of-the-art on the preparation, modification, and application of biomass-derived carbon quantum dots. *Ind. Eng. Chem. Res.* **2020**, *59*, 22017–22039.
[114] Mehta, V. N.; Jha, S.; Basu, H.; Singhal, R. K.; Kailasa, S. K. One-step hydrothermal approach to fabricate carbon dots from apple juice for imaging of mycobacterium and fungal cells. *Sens. Actuators B: Chem.* **2015**, *213*, 434–443.
[115] De, B.; Karak, N. A green and facile approach for the synthesis of water soluble fluorescent carbon dots from banana juice. *RSC Adv.* **2013**, *3*, 8286–8290.
[116] Desa, S. S.; Ishii, T.; Nueangnoraj, K. Sulfur-doped carbons from durian peels, their surface characteristics, and electrochemical behaviors. *ACS Omega* **2021**, *6*, 24902–24909.
[117] Jayaweera, S.; Yin, K.; Ng, W. J. Nitrogen-doped durian shell derived carbon dots for inner filter effect mediated sensing of tetracycline and fluorescent ink. *J. Fluoresc.* **2019**, *29*, 221–229.
[118] Thongsai, N.; Tanawannapong, N.; Praneerad, J.; Kladsomboon, S.; Jaiyong, P.; Paoprasert, P. Real-time detection of alcohol vapors and volatile organic compounds via optical electronic nose using carbon dots prepared from rice husk and density functional theory calculation. *Colloids Surf. A* **2019**, *560*, 278–287.
[119] Wang, C. F.; Sun, D.; Zhuo, K. L.; Zhang, H. C.; Wang, J. J. Simple and green synthesis of nitrogen-, sulfur-, and phosphorus-co-doped carbon dots with tunable luminescence properties and sensing application. *RSC Adv.* **2014**, *4*, 54060–54065.
[120] Chen, W. F.; Li, D. J.; Tian, L.; Xiang, W.; Wang, T. Y.; Hu, W. M.; Hu, Y. L.; Chen, S. N.; Chen, J. F.; Dai, Z. X. Synthesis of graphene quantum dots from natural polymer starch for cell imaging. *Green Chem.* **2018**, *20*, 4438–4442.
[121] Xie, Y. D.; Cheng, D. D.; Liu, X. L.; Han, A. X. Green hydrothermal synthesis of N-doped carbon dots from biomass highland barley for the detection of Hg^{2+}. *Sensors* **2019**, *19*, 3169.
[122] Liu, J.; Kong, T.; Xiong, H.-M. Mulberry-leaves-derived red-emissive carbon dots for feeding silkworms to produce brightly fluorescent silk. *Adv. Mater.* **2022**, *34*, 2200152.
[123] Mou, Z. H.; Yang, Q. B.; Zhao, B.; Li, X. Q.; Xu, Y. X.; Gao, T. T.; Zheng, H.; Zhou, K.; Xiao, D. Scalable and sustainable synthesis of carbon dots from biomass as efficient friction modifiers for polyethylene glycol synthetic oil. *ACS Sustainable Chem. Eng.* **2021**, *9*, 14997–15007.
[124] Xu, J.; Jie, X.; Xie, F. F.; Yang, H. M.; Wei, W. L.; Xia, Z. N. Flavonoid moiety-incorporated carbon dots for ultrasensitive and highly selective fluorescence detection and removal of Pb^{2+}. *Nano Res.* **2018**, *11*, 3648–3657.
[125] Amer, W. A.; Rehab, A. F.; Abdelghafar, M. E.; Torad, N. L.; Atlam, A. S.; Ayad, M. M. Green synthesis of carbon quantum dots from purslane leaves for the detection of formaldehyde using quartz crystal microbalance. *Carbon* **2021**, *179*, 159–171.
[126] Long, W. J.; Li, X. Q.; Yu, Y.; He, C. Green synthesis of biomass-derived carbon dots as an efficient corrosion inhibitor. *J. Mol. Liq.* **2022**, *360*, 119522.
[127] Sharma, V.; Singh, S. K.; Mobin, S. M. Bioinspired carbon dots: From rose petals to tunable emissive nanodots. *Nanoscale Adv.* **2019**, *1*, 1290–1296.
[128] Gu, D.; Hong, L.; Zhang, L.; Liu, H.; Shang, S. M. Nitrogen and sulfur co-doped highly luminescent carbon dots for sensitive detection of Cd(II) ions and living cell imaging applications. *J. Photochem. Photobiol. B: Biol.* **2018**, *186*, 144–151.
[129] Campalani, C.; Cattaruzza, E.; Zorzi, S.; Vomiero, A.; You, S. J.; Matthews, L.; Capron, M.; Mondelli, C.; Selva, M.; Perosa, A. Biobased carbon dots: From fish scales to photocatalysis. *Nanomaterials* **2021**, *11*, 524.
[130] Mandani, S.; Dey, D.; Sharma, B.; Sarma, T. K. Natural occurrence of fluorescent carbon dots in honey. *Carbon* **2017**, *119*, 569–572.
[131] Wang, D.; Zhu, L.; Mccleese, C.; Burda, C.; Chen, J. F.; Dai, L. M. Fluorescent carbon dots from milk by microwave cooking. *RSC Adv.* **2016**, *6*, 41516–41521.
[132] Gu, D.; Zhang, P. B.; Zhang, L.; Liu, H.; Pu, Z. B.; Shang, S. M. Nitrogen and phosphorus co-doped carbon dots derived from lily bulbs for copper ion sensing and cell imaging. *Opt. Mater.* **2018**, *83*, 272–278.
[133] Yang, W.; Shimanouchi, T.; Kimura, Y. Characterization of the residue and liquid products produced from husks of nuts from *Carya cathayensis* sarg by hydrothermal carbonization. *ACS Sustainable Chem. Eng.* **2015**, *3*, 591–598.
[134] Sachdev, A.; Gopinath, P. Green synthesis of multifunctional carbon dots from coriander leaves and their potential application as antioxidants, sensors and bioimaging agents. *Analyst* **2015**, *140*, 4260–4269.
[135] Wang, Q.; Liu, X.; Zhang, L. C.; Lv, Y. Microwave-assisted synthesis of carbon nanodots through an eggshell membrane and their fluorescent application. *Analyst* **2012**, *137*, 5392–5397.
[136] Wang, J.; Wang, C. F.; Chen, S. Amphiphilic egg-derived carbon dots: Rapid plasma fabrication, pyrolysis process, and multicolor printing patterns. *Angew. Chem., Int. Ed.* **2012**, *51*, 9297–9301.
[137] Chen, J.; Wang, Y. T.; Wang, L.; Liu, M. J.; Fang, L. L.; Chu, P.; Gao, C. Z.; Chen, D. P.; Ren, D. Z.; Zhang, J. B. Multi-applications of carbon dots and polydopamine-coated carbon dots for Fe^{3+} detection, bioimaging, dopamine assay and photothermal therapy. *Discover Nano* **2023**, *18*, 30.
[138] Zhang, Z. H.; Sun, W. H.; Wu, P. Y. Highly photoluminescent carbon dots derived from egg white: Facile and green synthesis, photoluminescence properties, and multiple applications. *ACS Sustainable Chem. Eng.* **2015**, *3*, 1412–1418.
[139] Wang, C. J.; Shi, H. X.; Yang, M.; Yan, Y.; Liu, E. Z.; Ji, Z.; Fan, J. Facile synthesis of novel carbon quantum dots from biomass waste for highly sensitive detection of iron ions. *Mater. Res. Bull.* **2020**, *124*, 110730.
[140] Li, L.; Shi, L. H.; Jia, J.; Chang, D.; Dong, C.; Shuang, S. M. Fe^{3+} detection, bioimaging, and patterning based on bright blue-fluorescent N-doped carbon dots. *Analyst* **2020**, *145*, 5450–5457.
[141] Gu, L.; Zhang, J. R.; Yang, G. X.; Tang, Y. Y.; Zhang, X.; Huang, X. Y.; Zhai, W. L.; Fodjo, E. K.; Kong, C. Green preparation of carbon quantum dots with wolfberry as on-off-on nanosensors for the detection of Fe^{3+} and l-ascorbic acid. *Food Chem.* **2022**, *376*, 131898.
[142] Zhao, W. B.; Liu, K. K.; Song, S. Y.; Zhou, R.; Shan, C. X. Fluorescent nano-biomass dots: Ultrasonic-assisted extraction and their application as nanoprobe for Fe^{3+} detection. *Nanoscale Res. Lett.* **2019**, *14*, 130.
[143] Wang, Z. Y.; Sheng, L. N.; Yang, X. X.; Sun, J. D.; Ye, Y. L.; Geng, S. X.; Ning, D. L.; Zheng, J. Y.; Fan, M. H.; Zhang, Y. Z. et al. Natural biomass-derived carbon dots as potent antimicrobial agents against multidrug-resistant bacteria and their biofilms. *Sustainable Mater. Technol.* **2023**, *36*, e00584.
[144] Chen, K.; Qing, W. X.; Hu, W. P.; Lu, M. H.; Wang, Y.; Liu, X. H. On-off-on fluorescent carbon dots from waste tea: Their properties, antioxidant and selective detection of CrO_4^{2-}, Fe^{3+}, ascorbic acid and L-cysteine in real samples. *Spectrochim. Acta Part A* **2019**, *213*, 228–234.
[145] Murru, C.; Badia-Laino, R.; Diaz-Garcia, M. E. Synthesis and

characterization of green carbon dots for scavenging radical oxygen species in aqueous and oil samples. *Antioxidants* **2020**, *9*, 1147.

[146] Šafranko, S.; Stanković, A.; Hajra, S.; Kim, H. J.; Strelec, I.; Dutour-Sikirić, M.; Weber, I.; Bosnar, M. H.; Grbčić, P.; Pavelić, S. K. et al. Preparation of multifunctional N-doped carbon quantum dots from *Citrus clementina* peel: Investigating targeted pharmacological activities and the potential application for Fe^{3+} sensing. *Pharmaceuticals* **2021**, *14*, 857.

[147] Das, B.; Dadhich, P.; Pal, P.; Srivas, P. K.; Bankoti, K.; Dhara, S. Carbon nanodots from date molasses: New nanolights for the *in vitro* scavenging of reactive oxygen species. *J. Mater. Chem. B* **2014**, *2*, 6839–6847.

[148] Wang, H. B.; Zhang, M. L.; Ma, Y. R.; Wang, B.; Shao, M. W.; Huang, H.; Liu, Y.; Kang, Z. H. Selective inactivation of Gram-negative bacteria by carbon dots derived from natural biomass: *Artemisia argyi* leaves. *J. Mater. Chem. B* **2020**, *8*, 2666–2672.

[149] Tang, H. J.; Song, P.; Li, J.; Zhao, D. S. Effect of *Salvia miltiorrhiza* on acetylcholinesterase: Enzyme kinetics and interaction mechanism merging with molecular docking analysis. *Int. J. Biol. Macromol.* **2019**, *135*, 303–313.

[150] Wang, W. H.; Hsuan, K. Y.; Chu, L. Y.; Lee, C. Y.; Tyan, Y. C.; Chen, Z. S.; Tsai, W. C. Anticancer effects of *Salvia miltiorrhiza* alcohol extract on oral squamous carcinoma cells. *Evid. Based. Complement. Alternat. Med.* **2017**, *2017*, 5364010.

[151] Meng, X. G.; Jiang, J. J.; Pan, H.; Wu, S. Y.; Wang, S. W.; Lou, Y. F.; Fan, G. R. Preclinical absorption, distribution, metabolism, and excretion of sodium danshensu, one of the main water-soluble ingredients in *Salvia miltiorrhiza*, in Rats. *Front. Pharmacol.* **2019**, *10*, 554.

[152] Li, Y. J.; Li, W.; Yang, X.; Kang, Y. Y.; Zhang, H. R.; Liu, Y. L.; Lei, B. F. *Salvia miltiorrhiza*-derived carbon dots as scavengers of reactive oxygen species for reducing oxidative damage of plants. *ACS Appl. Nano Mater.* **2021**, *4*, 113–120.

[153] Pichardo-Molina, J. L.; Cardoso-Avila, P. E.; Flores-Villavicencio, L. L.; Gomez-Ortiz, N. M.; Rodriguez-Rivera, M. A. Fluorescent carbon nanoparticles synthesized from bovine serum albumin nanoparticles. *Int. J. Biol. Macromol.* **2020**, *142*, 724–731.

[154] Ding, S. C.; Zhang, N.; Lyu, Z. Y.; Zhu, W. L.; Chang, Y. C.; Hu, X. L.; Du, D.; Lin, Y. H. Protein-based nanomaterials and nanosystems for biomedical applications: A review. *Mater. Today* **2021**, *43*, 166–184.

[155] Maity, S.; Bhat, A. H.; Giri, K.; Ambatipudi, K. BoMiProt: A database of bovine milk proteins. *J. Proteomics* **2020**, *215*, 103648.

[156] Sugár, S.; Turiák, L.; Vékey, K.; Drahos, L. Widespread presence of bovine proteins in human cell lines. *J. Mass Spectrom.* **2020**, *55*, e4464.

[157] Tang, M. H.; Teng, P.; Long, Y. J.; Wang, X. L.; Liang, L. P.; Shen, D. J.; Wang, J.; Zheng, H. Z. Hollow carbon dots labeled with FITC or TRITC for use in fluorescent cellular imaging. *Microchim. Acta* **2018**, *185*, 223.

[158] Xu, Y. L.; Wang, C.; Wu, T.; Ran, G. X.; Song, Q. J. Template-free synthesis of porous fluorescent carbon nanomaterials with gluten for intracellular imaging and drug delivery. *ACS Appl. Mater. Interfaces* **2022**, *14*, 21310–21318.

[159] Carbonaro, C. M.; Corpino, R.; Salis, M.; Mocci, F.; Thakkar, S. V.; Olla, C.; Ricci, P. C. On the emission properties of carbon dots: Reviewing data and discussing models. *J. Carbon Res.* **2019**, *5*, 60.

[160] Alivisatos, A. P. Semiconductor Clusters, Nanocrystals, and quantum dots. *Science* **1996**, *271*, 933–937.

[161] Sk, M. A.; Ananthanarayanan, A.; Huang, L.; Lim, K. H.; Chen, P. Revealing the tunable photoluminescence properties of graphene quantum dots. *J. Mater. Chem. C* **2014**, *2*, 6954–6960.

[162] Yuan, F. L.; Yuan, T.; Sui, L. Z.; Wang, Z. B.; Xi, Z. F.; Li, Y. C.; Li, X. H.; Fan, L. Z.; Tan, Z. A.; Chen, A. M. et al. Engineering triangular carbon quantum dots with unprecedented narrow bandwidth emission for multicolored LEDs. *Nat. Commun.* **2018**, *9*, 2249.

[163] Wang, L.; Li, W. T.; Yin, L. Q.; Liu, Y. J.; Guo, H. Z.; Lai, J. W.; Han, Y.; Li, G.; Li, M.; Zhang, J. H. et al. Full-color fluorescent carbon quantum dots. *Sci. Adv.* **2020**, *6*, eabb6772.

[164] Li, H. J.; Han, S. C.; Lyu, B. W.; Hong, T.; Zhi, S. B.; Xu, L.; Xue, F. F.; Sai, L. M.; Yang, J. H.; Wang, X. Y. et al. Tunable light emission from carbon dots by controlling surface defects. *Chin. Chem. Lett.* **2021**, *32*, 2887–2892.

[165] Yuan, K.; Zhang, X. H.; Qin, R. H.; Ji, X. F.; Cheng, Y. H.; Li, L. L.; Yang, X. J.; Lu, Z. M.; Liu, H. Surface state modulation of red emitting carbon dots for white light-emitting diodes. *J. Mater. Chem. C* **2018**, *6*, 12631–12637.

[166] Song, Y. B.; Zhu, S. J.; Zhang, S. T.; Fu, Y.; Wang, L.; Zhao, X. H.; Yang, B. Investigation from chemical structure to photoluminescent mechanism: A type of carbon dots from the pyrolysis of citric acid and an amine. *J. Mater. Chem. C* **2015**, *3*, 5976–5984.

[167] Shi, L.; Yang, J. H.; Zeng, H. B.; Chen, Y. M.; Yang, S. C.; Wu, C.; Zeng, H.; Yoshihito, O.; Zhang, Q. Q. Carbon dots with high fluorescence quantum yield: The fluorescence originates from organic fluorophores. *Nanoscale* **2016**, *8*, 14374–14378.

[168] Kasprzyk, W.; Świergosz, T.; Bednarz, S.; Walas, K.; Bashmakova, N. V.; Bogdał, D. Luminescence phenomena of carbon dots derived from citric acid and urea—A molecular insight. *Nanoscale* **2018**, *10*, 13889–13894.

[169] Cao, L.; Zan, M. H.; Chen, F. M.; Kou, X. Y.; Liu, Y. L.; Wang, P. Y.; Mei, Q.; Hou, Z.; Dong, W. F.; Li, L. Formation mechanism of carbon dots: From chemical structures to fluorescent behaviors. *Carbon* **2022**, *194*, 42–51.

[170] Soni, N.; Singh, S.; Sharma, S.; Batra, G.; Kaushik, K.; Rao, C.; Verma, N. C.; Mondal, B.; Yadav, A.; Nandi, C. K. Absorption and emission of light in red emissive carbon nanodots. *Chem. Sci.* **2021**, *12*, 3615–3626.

[171] Wang, B. Y.; Song, H. Q.; Tang, Z. Y.; Yang, B.; Lu, S. Y. Ethanol-derived white emissive carbon dots: The formation process investigation and multi-color/white LEDs preparation. *Nano Res.* **2021**, *15*, 942–949.

[172] Wang, F.; Wang, C. L.; Chen, M. L.; Gong, W. L.; Zhang, Y.; Han, S. S.; Situ, G. H. Far-field super-resolution ghost imaging with a deep neural network constraint. *Light Sci. Appl.* **2022**, *11*, 1.

[173] Lin, Y. C.; Zheng, Y. F.; Guo, Y. C.; Yang, Y. L.; Li, H. B.; Fang, Y.; Wang, C. Peptide-functionalized carbon dots for sensitive and selective Ca^{2+} detection. *Sens. Actuators B: Chem.* **2018**, *273*, 1654–1659.

[174] Yang, J.; Jin, X. L.; Cheng, Z.; Zhou, H. W.; Gao, L. N.; Jiang, D. L.; Jie, X. L.; Ma, Y. T.; Chen, W. X. Facile and green synthesis of bifunctional carbon dots for detection of Cu^{2+} and ClO^- in aqueous solution. *ACS Sustainable Chem. Eng.* **2021**, *9*, 13206–13214.

[175] Feng, J.; Zhao, X. R.; Bian, W.; Tang, X. J. Microwave-assisted synthesis of nitrogen-rich carbon dots as effective fluorescent probes for sensitive detection of Ag^+. *Mater. Chem. Front.* **2019**, *3*, 2751–2758.

[176] Sun, Z. S.; Zhou, Y. P.; Zhou, W. Y.; Luo, J. B.; Liu, R. Y.; Zhang, X. G.; Zhou, L. Y.; Pang, Q. Pb(II) detection and versatile bio-imaging of green-emitting carbon dots with excellent stability and bright fluorescence. *Nanoscale* **2021**, *13*, 2472–2480.

[177] Wei, S. S.; Tan, L. H.; Yin, X. Y.; Wang, R. M.; Shan, X. R.; Chen, Q.; Li, T. H.; Zhang, X. Y.; Jiang, C. Z.; Sun, G. Y. A sensitive "on-off" fluorescent probe based on carbon dots for Fe^{2+} detection and cell imaging. *Analyst* **2020**, *145*, 2357–2366.

[178] Wang, B. B.; Jin, J. C.; Xu, Z. Q.; Jiang, Z. W.; Li, X.; Jiang, F. L.; Liu, Y. Single-step synthesis of highly photoluminescent carbon dots for rapid detection of Hg^{2+} with excellent sensitivity. *J. Colloid Interface Sci.* **2019**, *551*, 101–110.

[179] Wang, N.; Chai, H. J.; Dong, X. L.; Zhou, Q.; Zhu, L. H. Detection of Fe(III)EDTA by using photoluminescent carbon dot with the aid of F^- ion. *Food Chem.* **2018**, *258*, 51–58.

[180] Wang, L. L.; Jana, J.; Chung, J. S.; Choi, W. M.; Hur, S. H. Designing an intriguingly fluorescent N, B-doped carbon dots based fluorescent probe for selective detection of NO_2^- ions. *Spectrochim. Acta Part A* **2022**, *268*, 120657.

[181] Liu, Q. L.; Niu, X. Y.; Xie, K. X.; Yan, Y. M.; Ren, B. R.; Liu, R. R.; Li, Y. X.; Li, L. Fluorescent carbon dots as nanosensors for monitoring and imaging Fe^{3+} and $[HPO_4]^{2-}$ ions. *ACS Appl. Nano Mater.* **2021**, *4*, 190–197.

[182] Liu, A. K.; Cai, H. J.; Xu, Z. B.; Li, J. L.; Weng, X. Y.; Liao, C. R.;

He, J.; Liu, L. W.; Wang, Y. P.; Qu, J. L. et al. Multifunctional carbon dots for glutathione detection and Golgi imaging. *Talanta* **2023**, *259*, 124520.

[183] Yu, X.; Zhang, C. X.; Zhang, L. N.; Xue, Y. R.; Li, H. W.; Wu, Y. Q. The construction of a FRET assembly by using gold nanoclusters and carbon dots and their application as a ratiometric probe for cysteine detection. *Sens. Actuators B: Chem.* **2018**, *263*, 327–335.

[184] Li, F.; Chen, J.; Wen, J. Y.; Peng, Y. Y.; Tang, X. M.; Qiu, P. Ratiometric fluorescence and colorimetric detection for uric acid using bifunctional carbon dots. *Sens. Actuators B: Chem.* **2022**, *369*, 132381.

[185] Wang, B.; Liu, F.; Wu, Y. Y.; Chen, Y. F.; Weng, B.; Li, C. M. Synthesis of catalytically active multielement-doped carbon dots and application for colorimetric detection of glucose. *Sens. Actuators B: Chem.* **2018**, *255*, 2601–2607.

[186] Yang, H.; Long, Y. W.; Li, H. X.; Pan, S.; Liu, H.; Yang, J. D.; Hu, X. L. Carbon dots synthesized by hydrothermal process via sodium citrate and NH_4HCO_3 for sensitive detection of temperature and sunset yellow. *J. Colloid Interface Sci.* **2018**, *516*, 192–201.

[187] Shi, W. L.; Guo, F.; Han, M. M.; Yuan, S. L.; Guan, W. S.; Li, H.; Huang, H.; Liu, Y.; Kang, Z. H. N,S co-doped carbon dots as a stable bio-imaging probe for detection of intracellular temperature and tetracycline. *J. Mater. Chem. B* **2017**, *5*, 3293–3299.

[188] Liao, X. F.; Chen, C. J.; Wang, P. W.; Zhou, R. X.; Zhao, X. L.; Fan, H.; Huang, Z. Q. Carbon dots derived from cellobiose for temperature and phosalone detection. *Mater. Res. Bull.* **2022**, *151*, 111790.

[189] Wang, C.; He, Y. M.; Xu, Y. L.; Sui, L. Z.; Jiang, T.; Ran, G. X.; Song, Q. J. "Light on" fluorescence carbon dots with intramolecular hydrogen bond-regulated co-planarization for cell imaging and temperature sensing. *J. Mater. Chem. A* **2022**, *10*, 2085–2095.

[190] Wang, C.; He, Y. M.; Huang, J. F.; Sui, L. Z.; Ran, G. X.; Zhu, H.; Song, Q. J. Intramolecular hydrogen bond-tuned thermal-responsive carbon dots and their application to abnormal body temperature imaging. *J. Colloid Interface Sci.* **2023**, *634*, 221–230.

[191] Zhai, X. Y.; Zhang, P.; Liu, C. J.; Bai, T.; Li, W. C.; Dai, L. M.; Liu, W. G. Highly luminescent carbon nanodots by microwave-assisted pyrolysis. *Chem. Commun.* **2012**, *48*, 7955–7957.

[192] Casey, J. R.; Grinstein, S.; Orlowski, J. Sensors and regulators of intracellular pH. *Nat. Rev. Mol. Cell Biol.* **2010**, *11*, 50–61.

[193] Geng, X.; Sun, Y. Q.; Li, Z. H.; Yang, R.; Zhao, Y. M.; Guo, Y. F.; Xu, J. J.; Li, F. T.; Wang, Y.; Lu, S. Y. et al. Retrosynthesis of tunable fluorescent carbon dots for precise long-term mitochondrial tracking. *Small* **2019**, *15*, 1901517.

[194] Wei, Y. Y.; Chen, L.; Zhang, X.; Du, J. L.; Li, Q.; Luo, J.; Liu, X. G.; Yang, Y. Z.; Yu, S. P.; Gao, Y. D. Orange-emissive carbon quantum dots for ligand-directed Golgi apparatus-targeting and *in vivo* imaging. *Biomater. Sci.* **2022**, *10*, 4345–4355.

[195] Shuang, E.; Mao, Q. X.; Wang, J. H.; Chen, X. W. Carbon dots with tunable dual emissions: From the mechanism to the specific imaging of endoplasmic reticulum polarity. *Nanoscale* **2020**, *12*, 6852–6860.

[196] Chen, J. Y.; Li, F.; Gu, J.; Zhang, X.; Bartoli, M.; Domena, J. B.; Zhou, Y. Q.; Zhang, W.; Paulino, V.; Ferreira, B, C. L. B. et al. Cancer cells inhibition by cationic carbon dots targeting the cellular nucleus. *J. Colloid Interface Sci.* **2023**, *637*, 193–206.

[197] Guo, S.; Sun, Y. Q.; Geng, X.; Yang, R.; Xiao, L. H.; Qu, L. B.; Li, Z. H. Intrinsic lysosomal targeting fluorescent carbon dots with ultrastability for long-term lysosome imaging. *J. Mater. Chem. B* **2020**, *8*, 736–742.

[198] Dai, R. Y.; Chen, X. P.; Ouyang, N.; Hu, Y. P. A pH-controlled synthetic route to violet, green, and orange fluorescent carbon dots for multicolor light-emitting diodes. *Chem. Eng. J.* **2022**, *431*, 134172.

[199] Shen, J.; Zheng, X. J.; Lin, L. L.; Xu, H. J.; Xu, G. H. Reaction time-controlled synthesis of multicolor carbon dots for white light-emitting diodes. *ACS Appl. Nano Mater.* **2023**, *6*, 2478–2490.

[200] Han, Q. R.; Xu, W. J.; Ji, C. Y.; Xiong, G. Y.; Shi, C. S.; Zhang, D. M.; Shi, W. Q.; Jiang, Y. X.; Peng, Z. L. Multicolor and single-component white light-emitting carbon dots from a single precursor for light-emitting diodes. *ACS Appl. Nano Mater.* **2022**, *5*, 15914–15924.

[201] Wang, Z. B.; Jiang, N. Z.; Liu, M. L.; Zhang, R. D.; Huang, F.; Chen, D. Q. Bright electroluminescent white-light-emitting diodes based on carbon dots with tunable correlated color temperature enabled by aggregation. *Small* **2021**, *17*, 2104551.

[202] Wang, B. Y.; Lu, S. Y. The light of carbon dots: From mechanism to applications. *Matter* **2022**, *5*, 110–149.

[203] Zhu, L. L.; Shen, D. K.; Wang, Q.; Luo, K. H. Green synthesis of tunable fluorescent carbon quantum dots from lignin and their application in anti-counterfeit printing. *ACS Appl. Mater. Interfaces* **2021**, *13*, 56465–56475.

[204] Wang, C.; Huang, J. F.; He, Y. M.; Ran, G. X.; Song, Q. J. Preparation of multicolor carbon dots with thermally turn-on fluorescence for multidimensional information encryption. *Chin. Chem. Lett.*, in press, https://doi.org/10.1016/j.cclet.2023.108420.

[205] Tao, S. Y.; Lu, S. Y.; Geng, Y. J.; Zhu, S. J.; Redfern, S. A. T.; Song, Y. B.; Feng, T. L.; Xu, W. Q.; Yang, B. Design of metal-free polymer carbon dots: A new class of room-temperature phosphorescent materials. *Angew. Chem., Int. Ed.* **2018**, *57*, 2393–2398.

[206] Wang, C.; Chen, Y. Y.; Hu, T. T.; Chang, Y.; Ran, G. X.; Wang, M.; Song, Q. J. Color tunable room temperature phosphorescent carbon dot based nanocomposites obtainable from multiple carbon sources via a molten salt method. *Nanoscale* **2019**, *11*, 11967–11974.

[207] Qiao, L.; Zhou, M. J.; Shi, G.; Cui, Z.; Zhang, X. M.; Fu, P.; Liu, M. Y.; Qiao, X. G.; He, Y. J.; Pang, X. C. Ultrafast visible-light-induced ATRP in aqueous media with carbon quantum dots as the catalyst and its application for 3D printing. *J. Am. Chem. Soc.* **2022**, *144*, 9817–9826.

[208] Su, W.; Guo, R. H.; Yuan, F. L.; Li, Y. C.; Li, X. H.; Zhang, Y.; Zhou, S. X.; Fan, L. Z. Red-emissive carbon quantum dots for nuclear drug delivery in cancer stem cells. *J. Phys. Chem. Lett.* **2020**, *11*, 1357–1363.

[209] Shivalkar, S.; Gautam, P. K.; Verma, A.; Maurya, K.; Sk, P.; Samanta, S. K.; Sahoo, A. K. Autonomous magnetic microbots for environmental remediation developed by organic waste derived carbon dots. *J. Environ. Manage.* **2021**, *297*, 113322.

[210] Chen, L. T.; Wang, C. F.; Liu, C.; Chen, S. Facile access to fabricate carbon dots and perspective of large-scale applications. *Small*, in press, https://doi.org/10.1002/smll.202206671.

[211] Li, W.; Wu, S. S.; Zhang, H. R.; Zhang, X. J.; Zhuang, J. L.; Hu, C. F.; Liu, Y. L.; Lei, B. F.; Ma, L.; Wang, X. J. Enhanced biological photosynthetic efficiency using light-harvesting engineering with dual-emissive carbon dots. *Adv. Funct. Mater.* **2018**, *28*, 1804004.

[212] Chen, J.; Guo, Y. X.; Zhang, X. L.; Liu, J. H.; Gong, P.; Su, Z. Q.; Fan, L. H.; Li, G. L. Emerging nanoparticles in food: Sources, application, and safety. *J. Agric. Food Chem.* **2023**, *71*, 3564–3582.

[213] Wang, Q. L.; Huang, X. X.; Long, Y. J.; Wang, X. L.; Zhang, H. J.; Zhu, R.; Liang, L. P.; Teng, P.; Zheng, H. Z. Hollow luminescent carbon dots for drug delivery. *Carbon* **2013**, *59*, 192–199.

[214] Wang, S. P.; Zhao, H. R.; Yang, J. L.; Dong, Y. H.; Guo, S. Z.; Cheng, Q.; Li, Y.; Liu, S. X. Preparation of multicolor biomass carbon dots based on solvent control and their application in Cr(VI) detection and advanced anti-counterfeiting. *ACS Omega* **2023**, *8*, 6550–6558.

[215] Liu, J. J.; Geng, Y. J.; Li, D. W.; Yao, H.; Huo, Z. P.; Li, Y. F.; Zhang, K.; Zhu, S. J.; Wei, H. T.; Xu, W. Q. et al. Deep red emissive carbonized polymer dots with unprecedented narrow full width at half maximum. *Adv. Mater.* **2020**, *32*, 1906641.

[216] John, V. L.; Nayana, A. R.; Keerthi, T. R.; K. A, A. K.; Sasidharan, B. C. P.; T. P, V. Mulberry leaves (*Morus rubra*)-derived blue-emissive carbon dots fed to silkworms to produce augmented silk applicable for the ratiometric detection of dopamine. *Macromol. Biosci.*, in press, https://doi.org/10.1002/mabi.202300081 .

[217] Huang, K.; He, Q.; Sun, R. S.; Fang, L. L.; Song, H. Y.; Li, L.; Li, Z.; Tian, Y.; Cui, H. X.; Zhang, J. B. Preparation and application of carbon dots derived from cherry blossom flowers. *Chem. Phys. Lett.* **2019**, *731*, 136586.

[218] Qi, H. Y.; Liu, C. T.; Jing, J.; Jing, T.; Zhang, X. H.; Li, J. L.; Luo, C.; Qiu, L. X.; Li, Q. Y. Two kinds of biomass-derived carbon dots with one-step synthesis for Fe^{3+} and tetracyclines detection. *Dyes Pigm.* **2022**, *206*, 110555.
[219] Wu, L.; Pan, W. Y.; Ye, H.; Liang, N.; Zhao, L. S. Sensitive fluorescence detection for hydrogen peroxide and glucose using biomass carbon dots: Dual-quenching mechanism insight. *Colloids Surf. A* **2022**, *638*, 128330.
[220] Xu, L. N.; Fan, H.; Huang, L. X.; Xia, J. L.; Huang, J. R.; Li, M.; Ding, H. Y.; Huang, K.; Li, S. H. Eosinophilic nitrogen-doped carbon dots derived from tribute chrysanthemum for label-free detection of Fe^{3+} ions and hydrazine. *J. Taiwan Inst. Chem. Eng.* **2017**, *78*, 247–253.
[221] Yang, X. M.; Zhuo, Y.; Zhu, S. S.; Luo, Y. W.; Feng, Y. J.; Dou, Y. Novel and green synthesis of high-fluorescent carbon dots originated from honey for sensing and imaging. *Biosens. Bioelectron.* **2014**, *60*, 292–298.
[222] Dong, Y.; Zhang, Y. D.; Zhi, S. M.; Yang, X. Y.; Yao, C. Green synthesized fluorescent carbon dots from *Momordica charantia* for selective and sensitive detection of Pd^{2+} and Fe^{3+}. *ChemistrySelect* **2021**, *6*, 123–130.
[223] Sahoo, N. K.; Jana, G. C.; Aktara, M. N.; Das, S.; Nayim, S.; Patra, A.; Bhattacharjee, P.; Bhadra, K.; Hossain, M. Carbon dots derived from lychee waste: Application for Fe^{3+} ions sensing in real water and multicolor cell imaging of skin melanoma cells. *Mater. Sci. Eng. C* **2020**, *108*, 110429.
[224] Emami, E.; Mousazadeh, M. H. Nitrogen-doped carbon dots for sequential "on-off-on" fluorescence probe for the sensitive detection of Fe^{3+} and l-alanine/l-histidine. *J. Photochem. Photobiol. A: Chem.* **2023**, *438*, 114536.
[225] Durrani, S.; Zhang, J.; Mukramin; Wang, H. Y.; Wang, Z. H.; Khan, L. U.; Zhang, F. N.; Durrani, F.; Wu, F. G.; Lin, F. M. Biomass-based carbon dots for Fe^{3+} and adenosine triphosphate detection in mitochondria. *ACS Appl. Nano Mater.* **2023**, *6*, 76–85.
[226] Zulfajri, M.; Gedda, G.; Chang, C. J.; Chang, Y. P.; Huang, G. G. Cranberry beans derived carbon dots as a potential fluorescence sensor for selective detection of Fe^{3+} ions in aqueous solution. *ACS Omega* **2019**, *4*, 15382–15392.
[227] Picard, M.; Thakur, S.; Misra, M.; Mohanty, A. K. *Miscanthus* grass-derived carbon dots to selectively detect Fe^{3+} ions. *RSC Adv.* **2019**, *9*, 8628–8637.
[228] Wang, W. X.; Chen, J.; Wang, D. K.; Shen, Y. M.; Yang, L. K.; Zhang, T.; Ge, J. Facile synthesis of biomass waste-derived fluorescent N, S, P co-doped carbon dots for detection of Fe^{3+} ions in solutions and living cells. *Anal. Methods* **2021**, *13*, 789–795.
[229] Ma, H. T.; Guan, L.; Chen, M. J.; Zhang, Y.; Wu, Y.; Liu, Z. Y.; Wang, D. W.; Wang, F. H.; Li, X. Synthesis and enhancement of carbon quantum dots from Mopan persimmons for Fe^{3+} sensing and anti-counterfeiting applications. *Chem. Eng. J.* **2023**, *453*, 139906.
[230] Zhao, P.; Zhang, Q.; Cao, J. J.; Qian, C.; Ye, J.; Xu, S. Y.; Zhang, Y. G.; Li, Y. B. Facile and green synthesis of highly fluorescent carbon quantum dots from water hyacinth for the detection of ferric iron and cellular imaging. *Nanomaterials* **2022**, *12*, 1528.
[231] Wang, B. Y.; Guo, L. J.; Yan, X. T.; Hou, F. J.; Zhong, L. L.; Xu, H. Dual-mode detection sensor based on nitrogen-doped carbon dots from pine needles for the determination of Fe^{3+} and folic acid. *Spectrochim. Acta Part A* **2023**, *285*, 121891.
[232] Atchudan, R.; Edison, T. N. J. I.; Perumal, S.; Muthuchamy, N.; Lee, Y. R. Hydrophilic nitrogen-doped carbon dots from biowaste using dwarf banana peel for environmental and biological applications. *Fuel* **2020**, *275*, 117821.
[233] Zhang, D. W.; Zhang, F. R.; Liao, Y. H.; Wang, F. H.; Liu, H. L. Carbon quantum dots from pomelo peel as fluorescence probes for "turn-off-on" high-sensitivity detection of Fe^{3+} and L-cysteine. *Molecules* **2022**, *27*, 4099.
[234] Liu, H. C.; Ding, J.; Chen, L. G.; Ding, L. A novel fluorescence assay based on self-doping biomass carbon dots for rapid detection of dimethoate. *J. Photochem. Photobiol. A: Chem.* **2020**, *400*, 112724.
[235] Deng, X. Y.; Feng, Y. L.; Li, H. R.; Du, Z. W.; Teng, Q.; Wang, H. J. N-doped carbon quantum dots as fluorescent probes for highly selective and sensitive detection of Fe^{3+} ions. *Particuology* **2018**, *41*, 94–100.
[236] Yuan, H. R.; Zhang, X.; Li, D. N.; Chen, Y. Strongly fluorescent carbon quantum dots from biomass tar as highly selective and sensitive probe for Fe^{3+} detection. *Nano* **2018**, *13*, 1850043.
[237] Chen, M. L.; Zhai, J. C.; An, Y. L.; Li, Y.; Zheng, Y. W.; Tian, H.; Shi, R.; He, X. H.; Liu, C.; Lin, X. Solvent-free pyrolysis strategy for the preparation of biomass carbon dots for the selective detection of Fe^{3+} ions. *Front. Chem.* **2022**, *10*, 940398.
[238] Krishnaiah, P.; Atchudan, R.; Perumal, S.; Salama, E. S.; Lee, Y. R.; Jeon, B. H. Utilization of waste biomass of *Poa pratensis* for green synthesis of n-doped carbon dots and its application in detection of Mn^{2+} and Fe^{3+}. *Chemosphere* **2022**, *286*, 131764.
[239] Huang, J.; Deng, Z. Q.; Ding, C. H.; Jin, Y. Z.; Wang, B.; Chen, J. C. Peroxyoxalate/carbon dots chemiluminescent reaction for fluorescent and visual determination of Fe^{3+}. *Microchem. J.* **2022**, *181*, 107782.
[240] Zhang, W. Y.; Jia, L. H.; Guo, X. F.; Yang, R.; Zhang, Y.; Zhao, Z. L. Green synthesis of up- and down-conversion photoluminescent carbon dots from coffee beans for Fe^{3+} detection and cell imaging. *Analyst* **2019**, *144*, 7421–7431.
[241] Ge, L.; Yu, H. L.; Ren, H. T.; Shi, B.; Guo, Q.; Gao, W. S.; Li, Z. Q.; Li, J. G. Photoluminescence of carbon dots and their applications in Hela cell imaging and Fe^{3+} ion detection. *J. Mater. Sci.* **2017**, *52*, 9979–9989.
[242] Guo, Z. C.; Liu, X. R.; Yu, H. Y.; Hou, F. J.; Gao, S. M.; Zhong, L. L.; Xu, H.; Yu, Y.; Meng, J. L.; Wang, R. R. Continuous response fluorescence sensor for three small molecules based on nitrogen-doped carbon quantum dots from prunus lannesiana and their logic gate operation. *Spectrochim. Acta Part A* **2021**, *257*, 119774.
[243] Qiu, Y. J.; Li, D. N.; Li, Y. C.; Ma, X. J.; Li, J. N. Green carbon quantum dots from sustainable lignocellulosic biomass and its application in the detection of Fe^{3+}. *Cellulose* **2021**, *29*, 367–378.
[244] Jagannathan, M.; Dhinasekaran, D.; Soundharraj, P.; Rajendran, S.; Vo, D. V. N.; Prakasarao, A.; Ganesan, S. Green synthesis of white light emitting carbon quantum dots: Fabrication of white fluorescent film and optical sensor applications. *J. Hazard. Mater.* **2021**, *416*, 125091.
[245] Zhu, L. L.; Shen, D. K.; Liu, Q.; Wu, C. F.; Gu, S. Sustainable synthesis of bright green fluorescent carbon quantum dots from lignin for highly sensitive detection of Fe^{3+} ions. *Appl. Surface Sci.* **2021**, *565*, 150526.
[246] Zhang, L.; Li, B.; Zhou, Y.; Wu, Y.; Le, T.; Sun, Q. Green synthesis of cow milk-derived carbon quantum dots and application for Fe^{3+} detection. *J. Sol-Gel Sci. Technol.* **2023**, *106*, 173–185.
[247] Ding, S.; Gao, Y.; Ni, B. S.; Yang, X. D. Green synthesis of biomass-derived carbon quantum dots as fluorescent probe for Fe^{3+} detection. *Inorg. Chem. Commun.* **2021**, *130*, 108636.
[248] Xia, L.; Li, X. J.; Zhang, Y. H.; Zhou, K.; Yuan, L.; Shi, R.; Zhang, K. L.; Fu, Q. F. Sustainable and green synthesis of waste-biomass-derived carbon dots for parallel and semi-quantitative visual detection of Cr(VI) and Fe^{3+}. *Molecules* **2022**, *27*, 1258.
[249] Zhang, J. B.; Zheng, G. S.; Tian, Y.; Zhang, C. H.; Wang, Y. T.; Liu, M. J.; Ren, D. Z.; Sun, H. J.; Yu, W. T. Green synthesis of carbon dots from elm seeds via hydrothermal method for Fe^{3+} detection and cell imaging. *Inorg. Chem. Commun.* **2022**, *144*, 109837.
[250] Murugan, N.; Sundramoorthy, A. K. Green synthesis of fluorescent carbon dots from *Borassus flabellifer* flowers for label-free highly selective and sensitive detection of Fe^{3+} ions. *New J. Chem.* **2018**, *42*, 13297–13307.